SUBJECT

EFFECTIVE MASS ERRORS

NAME Orin Dahl

DATE 4-16-64

In using fitted data to calculate effective masses, we may proceed in either of two ways.

1. Calculate the effective mass of the particles of interest.

2. Calculate the missing mass of the rest of the system.

For example, in the reaction $K^-+p \rightarrow \Lambda +\pi^+ +\pi^-$ we may calculate the $\pi\pi$ mass either by calculating the effective mass of the two pions or by calculating the missing mass from the K^-, p, and

Using either method we will obviously get the same value of the mass. (We are discussing fitted data). However, it is not obvious that the error calculated for the mass will be the same for the two calculations. (Neither Guts nor Fit do a true linear propagation of errors).

In this note we show that if we use the errors as formed in either Guts or Fit, we will get the same calculated error for either method of calculating the mass.

In Guts we have two types of variables; measured variables (and their corresponding fitted values) and massing variables. Thus we may form derivatives by treating only the measured variables as independent (and the missing variables as functions of these measured variables) or by treating both the measured and the missing variables as independent. We also have two types of constraint equations; those balanced by the fitting procedure and those used to solve for the missing variables.

Let us first define a few sets of variables

x_i = measured variables

$$\begin{pmatrix} x_i^m = \text{measured values} \\ x_i^f = \text{fitted values} \end{pmatrix}$$

y_α = missing variables

f_λ = constraints balanced in the fitting procedure

k_α = constraints used to eliminate missing variables

$$F_{i\lambda} = \frac{\partial f_\lambda(x)}{\partial x_i} \quad \text{(x's only independent)}$$

SUBJECT EFFECTIVE MASS ERRORS
NAME Orin Dahl
DATE 4-16-64

$$F^*_{i\lambda} = \frac{\partial f_\lambda(x,y)}{\partial x_i}$$ (x's and y's independent)

$$T_{\alpha\lambda} = \frac{\partial f_\lambda(x,y)}{\partial y_\alpha}$$ (x's and y's independent)

$$K^*_{i\alpha} = \frac{\partial k_\alpha(x,y)}{\partial x_i}$$ (x's and y's independent)

$$U_{\alpha\beta} = \frac{\partial k_\beta(x,y)}{\partial y_\alpha}$$ (x's and y's independent)

$$V_{i\alpha} = \frac{\partial y_\alpha}{\partial x_i}$$

In the Guts method, the error matrix for the fitted variables is given by:

$$G^{*-1} = \tilde{A}G^{-1}A = (1 + QR)^{-1}Q(1+RQ)^{-1}$$

where $Q = G^{-1} - G^{-1}FH^{-1}\tilde{F}G^{-1}$

and $H = \tilde{F}G^{-1}F$

Here $G^{*-1}_{ij} = \overline{\delta x_i^f \delta x_j^f}$ = error matrix for fitted variables (measured)

$G^{-1}_{ij} = \overline{\delta x_i^m \delta x_j^m}$ = error matrix for measured variables

$F_{i\lambda} = \frac{\partial f_\lambda}{\partial x_i}$ = matrix of constraint derivatives (as previously defined)

R = matrix of second derivatives of constraints (R=0 for linear constraints)

$$A_{ij}^{\prime} = \frac{\partial x_i^f}{\partial x_i^m}$$

In calculating G^{*-1} Guts assumes that the constraints are linear and hence replaces G^{*-1} by Q.

Guts then augments the error matrix to include the missing variables by forming

$$C = QV \simeq G^{*-1}V = \sum_j \overline{\delta x_i^f \delta x_j^f}\, \frac{\partial y_\alpha}{\partial x_j} = \overline{\delta x_i^f \delta y_\alpha^f}$$

$$M = \tilde{V}QV \simeq \tilde{V}G^{*-1}V = \sum_{i,j} \frac{\partial y_\alpha}{\partial x_i}\, \overline{\delta x_i^f \delta x_j^f}\, \frac{\partial y_\beta}{\partial x_j} = \overline{\delta y_\alpha^f \delta y_\beta^f}$$

Thus we may form an augmented error matrix

$$Q' = \begin{bmatrix} Q & C \\ \tilde{C} & M \end{bmatrix}$$

NAME Orin Dahl

DATE 4-16-64

SUBJECT

EFFECTIVE MASS ERRORS

We may also form an augmented matrix of the constraint derivates by forming

$$F' = \begin{bmatrix} F^* & K^* \\ T & U \end{bmatrix}$$

This augmented matrix F' is the full constraint derivative matrix for both the f's and the k's (treating both x's and y's as independent).

Now we shall proved that

$Q'F' = 0$

The equation may be broken down into four pieces

$QF^* + CT = 0$ 1)

$\tilde{C}F^* + MT = 0$ 2)

$QK^* + CU = 0$ 3)

$\tilde{C}K^* + MU = 0$ 4)

Now we must consider the constraint derivatives. First consider the equations $k_\alpha(x,y) = 0$

If we differentiate we get (since this equation is the definition of y)

$$0 = \frac{\partial k_\alpha(x)}{\partial x_i} = \frac{\partial k_\alpha(x,y)}{\partial x_i} + \sum_\beta \frac{\partial y_\beta}{\partial x_i}\frac{\partial k_\alpha(x,y)}{\partial y_\beta}$$

or $K^* + VU = 0$

But $QK^* + CU = QK^* + QVU = Q(K^* + VU) = 0$

and $\tilde{C}K^* + MU = \tilde{V}QK^* + \tilde{V}CU = \tilde{V}(QK^* + CU) = 0$

Also we have

$$\frac{\partial f_\lambda(x)}{\partial x_i} = \frac{\partial f_\lambda(x,y)}{\partial x_i} + \sum_\alpha \frac{\partial y_\alpha}{\partial x_i}\frac{\partial f_\lambda(x,y)}{\partial y_\alpha}$$

or $F = F^* + VT$

Now consider $QF = G^{-1}F - G^{-1}FH^{-1}(\tilde{F}G^{-1}F) = G^{-1}F - G^{-1}FH^{-1}H = 0$

Also $G^{*-1}F = \tilde{A}G^{-1}AF = 0$ since

$$AF = \sum_j \frac{\partial x_j^f}{\partial x_i^m}\frac{\partial f_\lambda(x^f)}{\partial x_i^f} = \frac{\partial f_\lambda(x^f)}{\partial x_i^m} = 0$$

Thus

$$QF^* + CT = QF^* + QVT = Q(F^* + VT) = QF = 0$$

$$\tilde{C}F^* + MT = \tilde{V}QF^* + \tilde{V}CT = \tilde{V}(QF^* + CT) = 0$$

ie $Q'F' = 0$

Note that if in forming Q' we had used G^{*-1} instead of Q we would still get $Q'F' = 0$ since $G^{*-1}F = 0$.

In Fit the error matrix is given by (see Fit writeup for notation)

$$Q = \overline{\delta\tilde{x}\,\delta x} = G^{-1} - G^{-1}\tilde{B}H^{-1}BG^{-1} + G^{-1}\tilde{B}H^{-1}B^*(1-tG^*)K^{-1}\tilde{B}^*H^{-1}BG^{-1}$$

$$Q^* = \overline{\delta\tilde{x}^*\,\delta x^*} = K^{-1}(1-At)$$

$$C = \overline{\delta\tilde{x}\,\delta x^*} = -G^{-1}\tilde{B}H^{-1}B^*\tilde{K}^{-1}$$

where

$$K = G^* + A(1-tG^*)$$

$$A = \tilde{B}^*H^{-1}B^*$$

$$H = BG^{-1}\tilde{B} + B^*t\tilde{B}^*$$

We wish to show that $Q'F' = 0$

where

$$Q' = \begin{pmatrix} Q & C \\ \tilde{C} & Q^* \end{pmatrix} \quad \text{and} \quad F' = \begin{pmatrix} \tilde{B} \\ \tilde{B}^* \end{pmatrix}$$

This is equivalent to the two equations

$$Q\tilde{B} + C\tilde{B}^* = 0$$

$$\tilde{C}\tilde{B} + Q^*\tilde{B}^* = 0$$

Now we have

$$Q\tilde{B} + C\tilde{B}^* = \tilde{Q}\tilde{B} + C\tilde{B}^*$$

$$= G^{-1}\tilde{B} - G^{-1}\tilde{B}H^{-1}BG^{-1}\tilde{B} + G^{-1}\tilde{B}H^{-1}B^*\tilde{K}^{-1}(1-G^*t)\,\tilde{B}^*H^{-1}BG^{-1}\tilde{B} - G^{-1}\tilde{B}H^{-1}B^*\tilde{K}^{-1}\tilde{B}^*$$

But $H^{-1}BG^{-1}\tilde{B} = H^{-1}(H - B^*t\tilde{B}^*) = 1 - H^{-1}B^*t\tilde{B}^*$

Thus $$Q\tilde{B} + C\tilde{B}^* = G^{-1}\tilde{B}H^{-1}B^*\left\{t\tilde{B}^* + \tilde{K}^{-1}(1-G^*t)\tilde{B}^*(1-H^{-1}B^*t\tilde{B}^*) - \tilde{K}^{-1}\tilde{B}^*\right\}$$

$$= G^{-1}\tilde{B}H^{-1}B^*\left\{t + \tilde{K}^{-1}(1-G^*t)(1-At) - \tilde{K}^{-1}\right\}\tilde{B}^*$$

SUBJECT: EFFECTIVE MASS ERRORS

NAME: Orin Dahl

DATE: 4-16-64

$$= G^{-1}\tilde{B}H^{-1}B^{*}\left\{t-\tilde{K}^{-1}(G^{*}+A - G^{*}tA)t\right\}\tilde{B}^{*} = G^{-1}\tilde{B}H^{-1}B^{*}\left\{t-\tilde{K}^{-1}\tilde{K}t\right\}\tilde{B}^{*}$$

or $Q\tilde{B} + C\tilde{B}^{*} = 0$

Also $\tilde{C}\tilde{B} + Q^{*}\tilde{B}^{*} = -K^{-1}\tilde{B}^{*}H^{-1}BG^{-1}\tilde{B} + K^{-1}(1-At)\tilde{B}^{*}$

$$= K^{-1}\left\{-\tilde{B}^{*}(1-H^{-1}B^{*}t\tilde{B}^{*}) + (1-At)\tilde{B}^{*}\right\} = K^{-1}\left\{-1+At+(1-At)\right\}\tilde{B}^{*}$$

or $\tilde{C}\tilde{B} + Q^{*}\tilde{B}^{*} = 0$

Thus $Q'F' = 0$

From now on we shall only consider the augmented matrices Q' and F' and augmented variable vectors and constraint vectors

$$x' = \begin{pmatrix}(x)\\(y)\end{pmatrix} \quad \text{and } f' = \begin{pmatrix}(f)\\(k)\end{pmatrix}$$

Now suppose we have another set of constraints p which are functions of the original set f'.

We have $p(f') = 0$

Thus we have

$$P \equiv \frac{\partial p_\lambda}{\partial x_i'} = \sum_\lambda \frac{\partial f_\lambda'}{\partial x_i'}\frac{\partial p_\mu}{\partial f_\lambda'} = F'L \quad ; \quad L_{\lambda\mu} = \frac{\partial p_\mu}{\partial f_\lambda}$$

Now

$Q'P = Q'F'L = 0$

Now suppose that we can split up the variables into two groups so that we can write the constraints as

$$0 = p = p_1+p_2$$

where p_1 is a function only of the variables in the first group and p_2 is a function only of the variables in the second group.*

---

* In our example $K^{-}p \longrightarrow \Lambda + \pi^{+} + \pi^{-}$ where we wanted the $\pi\pi$ mass, we put the K^{-}, p, and Λ in one group and the two pions in the other. The constraints we use are the energy momentum 4-vector.

Thus $p_1 = p_{\pi+} + p_{\pi-}$ } these are 4-vectors

[illegible]

SUBJECT: EFFECTIVE MASS ERRORS

NAME: Orin Dahl

DATE: 4-16-64

Now we may calculate $\overline{\delta p_1 \delta p_1}$ and $\overline{\delta p_2 \delta p_2}$

(These are matrices)

We have $$\overline{\delta p_1 \delta p_1} = \frac{\partial p_1}{\partial x} \overline{\delta x \delta x} \frac{\partial p_1}{\partial x} = \tilde{P}_1 Q' P_1$$

and similarly $$\overline{\delta p_2 \delta p_2} = \tilde{P}_2 Q' P_2$$

However we now note that $P = P_1 + P_2$ since $\frac{\partial p_1}{\partial x_2} = 0$ and $\frac{\partial p_2}{\partial x_1} = 0$

Thus $$\overline{\delta p_1 \delta p_1} - \overline{\delta p_2 \delta p_2} = \tilde{P}_1 Q' P_1 - \tilde{P}_2 Q' P_2$$

$$= (\tilde{P}_1 Q' P_1 + \tilde{P}_1 Q' P_2) - (\tilde{P}_1 Q' P_2 + \tilde{P}_2 Q' P_2)$$

$$= \tilde{P}_1 Q'(P_1 + P_2) - (\tilde{P}_1 + \tilde{P}_2) Q' P_2 = \tilde{P}_1 (Q'P) - (\widetilde{Q'P}) P_2 = 0$$

since $QP = 0$

ie $$\overline{\delta p_1 \delta p_1} = \overline{\delta p_2 \delta p_2}$$

Now suppose we have a quantity z which is a function only of the elements of p_1.+

We may calculate $Z_1 = Z(+p_1)$ or (since $p_2 = -p_1$) $Z_2 = Z(-p_2)$

Now $$\overline{(\delta Z_1)^2} = \frac{\partial Z}{\partial p_1} \overline{\delta p_1 \delta p_1} \frac{\partial Z}{\partial p_1}$$

and $$\overline{(\delta Z_2)^2} = \frac{\partial Z}{\partial p_2} \overline{\delta p_2 \delta p_2} \frac{\partial Z}{\partial p_2}$$

But since $\frac{\partial Z}{\partial p_2} = -\frac{\partial Z}{\partial p_1}$ and $\overline{\delta p_2 \delta p_2} = \overline{\delta p_1 \delta p_1}$

we get $$\overline{(\delta Z_1)^2} = \frac{\partial Z}{\partial p_1} \overline{\delta p_1 \delta p_1} \frac{\partial Z}{\partial p_1} = \frac{\partial Z}{\partial p_2} \overline{\delta p_2 \delta p_2} \frac{\partial Z}{\partial p_2} = \overline{(\delta Z_2)^2}$$

Thus in our original problem we may calculate the error in the effective mass in either way and will get identical results.

+ In our example

$$Z = M^2 = (E_1)^2 - (p_1^x)^2 - (p_1^y)^2 - (p_1^z)^2$$
$$= (-E_2)^2 - (-p_2^x)^2 - (-p_2^y)^2 - (-p_2^z)^2$$

SUBJECT

ELECTROSTATIC POTENTIAL OF THE EARTH AND MOON

NAME Alvarez/Golden/Judd

DATE April 16, 1964

I. Introduction

The possibility that electrostatic fields might play an important role in astrophysics has often been dismissed with the statement that such fields would quickly be neutralized by the consequent motion of positive and negative charges. Five years ago, anyone who had thought even briefly of the possibility that the earth might have a significant electrostatic charge would have quickly convinced himself that the idea was untenable; the charge would have been neutralized almost instantaneously by a flow of current down the geomagnetic polar lines of force. But now that satellite measurements have shown that the magnetosphere is not azimuthally symmetric, it is clear that there are no magnetic field lines that are everywhere straight and radial. This makes it less clear that the charge would be neutralized with a very short time constant.

The equivalent circuit of the earth is show in Figure 1.

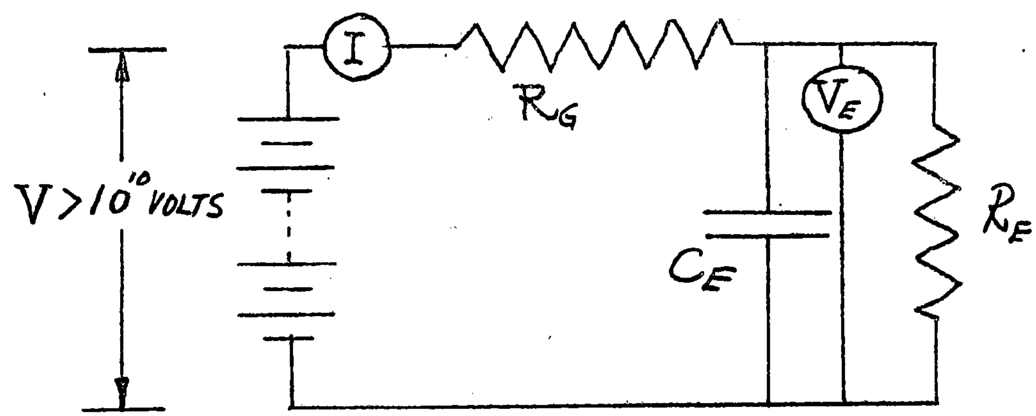

Figure 1

The capacitance of the earth is approximately its radius in centimeters, r_e, with 1 $\mu\mu f \approx 1$ cm. So $C_e = 6.3 \times 10^8$ cm = 7.6×10^{-4} farads. I is the cosmic ray current to the earth. From the tabulated flux as a function of magnetic latitude, J_θ (cm^{-2} sec^{-1} $ster^{-1}$),

$$I = 8\pi^2 r_e^2 \bar{q} \int_0^{\pi/2} J_\theta \cos\theta \, d\theta$$

where $\bar{q}$ is the average charge of the cosmic ray particles.

To within a factor of two,

$$I = 0.6 \text{ ampere.} \qquad (1)$$

In Figure 1, the current I is constant, independent of multimillion volt variations of the potential difference, V_E, across the capacitance C_E. In the absence of the discharging resistance, R_E, the electrostatic potential of the earth would rise at a rate

$$\frac{dV}{dt} = \frac{1}{C}\frac{dQ}{dt} = \frac{I}{C} \qquad (2)$$

With the constants tabulated,

$$\frac{dV}{dt} = 850 \frac{\text{Volts}}{\text{second}} \qquad (3)$$

If we now insert R_E into the circuit, the potential of the earth will level off at the asymptotic value,

$$V = \frac{dV}{dt} \times \left(R_E \times C_E\right) \qquad (4)$$

where R_E C_E is the discharge time constant of the capacitance C_E. If the value of R_E C_E is as long as one hour, then

$$V = 3 \text{ Million Volts} \qquad (5)$$

II. Discussion.

Our attention was drawn to this question by conversations with E. G. Bowen, concerning the possibility that the moon might have an electrostatic charge.[1, 2, 3] Bowen and others[4, 5] had demonstrated a striking dependence of rainfall intensity on the lunar phase. According to Bowen's well known theory relating rainfall intensity to meteoric dust in the atmosphere, the observed correlation would require a strong modulation of the intensity of meteoric dust at the earth by the moon. The modulation index was too great to be accounted for by simple interception of the dust by the moon, or by gravitational effects. Bowen suggested that the dust would be charged positively by the photoelectric action of the sun's rays, and that the charged dust could be "Rutherford scattered" by the moon, with a large effective "lunar cross section". Bowen suggested no mechanism by which the moon might retain the approximately 10^7 Volt positive potential he computed would be required to produce the observed rainfall modulation.

---

1. E. G. Bowen, J. Geophys. Res. 68: 1401 (1963)
2. E. K. Bigg, J. Geophys. Res. 68: 1409 (1963)
3. J. Telford, Australian Jour. of Physics, 16, 464 (1963)
4. D.A.Bradley, M.A.Woodbury, and G.W.Brier, Science, 137, 748, (1962)
5. E.E.Adderley and E.G.Bowen, Science, 137, 749, (1962)

While considering various methods by which one could detect the potential postulated by Bowen, our attention was drawn to a recent paper by Fan, Simpson and Stone.[6] These authors describe a polar-satellite measurement of the flux of 1.5 Mev protons. According to the Störmer theory, such low energy particles should be observable only at geomagnetic latitudes greater than 75°. However, the experiment showed that the protons appeared abruptly at about 65° north and south geomagnetic latitude, where the ~~Störmer~~ EXPECTED PROTON cutoff energy is ~~about~~ AT LEAST 15 MeV, and had constant intensity at greater latitudes. Although at the time we knew of no mechanism for increasing the relaxation time for neutralization of the earth's charge, we nonetheless decided that it would be instructive to trace particle orbits in a combined magnetic dipole field and electric monopole field. The orbits were integrated, using two quite different methods, on the Laboratory's 7044 and 7094 computers.

During this time it was found possible to establish a new generalized Störmer cutoff criterion without recourse to numerical integration. Subject to corrections of a few percent, this criterion predicts that particles which could barely penetrate at any high latitude without the electric field can still do so in its presence provided the electrostatic potential is not so great as to exclude them. This prediction was checked with the computer.

Although there may be other perturbations that might change the simple Störmer cutoff, it seems that the effects observed by Fan, Simpson and Stone

---

6. C. Y. Fan, J. A. Simpson, and Edward C. Stone, Physical Review Letters, 12, 269 (1964).

could have been caused by the presence on the earth of a positive electrostatic charge, raising the potential to the order of 15 Million Volts.

III. Conclusions.

Since none of us is as yet familiar enough with modern knowledge concerning the magnetosphere, we cannot assess the value of the observations we make in this note. In fact, we were very recently about to abandon the whole idea as incompatible with the known density of the interplanetory plasma. But then a casual glance at a field plot of the distorted lines of force in the magnetosphere revived our interest. In appeared from this diagram that the earth's distorted magnetosphere might actually be a good approximation to the elusive "tight magnetic bottle" of the Project Sherwood Physicsists' dreams. Although we have not yet proved the "bottle" to be "vacuum tight", our confidence that it may turn out to have a reasonable long time constant has increased each day. Within the last day, we have obtained, through the courtesy of Professor David Beard, his analysis, with Dr. Gilbert Mead, of the earth's magnetosphere in associated spherical harmonics. The analysis has been made in terms of the interaction of the solar wind with the earth's dipole field, and it is apparently a good fit where it can be compared with experimental observations.

We are now "checking the bottle for tightness", on the computer, using the field shape of Beard and Mead. We have been encouraged to write this brief note by two factors: 1) Dr. Beard, who (unlike the authors) is experienced in these matters, feels it plausible that the bottle might have a time constant of the order of an hour, and 2) we would like to have the benefit of the criticism of these ideas by those attending the URSI-AGU-AAS Symposium on Solar-Terrestrial Relationships, early next week.

Too little is known of the moon's magnetic field, but this situation should be remedied in the near future. If the moon has an appreciable magnetic field, and if the theory of the charge as suggested in this note is correct, then Bowen's mechanism appears plausible.

SUBJECT
STUDY OF HIGH ENERGY INTERACTIONS, USING A "BEAM" OF PRIMARY COSMIC RAY PROTONS

NAME L. W. Alvarez

DATE 5/4/64

I. Introduction.

Until about ten years ago, the discovery of all unstable "fundamental particles" had come from cosmic ray experiments. The pion, the muon, the K mesons and the three hyperons (Λ, Σ and Ξ) were all seen first in cosmic ray experiments. In the past ten years, large accelerators have almost completely supplanted the cosmic radiation as a source of particles for studying the fundamental interactions. Cosmic ray physicists have for the most part abandoned their studies of the interactions of the particles, and have concentrated their attention on the cosmological aspects of the radiation. This situation has arisen from the well known fact that artificial beam intensities in the 1-25 Bev energy region far surpass those available in the cosmic radiation.

The situation in the 100-10,000 Bev energy range is strikingly different--there is no artificial intensity now available, and none will be available for the order of ten years. It has generally been thought that the cosmic ray intensity available in this region is so low as to make experiments with "natural beams" quite unattractive[1]. It is the purpose of this note to show that because of the almost simultaneous emergence of a number of seemingly unrelated techniques, cosmic ray experiments of a meaningful nature in the range 1000 Bev $\pm$ a factor of ten, can probably be carried out.

1. Lawrence W. Jones, "A Cosmic Ray Experiment Design to Explore Strong Interactions at 300 GeV", AR/Int SG/63-13; 29th March 1963. Unpublished document, apparently from CERN.

II. Nature of the Primary Radiation.

The intensity of primary protons in the energy range above 100 Bev is usually expressed in terms of an "integral flux", J_E, where J_E is the number of particles per cm^2, per steradian, per second, with energy greater than E. The flux, J_E, as a function of E, is shown in figure 1.

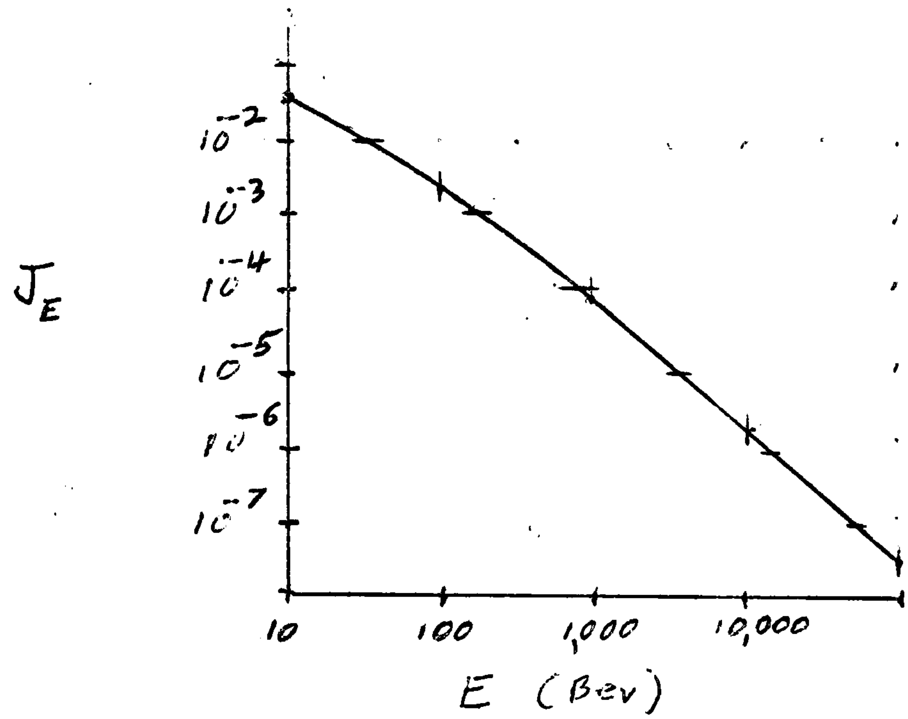

figure 1.

The mean slope of this integral curve is about -1.8. In other words,

$$J_E \propto \frac{1}{E^{1.8}}$$

with $J_{1000\ Bev} \cong 10^{-4.2}\ cm^{-2}\ sec^{-1}\ ster^{-1}$.

SUBJECT STUDY OF HIGH ENERGY INTERACTIONS, USING A "BEAM" OF PRIMARY COSMIC RAY PROTONS
NAME L. W. Alvarez
DATE 5/4/64

We shall now introduce a term which is common in the cosmic ray literature: the geometrical factor is the product of the detector area and the effective solid angle of the detection system. If we have a flux of J, and a geometrical factor G, the counting rate R is given by

$$R = J\,G \quad \text{events per second.}$$

To take a numerical example, let the detector area be 1 square meter, and the solid angle be 0.2 steradians ($\pm 13^{\circ}$ acceptance angle in two orthogonal directions). The G factor is then 2×10^{3} cm^{2} steradians. The counting rate of protons with an energy greater than 300 Bev is then ($J_{300} = 3 \times 10^{-4}$)

$$R = 3 \times 10^{-4} \times 2 \times 10^{3}$$

$$R_{E} > 300 \text{ Bev} = 0.6 \text{ per second}$$

$$= 36 \text{ per minute}$$

To put this number of high energy protons into proper perspective, we may remember that the 72 inch bubble chamber pulses 10 times per minute, and it has often operated usefully for long periods of time with approximately 3.6 K^{-} mesons incident per picture. We therefore see that the cosmic ray beam can supply interesting numbers of very high energy protons for possible experiments, not only at 300 Bev, but also at higher energies. Because of the character of the cosmic ray spectrum, about 10% of the events counted under the conditions just specified have energies greater than 1000 Bev, and 1% have energies greater than 3,000 Bev.

If one allows these high energy protons to fall on a liquid (or solid) hydrogen target two meters long (volume ≅ 3 cubic meters), the probability of an interaction is about 30% per traversal, so one should expect to observe about 10 interactions per minute, or 5,000 per 8 hour flight. (Again, note that 500 of these are at energies greater than 1000 Bev, and 50 are at energies greater than 3,000 Bev !)

III. Experimental Arrangement.

In the last paragraph, the word flight was introduced. The mean free path for high energy particle interactions in the atmosphere is roughly 50 gms per cm^2, so it is imperative that the detecting apparatus be lifted to "Balloon Altitudes". The density of liquid hydrogen is 0.07 gms/cm^3, so 200 cm of H_2 has a surface density of 14 gms/cm^2. At 100,000 feet altitude, the air mass above the apparatus is 9 gms per cm^2. If one compares these two surface densities with the atmospheric interaction "length" of 50 gms/cm^2, it is obvious that no useful purpose would be served by going to higher altitudes. For these reasons, we will consider that the normal balloon altitudes of 85,000 to 100,000 feet are adequate for the experiments under consideration.

Fortunately, at the present time, there are three commercial concerns offering their services to balloon users. These companies will handle all aspects of launching and recovery, at very reasonable rates. (As a rule of thumb, the flight of a balloon with a volume of V million cubic feet costs about $2V$ thousand dollars. For orientation, the 5 million cubic foot Stratoscope II balloon carried a 3-1/2 ton payload to 80,000 feet altitude.) We shall therefore assume that we do not have to become balloon experts in order to use the cosmic ray protons as bombarding particles.

SUBJECT STUDY OF HIGH ENERGY INTERACTIONS, USING A "BEAM" OF PRIMARY COSMIC RAY PROTONS
NAME L. W. Alvarez
DATE 5/4/64

The hydrogen target presents no problems at the present time, since the existence of "superinsulators" obviates the necessity of carrying dewar flasks to altitude. The weight of the hydrogen is small--3 cubic meters of liquid hydrogen weighs only 450 pounds.

The two remaining problems involve the identification of the "interesting" high energy particles from their more numerous "uninteresting" companions of lower energy. The first proposal in this area involved a large hodoscope plus magnetic field. Fortunately, Dr. William Humphrey has proposed a much simpler, lighter, and more elegant scheme. His Cerenkov counter is described in the following Physics Note. He makes use of his observation that at balloon altitudes, the air density is so low that protons cannot radiate Cerenkov light unless their energy is in the "interesting" region above a few hundred Bev. We shall therefore assume for the moment that we can identify the high energy primary protons as they enter the hydrogen target.

We now need a triggerable track chamber with a spatial resolution in a magnetic field comparable to that of a hydrogen bubble chamber. The recent development of the "wide gap spark chamber", or "discharge chamber", by Alikhanian and his collaborators, seems to meet these requirements. Chambers of this type have been built by Professor Karl Strauch at Harvard, and their performance is excellent in all desired respects. Strauch's chambers have the form shown in figure 2, page 6.

SUBJECT STUDY OF HIGH ENERGY INTERACTIONS, USING A "BEAM" OF PRIMARY COSMIC RAY PROTONS

NAME L. W. Alvarez

DATE 5/4/64

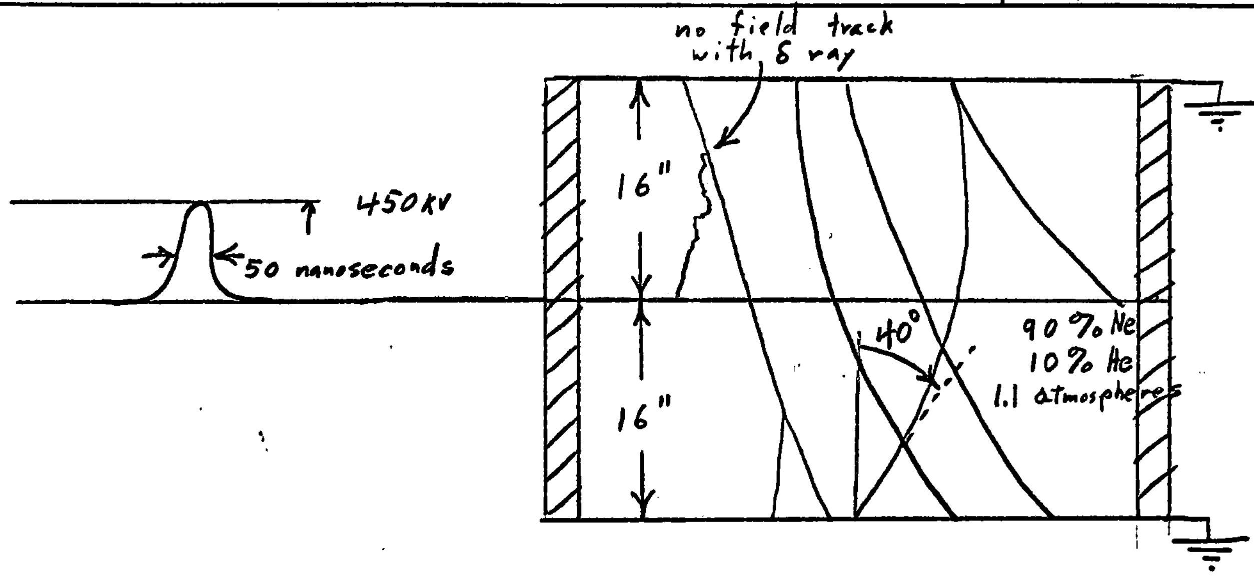

figure 2.

The chambers are sensitive for 5 μsec, and require no clearing field. The pulser is a Marx generator, using 15 standard "color television capacitors" charged in parallel to 30 KV, and discharged by spark gaps in series, to 450 KV. Tracks are seen to 40° from the electric field direction, which is probably quite adequate for very high energy interactions. The light intensity is high enough for photography at f 45, so good depth of focus can be obtained. Strauch advises taking two photographs, one at f 45 and another at f 12, on the chance that some fainter tracks may also be present. He shows pictures with about 20 tracks of good quality in the chamber simultaneously. Tracks can branch, as shown at the left-hand side of figure 2. Strauch compared the measured momentum of cosmic ray particles in the upper and lower halves of a 32" high double chamber, and found the RMS deviation at 1 Bev/c, in 15,000 gauss to be about 1.4%. This is quite comparable to modern bubble standards.

The discharge chamber thus appears to be ideally suited to the job at hand. The only item of equipment still needed is a magnet. Five years ago, one would have had to say "of course it is impossible to carry a useful magnet to high altitude." This is because we have in mind a magnet with several times the stored magnetic energy of the 60" cyclotron magnet. But fortunately, the discovery of "hard superconductors" has changed the situation by many orders of magnitude. One can now transport to balloon altitudes, a magnetic field of many thousands of kilogauss, over several cubic meters. This is the final development which was alluded to in the introduction.

Although the magnet has not yet been designed, it is instructive to note that the Avco Corporation has recently delivered a superconducting magnet (Helmholtz coil), with 11" inside diameter, to the Argonne Laboratory, for use with a bubble chamber. The useful field is approximately 50,000 gauss over approximately 1/2 cubic foot. If we increase the useful field volume by a factor of 100 (to about 1.5 cubic meters), we cut the magnetic field by a factor of 10 (assuming the energy storage to be constant). This crude calculation is only intended to show that it is not unreasonable to believe that useful magnetic fields over the required volume of discharge chamber can be carried aloft.

IV. Conclusions.

It appears to be technically and economically feasible to carry out meaningful experiments on p-p interactions in the energy range from 300 to 3,000 Bev. This is the energy range which would be available to the CERN experimenters if they build their storage rings-clashing beam facility (at a cost of about 50 million dollars).

It is perhaps appropriate to quote from a recent issue of the CERN Courrier[2]:

"The Storage rings should be regarded as an exploratory device. They will not produce super-high-energy beams of secondary particles and can only be used for the study of proton-proton interactions. They cannot therefore be thought of as an alternative to the 300 BeV accelerator. Nevertheless, they would provide a "window" through which the future course of experimental physics at the highest energy could be viewed."

This quotation appears to be equally applicable to the present proposal, which has the additional attractive feature of being less expensive by perhaps more than an order of magnitude than the storage rings.

---

2. CERN Courrier, Vol. 4, No. 2, page 17, 1964.

LAWRENCE RADIATION LABORATORY • UNIVERSITY OF CALIFORNIA PHYSICS NOTES	NFD	MEMO NO. 505.	PAGE 1
SUBJECT PROPOSED EXPERIMENTAL TECHNIQUES FOR USE IN HIGH ALTITUDE PARTICLE PHYSICS EXPERIMENTS		NAME William Humphrey; DATE April 29, 1964	

I. Introduction

Present day accelerators have been built which are capable of producing proton beams having an energy up to about 30 Bev. There are two design studies in progress for the construction of machines capable of producing 200 Bev and 1000 Bev proton beams. Neither of these proposed machines will probably be operating within 10 years from now. Dr. Luis Alvarez has been interested in the possibility of using natural cosmic ray protons which are incident on the earth's outer atmosphere as a source of "proton beam" for high energy particle physics experiments in the near future. Experiments with these cosmic rays would supplement that available from the proposed accelerators in the range above 1000 Bev, and might provide useful information to act as a guide in the design of accelerators and detecting equipment in the range below 1000 Bev.

This note deals with some possible techniques that might be used to reject the large number of unwanted particles (protons of less than about 200 Bev for example) that would be encountered while doing experiments with a high altitude (more than 25 kilometers) balloon, and some techniques which might be useful in making measurements of particles with energies of the order of 1000 Bev.

II. A Cerenkov detector which detects high energy protons

It turns out that at the balloon altitudes of about 25 kilometers, the Cerenkov threshold is in the region of 200 Bev, see Fig. 1. The Cerenkov light emitted by a proton having more than 200 Bev of energy as it moves into the earth's atmosphere may be collected and detected with a photomultiplier, while lower energy protons produce negligible light and hence produce no "count" at the photomultiplier. This provides a pulse which can be employed to trigger such devices as spark chambers that have a facility of time resolution, whenever a high energy proton traverses the experimental setup.

The Cerenkov light at the altitudes of interest is confined to a narrow angle (less than 10^{-2} radians full angle) so that the light given off by a particle may be collected over the last few hundred meters of path length by making use of a light collector of fairly modest size, say 2 meters diameter. Even so, the light emission is so weak that only a few hundred photons would be collected (see Fig. 2 and 3). In order to detect these photons, it is necessary to operate at night when the background photons would be of the order of 10^{10} in the visible region for a 2 meter light collector. The Cerenkov light may be separated from the background light by making use of the short duration of the Cerenkov pulse. Current electronics would limit the time resolution to about 10^{-9} sec, and in this interval of time the current due to the Cerenkov light is much greater than the background current due to background light, phototube noise, etc. In addition, the Cerenkov pulse must come in coincidence with a pulse from one or more particle detectors located in the experimental setup, which further reduces possible accidental counts. A further reduction of background can be achieved by making use of the narrow angular distribution of the Cerenkov light. These points will be clarified in an example which will be considered.

In principal, the Cerenkov light could be used for more than just a trigger pulse. Pulse height information could be used to measure the momentum of particles somewhat above threshold, or the direction of the particle could be measured by focusing the Cerenkov light on a pulsed image intensifier and taking a photograph. Unfortunately, these schemes are probably not very practical because of the low yield of photons and the low electron conversion efficiency of photocathode materials.

III. An example of a Cerenkov trigger system

In order to get an idea of the order of magnitude of quantities that enter into the problem, and the techniques which must be used, consider the Cerenkov trigger system diagrammed below:

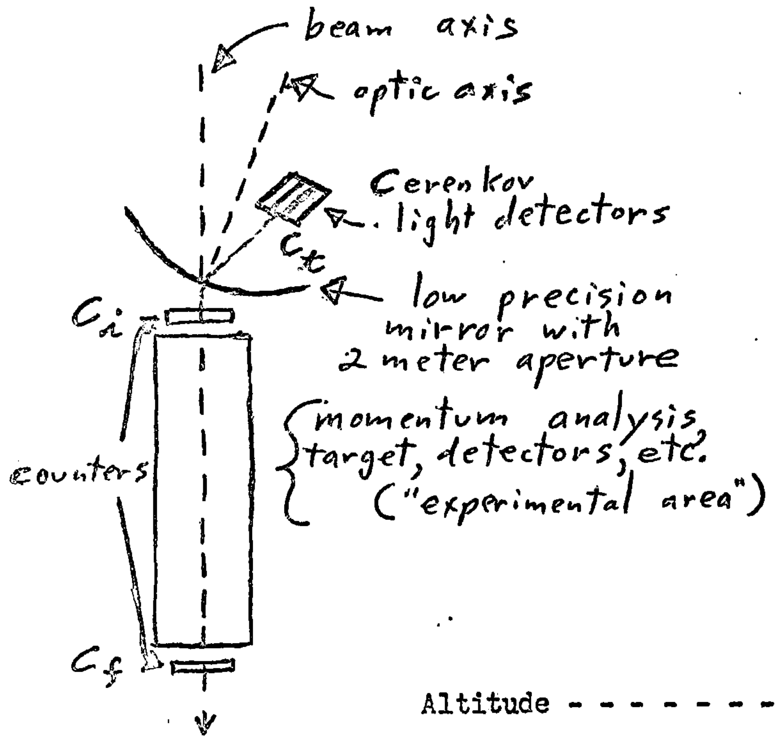

Experimental detecting equipment is triggered on a coincidence of $C_t + C_i + C_f$, where C_i and C_f are detectors which insure the particle passes through the "experimental area".

Let the parameters be as follows;

Altitude - - - - - - - - - - - -	25 km
Mirror - - - - - - - - - - - - -	1 m. radius
Cerenkov angle - - - - - - - - -	4.25×10^{-3} radians half angle
Counter angle - - - - - - - - -	$\sim 4 \times 10^{-2}$ radians half angle (80 °/o efficient)
Counters - - - - - - - - - - - -	7, sensitive from 4000 to 6000 Å with 10 °/o efficiency and 10^{-9} sec time resolution
Total solid angle - - - - - - -	.045 steradians

The background will be

$$N_B = (2.5 \times 10^8)(\pi \times 10^4)(8 \times 10^{-2})^2(.1) = 5.0 \times 10^9 \text{ e/sec counter}$$

The signal strength is

$$N_S = 15.3\text{e for } \eta \geq 1000$$

This means that the average number of electrons per light pulse will be 20.3. Imposing a threshold of 20.3 will give 50 °/o detection of the desired particles. The chances of an accidental are

SUBJECT PROPOSED EXPERIMENTAL TECHNIQUES FOR USE IN HIGH ALTITUDE PARTICLE PHYSICS EXPERIMENTS

NAME William Humphrey
DATE April 29, 1964

$$P = \frac{(5)^{20.3}e^{-5}}{20.3!} = 9.2 \times 10^{-7} \text{ per counter}$$ (plus probability for more than 20.3 counts)

or

2×10^{-5} for all seven counters for a given interval of 10^{-9} sec.

Requiring $C_i + C_f + C_t$ with $C_i + C_f$ having twice the solid angle of C_t, one has

$$\text{o/o background} = \frac{100 N \text{ above 1 bev/c}}{N \text{ above 1000 Bev/c}} = 100\frac{(2 \times 10^{-1} \times 2)(2 \times 10^{-5})}{10^{-4}\,(1/2)} = 16 \text{ o/o}$$

counting only the proton flux.

The counting rate might be about 30 per hour with $C_i = 50 \times 50$ cm.

This example points out the fact that a straight forward approach to the problem gives a system which is probably workable, but is very critical to some of the parameters, particularly the background. The background fluctuates somewhat with time, and reliable quantitative measurements are hard to find. The optical background problem is considered in more detail in an Appendix.

This first approximation might be improved in a variety of ways. For example increasing the number of counters from 7 to 10 would reduce the background by a factor of 30, assuming the same total solid angle. Or, shifting to the 3000 to 4000 Å band (which has the same signal strength and half the background) would reduce background coincidence by a factor of 100. If these changes were made the transmission of the desired particles could be greatly increased at the same time the background counts were reduced.

IV. Cerenkov light in an absorptive atmosphere.

Detection of Cerenkov light in the wavelength region from 3000 to 6000 A° has been considered in the previous section. In the region of wavelength greater than 6000 A°, the signal to noise ratio becomes worse. For wavelengths shorter than about 2000 A° light is strongly absorbed by oxygen and the air is essentially opaque. The one region left to be considered is the wavelength interval from 2000 to 3000 A°. This is a very interesting region because there is strong absorption of light by ozone molecules present in the region of interest. ~~Essentially all background light is absorbed out and it can be ignored.~~ The situation is much like looking for Cerenkov light from a particle traveling through a bottle of ink; if the ink is not too dense, the signal is attenuated much less than the background light and the Cerenkov pulse is easily detected.

To give an idea of the intense absorption of ozone, the usual total ozone content of the atmosphere is equivalent to a 2.5 mm thick layer of the gas at S.T.P. This thin layer reduces the transmitted intensity by a factor of 10^{40} at 2550 A°! At an altitude of 25 km, this represents a decay length at maximum absorption (2550 A°) of about 200 meters. This means that photons can be expected from only about the last 200 meters of air. At higher altitudes and other wavelengths, the decay length can be expected to increase. The ozone absorption is shown in Fig. 4 as a function of wavelength.

The absorption by the ozone is so strong that it might be possible to detect Cerenkov light at altitudes of 20 km or less during the day. Unfortunately there is too much air mass above this altitude to make such a Cerenkov detector useful for the purposes of this note.

The 2000 to 3000 A° band has another interesting property, and that is that the index of refraction is about 10 °/o higher due to the dispersion of air. This means a lower Cerenkov threshold and more photons per meter of track path length in the atmosphere. The influence of the absorption band of the ozone on the index of the air has been neglected.

SUBJECT: PROPOSED EXPERIMENTAL TECHNIQUES FOR USE IN HIGH ALTITUDE PARTICLE PHYSICS EXPERIMENTS

NAME: William Humphrey

DATE: April 29, 1964

V. An example of a Cerenkov trigger using the ozone absorption band

In the ozone absorption band, the feasibility of the Cerenkov technique depends only on how many Cerenkov photons can be collected, and not on background light considerations. ~~For this reason, the Cerenkov light detector should consist of as few photomultiplier tubes as possible so that the tube noise background will be reduced, and if more than one tube must be used, pulse height discrimination should be on the sum of the tube currents rather than having a separate discriminator for each tube as in the examples of section III. Tube noise can also be reduced by chilling the photomultiplier, as long as the temperature is not reduced past the point at which the photocathode becomes non-conductive.~~ Tube noise should not exceed about 10^4 electrons per second.

The Cerenkov photon yield have been calculated for two spectral intervals for the geometry outlined in section III. (see Fig. 5 and 6). The two spectral regions are 2100 to 2550 A° and 2550 to 3000 A°. These regions are considered separately because different light collection methods tend to vary greatly in efficiency for these two regions. The results of the calculations are summarized in table I. These calculations suggest that at 25 km it is probably practical to collect of the order of a hundred photons in the ozone absorption band using an aluminum coated mirror. Perhaps an average of 6 photoelectrons can be collected and amplified in the photomultiplier. Then for a counter threshold set to trigger on two or more photoelectrons, the chance of an accidental count from phototube noise in a given interval of 10^{-9} sec is:

$$P_B = \frac{(10^{-3})^2 \, e^{10^{-5}}}{2!} \sim 10^{-6}$$ (taking background ≐ 100 x (tube noise))

On the other hand, the probability that a desired particle will not pass the threshold is

$$P_R = \frac{(6)^1 \, e^{-6}}{1} + \frac{(6)^0 \, e^{-6}}{1} \sim 3 \times 10^{-2}$$

Therefore the transmission will be good, and the percentage of background will be very low (1/4 °/o). The primary source of background should then be particle background rather than background from various sources of extraneous photoelectrons. (There might actually be some background light in the region of 3000 A°, but the background can be controlled by the choice of the spectral window which is used, see fig. 6).

Again, the feasibility of this particle detection scheme depends on parameters of the upper atmosphere which are somewhat uncertain and variable. This is particularly true of the ozone concentration. At high altitudes, there are even appreciable seasonal variations in the ozone concentration which must be considered. A device operating in the ozone absorption band must have monitors of both the air density and ozone concentration in order to calibrate the measurement of the Cerenkov pulse height. The fact that there are only 2 parameters important to performance in the ozone absorption band is actually quite an advantage and simplification over the methods considered in section III.

VI. A Fully Enclosed Cerenkov Trigger

The obvious advantage of a fully enclosed Cerenkov counter is the freedom from background light, which plagues the previously described Cerenkov systems. Perhaps the most obvious possibility is to use the helium gas in the balloon. The trouble with this is that helium has a very small index of refraction and hence too high a Cerenkov threshold, as well as far too low a photon production rate. The index of the gas in the balloon can be increased by mixing in something such as methane with a high index and low density, but the lift will be drastically reduced before the index of air is achieved. Even at the index of air, more than a hundred meters of path length over perhaps .1 steradian would be required, and the balloon would have to be extremely well coated to eliminate background light.

Another approach is to make use of the fact that the photon yield increases in proportion to $(n-1)$ while the threshold only changes as $1/\sqrt{n-1}$. This suggests that perhaps a relatively short length of gas of index higher than that of air could be enclosed in some sort of opaque balloon-like structure. The gas should be light weight and have (n-1) several times that of air. Simple hydrocarbons are practically made to order. Butane is only twice as heavy as air, and has (n-1) five times that of air (based on interpolation between methane and pentane, whose indices are in the "Rubber Handbook") Propane or carbon tetrachloride might be other good possibilities. At some balloon altitudes heat is needed to maintain a gas, except possibly for butane.

Taking butane as an example, consider a 10 meter opaque container at 25 km. filled with butane at slightly above local atmospheric pressure. About 70 photons are produced in the wavelength interval of 3000 to 6000 A°, which should yield about 6 photoelectrons (taking into account optical efficiency and photo-cathode efficiency) with little more than phototube noise for background. From previous examples, this is clearly a very good trigger signal. The Cerenkov threshold would be about $\eta = 100$ ($\eta = P/M$). At higher altitudes pentane or carbon tetrachloride might be used at nearly local atmospheric pressure.

The interior surface of the container for the Cerenkov gas should be a metallic surface that is blackened to eliminate Cerenkov light from the container and to absorb ionization and recombination radiations. The non-Cerenkov light is normally negligible, but must be checked under conditions of low pressure. Jelley[4] claims less than 4×10^{-6} of the ionization energy for relativistic particles appears as visible light in air at S.T.P.

As a more concrete example of such a counter, consider a Cerenkov gas container in the shape of a pyramid with a depth of 10 m and a base of 17.3 m^2. Such a container would provide a 1 m^2 counter aperture with a solid angle of .1 steradian. The surface area of the container would be 120 m^2, which would weigh perhaps 100 pounds if it were formed of several layers of the mylar and aluminum sheets of the type employed in satellite balloons. The volume of butane required would be 75 m^3, which should weigh less than 6 pounds at balloon altitudes. At about 25 km, a little more than 6

SUBJECT PROPOSED EXPERIMENTAL TECHNIQUES FOR USE IN HIGH ALTITUDE PARTICLE PHYSICS EXPERIMENTS | NAME William Humphrey | DATE April 29, 1964

photoelectrons could be produced by the Cerenkov light in the pyramid (using an aluminum mirror light collector, quartz optics, a photomultiplier with extended S11 response, and allowing 20 o/o inefficiency due to reflections, etc.). The number of photons decreases as the η of the particle decreases, however the decrease is very slight until η is relatively close to the threshold of $\eta = 100$ (See Fig. 7). If the phototube pulse height discriminator is set for 2 photoelectrons, practically all particles with η above 200 are detected (See Fig. 8 and Fig. 9).

VII. Particle Background for a Cerenkov Trigger System

A Cerenkov counter can only be used to discriminate between particles of different η (P/M). In the case of the previous examples, there was a Cerenkov threshold at about $\eta = 250$. This means that there can be trigger pulses for 125 MeV electrons and 30 BeV pions in addition to the desired 250 BeV protons.

The electrons are particularly annoying, because there are so many ways of producing low energy electrons. Solar flares appear to produce fluxes of 100 MeV electrons far in excess of the cosmic ray flux for short periods of time. At low latitudes the earth's magnetic field will deflect these. Another source of electrons is the decay of π^0 mesons produced by primary cosmic ray interactions in the atmosphere. This is a two step process involving the production of ~~about 40 grams of atmosphere in which such a process can take place. The interaction length is about 50 grams and the radiation~~
a π^0 which decays into gamma rays which produce electrons. At 25 km, there are about 40 grams of atmosphere in which such a process can take place. The interaction length is about 50 grams and the radiation

SUBJECT PROPOSED EXPERIMENTAL TECHNIQUES FOR USE IN HIGH ALTITUDE PARTICLE PHYSICS EXPERIMENTS
NAME William Humphrey
DATE April 29, 1964

length is about 30 grams, so this mechanism might contribute background, expecially in view of the relatively large flux of protons below the Cerenkov threshold. Another important source of electrons would be the Dalitz production process. There are probably other sources of electrons than those mentioned, but the point is that provision might have to be made to eliminate trigger pulses arising from electrons. This must be done by momentum analysis. Some momentum analysis takes place as the electron moves through the atmosphere, and this causes the Cerenkov light to be spread in direction ($\lesssim 1°$) and reduces collection efficiency near the electron threshold. To obtain appreciable electron rejection, it is probably necessary to provide a sweeping field below the Cerenkov detector to bend the electrons out of the system before they can reach the last counter in the Cerenkov coincidence circuit (C_f of section III). This same magnetic field could be useful in momentum analyzing the desired particles, as will be discussed in the next section.

As far as pion background is concerned, if it is small, there is nothing to worry about. If it is large, then it is a good source of pions in an energy range above that available from present accelerators. The pions should be easily separated from protons by momentum analysis. To reduce the attenuationof the relatively rare protons and reduce the number of pions, the balloon should probably fly at an altitude greater than the 25 km used in the previous examples. At 30km there are only about 15 grams of atmosphere to deal with, but Cerenkov detection efficiency will probably be reduced.

This section serves only to indicate that particle background is probably not going to make the Cerenkov trigger scheme unworkable. Obviously, a great deal of work must be done to estimate the number and energy spectrum of the various kinds of detectable particles as a function of altitude.

SUBJECT: PROPOSED EXPERIMENTAL TECHNIQUES FOR USE IN HIGH ALTITUDE PARTICLE PHYSICS EXPERIMENTS

NAME: William Humphrey

DATE: April 29, 1964

VIII. Position and Angle measurements

For protons in the range of 1000 BeV, the measurement precision is a very important factor, For example, a scatter with a transverse momentum transfer of 250 MeV/c produces an angular deflection of .25 milliradians. On the other hand, multiple scattering is low, and measurements to 10 microradians might be meaningful. One way of acheiving this sort of precision would be to combine spark chambers and emulsion in order to obtain both time and spatial resolution. Such an angle measurement scheme is illustrated below.

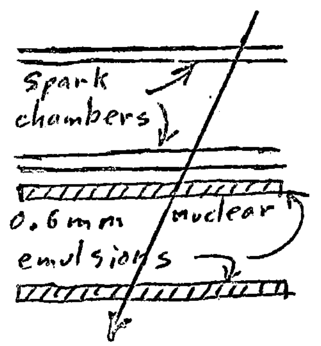

The path of the particle in the emulsion can be measured to about a micron, giving an angular resolution of about 3 microradians.

The particular particle can be located in the emulsion by calculating the particle orbit from the spark chamber information and scanning only a small area of emulsion for tracks having just the right direction. The direction can be easily recognized if the emulsion is oriented such that the desired particle will be vertical. Then if the microscope objective is moved up and down, only the desired particle will appear as a stationary spot in the emulsion. A minimum track would give perhaps a dozen developed grains in each emulsion.

Assuming a spark precision of about 1 mm, one heeds only scan a millimeter square of emulsion, which might have a thousand tracks in all directions. (After a couple of days in a balloon.) Of these, the direction information restricts the angular phase space by a factor of about a million, and background track coincidences should be very rare.

It might be possible to desensitize emulsions by freezing them if they are doped with some substance such as iodine. The emulsion scanning would be made easier if the emulsion could be exposed to radiation for only eight or ten hours and then desensitized. I understand that emulsions can be "erased" before use by warming them.

Other properties of emulsion might also be used to discriminate against background, for example non-minimum tracks or tracks with large scatter could be ignored. One nice thing about the emulsion -- there is no problem of optics calibration to ensure micron spatial resolution. An accurate grid can be printed on the emulsion and measurements are made with respect to the grid.

The precise relative spatial position of the emulsions might be calculated from the path of the higher energy particles, which are almost straight lines.

High precision emulsion measurements can provide useful momentum measurements, and in fact this might be their greatest value. For example, if an angle change of 10^{-4} radians is measurable to 10 °/o, then an integrated field of 3 kilogauss meters will give a 10 °/o estimate of momentum at 1000 BeV/c.

IX. Summary

From the rather meager and somewhat questionable information available about the upper atmosphere, it seems that a Cerenkov counter could be built that would trigger detecting equipment for particles having an η in excess of about 300. It is doubtful that the signal to noise ratio in the visible or near ultraviolet would permit Cerenkov operation in a single and reliable way. The most promising region to look for Cerenkov light is the region below 3000 Å. The rate at which a detector might be triggered by Cerenkov pulses would typically be a few times a minute.

It also seems practical to build a fully enclosed Cerenkov counter containing gas at local atmospheric pressure which could be used both during the day and at night. Although the threshold for Cerenkov radiation would be lower (say η = 100), the counting rate would be increased to perhaps 20 per minute. The biggest unknown in this scheme is the relative amount of light given off by particles from processes other than Cerenkov radiation. This source of background is negligible at atmospheric pressure (STP).

It is probably possible to measure angles to the order of 10^{-5} radians and positions to a few microns using combined spark-chamber-emulsion techniques. This should make practical 10 °/o momentum measurements at momenta up to 1000 BeV/c.

SUBJECT PROPOSED EXPERIMENTAL TECHNIQUES FOR USE IN HIGH ALTITUDE PARTICLE PHYSICS EXPERIMENTS

NAME William Humphrey

DATE April 29, 1964

X. Appendices

A. Background light

The qualitative features of light from the night sky are as follows. Starting from the short wavelength end, oxygen absorbs light strongly to 2000 Å, and ozone absorbs strongly to 3000 Å. A useful diagram of the penetration depth versus wavelength is available in reference 1, pg. 134. Beyond 3000 Å there is a region of about 100 Å of fairly low background light followed by a region of moderate emission from the Herzberg bands of oxygen. This emission region is characterized by many very pronounced and fairly narrow emission peaks. There is an interval of about 100 Å at 4000 Å that has quite a low background light level. Beyond 4000 Å there is a rapid increase in intensity to a high level peaking at about 4600 Å. This region consists of a continuation of the Hertzberg bands plus a continuum. Beyond 5000 Å, the background remains at a fairly high, constant level far into the infrared region. There are two very bright lines due to oxygen at 5577 Å and 6315 Å. A profile of the entire spectrum is available in the "atlas" reference 2. The sources of night sky light and their relative strengths are listed in one paper as follows[3]:

Atmospheric scattered star light - - - - -	7 %
Airglow - - - - - - - - - - - - - - - - - - -	40
Interplanetary light - - - - - - - - - - - -	20
Interstellar light - - - - - - - - - - - - -	20
Interstellar dust - - - - - - - - - - - - - -	13

I am informed that most of the gallactic light is due to a multitude of very faint, distant stars, and not the stars that are visible to the eye.

As far as more familiar sources of light are concerned, the relative "surface brightness" is as follows:

Sun - - - - - - - - - - - -	1
Moon - - - - - - - - - - - -	10^{-6}
Day sky at 80,000 ft	10^{-8}

SUBJECT PROPOSED EXPERIMENTAL TECHNIQUES FOR USE IN HIGH ALTITUDE PARTICLE PHYSICS EXPERIMENTS

NAME William Humphrey

DATE April 29, 1964

Quantitative information about sky brightness is very hard to find, and what there is differs from observer to observer. In the visible region, Jelley's book[4] on Cerenkov radiation has useful numbers in the chapter on detection of atmospheric electron showers. These numbers must be corrected for atmospheric absorption if they are to be applied to balloon experiments. In the near ultraviolet region (3000 to 4000 Å), a good source of numbers is the "Nightglow Atlas" (ref. 2) compiled from Russian measurements during the I.G.Y. Some of the values in the "Atlas" appear to be higher than those of other observers. The atlas gives intensities for the oxygen Hertzberg emission bands (which constitute most of the near ultraviolet background) in terms of both observed intensities and intensities at the source. Numerous other references to airglow work appear in reference 1 in this chapter on airglow by Bates.

The brightness of the night sky is quoted in a variety of different units. For example astronomers use "magnitudes per sec^2." while atmospheric physicists use "Rayleighs" or "ergs per cm^2 steradian sec." The best information I have (based on personal conversations and references) indicates that the photon flux in the visible region at high altitude is about 2.5×10^8 photons/cm^2 ster. sec. in the 4000 to 6000 Å band. The estimate of sky brightness in the 3000 to 4000 Å band is based on the Russian work in the atlas[2], and is 1.25×10^8 photons/cm^2 ster. sec. at high altitude.

In the ozone absorption band, there are two important considerations relative to absorption of background light. One is the absorption properties of ozone, which are well known.[5] Fig. 4 is derived from ~~their paper~~ ref. 5. The second factor is the distribution of ozone with altitude. The most complete set of measurements on this subject is probably the work of Brewer and Milford in England.[6] They made measurements in balloon flights on a number of different days. The value of 15×10^{-3} cm. of ozone per km which I have used in fig. 5, 6, and 7 is based on their work. Another unknown in the ozone absorption band is the intensity of sources of background light in this special range.

Zodiacal light and gallactic light are probably very low. A large background would have to come from a strong airglow emission.

All the Cerenkov trigger schemes depend on the Cerenkov light being the dominant source of light from particles. If stopping particles can produce appreciable light by ionization or excitation of the air (or other Cerenkov gas), then there will be a serious background problem to deal with. Several comments in Jelley's book[4] (pg 236 and Pg 94) suggest this is probably not a large background.

B. Optics and light detectors

Both of the most promising schemes for triggering on Cerenkov light profit by working with light in the far ultraviolet. Optics imposes a restriction on how much of the ultraviolet region is useful. For transparent materials, quartz is good to 2000 Å and Uviol crown is good to 3000 Å. There are filters for cutting out visible light. For example Jena glass UG5 transmits 93 °/o at 2810 Å and 11 °/o at 4360 Å. For reflective optics, aluminum is still 60 °/o reflective at 2500 Å. The "Handbook of Physics and Chemistry" lists other metals slightly more efficient in the far ultraviolet.

As far as light detectors are concerned, the new RCA C70045A[7] with a 1/2 n.sec. response time has an extended S11 light sensitivity which is usable to 2000 Å. There are other less expensive and useable tubes with quartz faces such as the 56UVP by Philips ($540). There are also special cathode materials such as S_iO_2-C_s-T_e which is good in the range 1600 to 3200 Å, but probably less sensitive than the usual C_s-S_b cathode. Opaque cathodes are usually more efficient because light must pass through the cathode material twice. Although an opaque cathode could be used, usually they are rather small, and would complicate the optics.

SUBJECT: PROPOSED EXPERIMENTAL TECHNIQUES FOR USE IN HIGH ALTITUDE PARTICLE PHYSICS EXPERIMENTS

NAME: William Humphrey
DATE: April 29, 1964

XI. References and other sources of information

Background light

1. "Physics of the Upper Atmosphere", edited by J.A. Ratcliffe (1960)

2. Atlas of the Airglow Spectrum 3000-12400 Å, V.I. Krassovsky, N.N. Shefov, V.I. Yarin. Planet. Space Sci., (1962) Vol. 9, pg. 883

3. New Frontiers of Astronomical Technology, A.B. Meinel. Science (1961), v. 134, pg. 1165

4. "Cerenkov Radiation and its Applications", J. V. Jelley (1958)

5. Absorption Coefficient of Ozone in the Ultraviolet and Visible Regions. Edward C. Y. Inn, Yoshio Tanaka. Journal of the Optical Society of America (1953), Vol. 43, p. 870

6. The Oxford-Kew Ozone Sonde. A.W. Brewer, J.R. Milford. Proc. Roy. Soc. A(G.B.), (1960), Vol. 256, pg. 470

In addition, daytime light level studies have been carried out by Gorden Newkirk (High Altitude Observatory, Boulder, Colorado) and Arthur Code (Washburn Observatory, University of Wisconsin). The work of Arthur Code includes 2500 Å studies from an X15 flight, and one night balloon flight.

Light detectors -- see ref. 4

7. Evaluation of the C-70045A High-Speed Photomultiplier. M. Birk, Q.A. Kerns, R.F. Tusting. UCRL-11147 (1964), unpublished.

Particle flux as a function of energy and sources of particle background

8. "Satellite Environment Handbook" editied by F.S. Johnson (1961)

Combined spark-chamber-emulsion techniques.

Conversations with W. Barkas indicate that the track density in emulsions is tolerable for exposures up to about two days. (The customary emulsion thickness is about .6 mm). Dr. Barkas thinks Prof. Burhop in London may be working on similar spark-chamber-emulsion techniques for use at CERN. Bogomolov may have information on desensitizing nuclear emulsion at low temperature by iodine contamination. John Dyer has made emulsion scanning equipment in which the emulsion is tilted and scanned. Barkas claims emulsions may be "erased" (by application of heat) to a large extent.

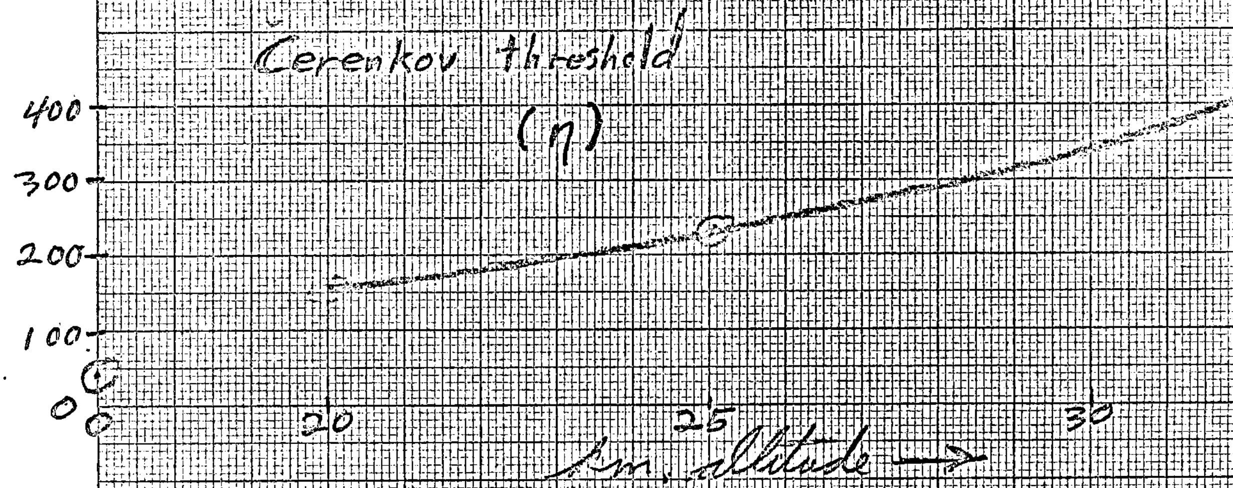

Fig. 1

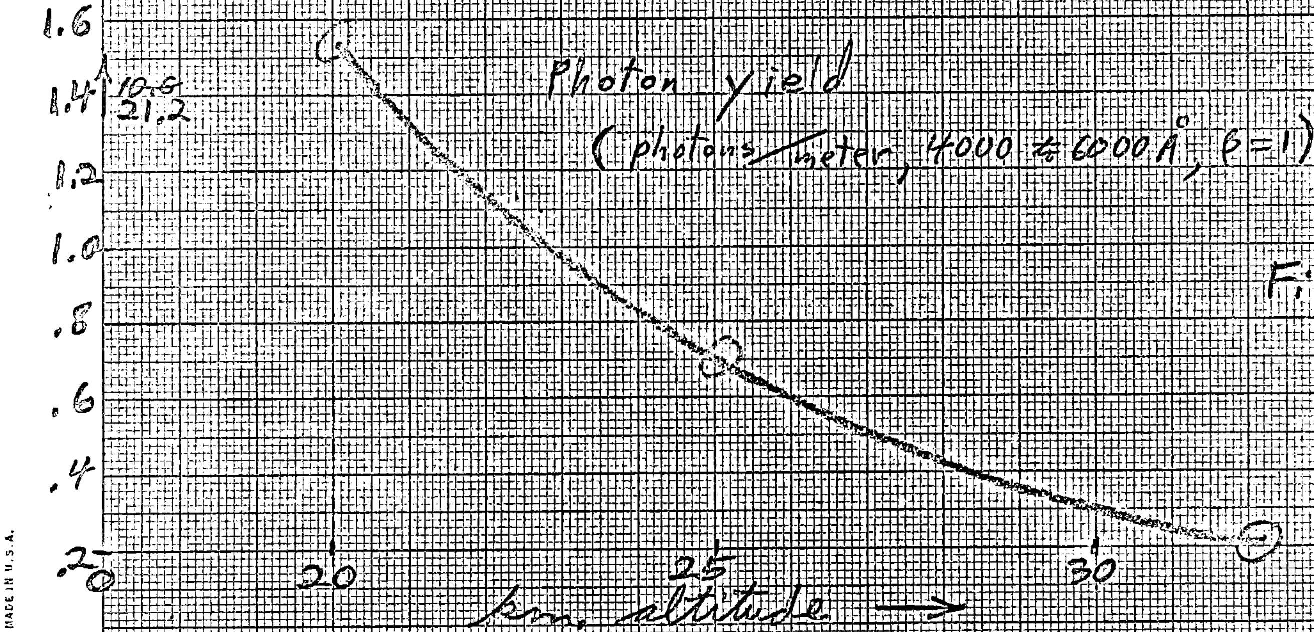

Fig. 2

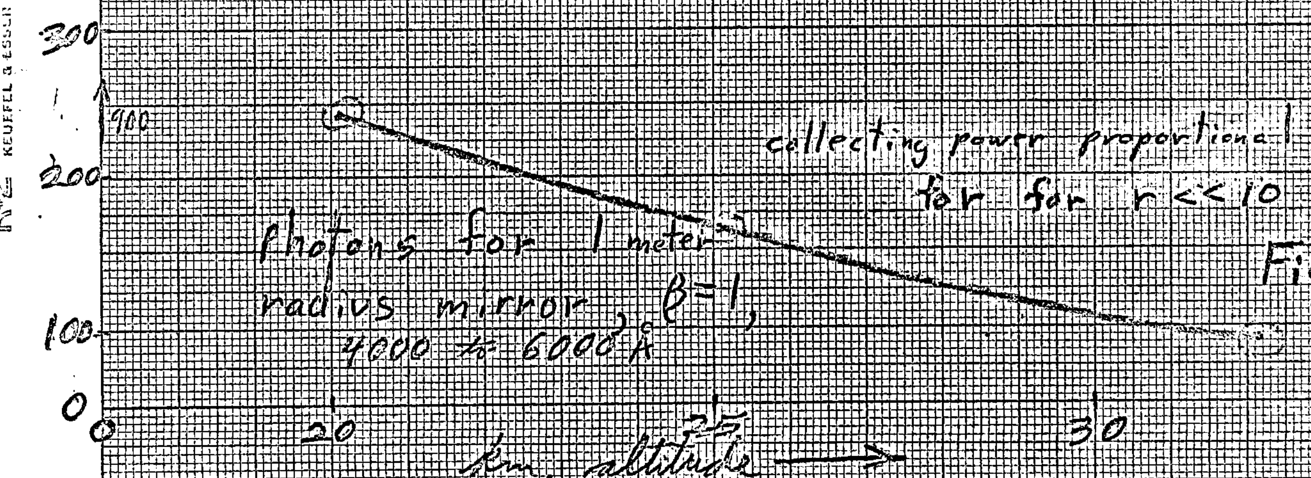

Fig. 3

4-29-64

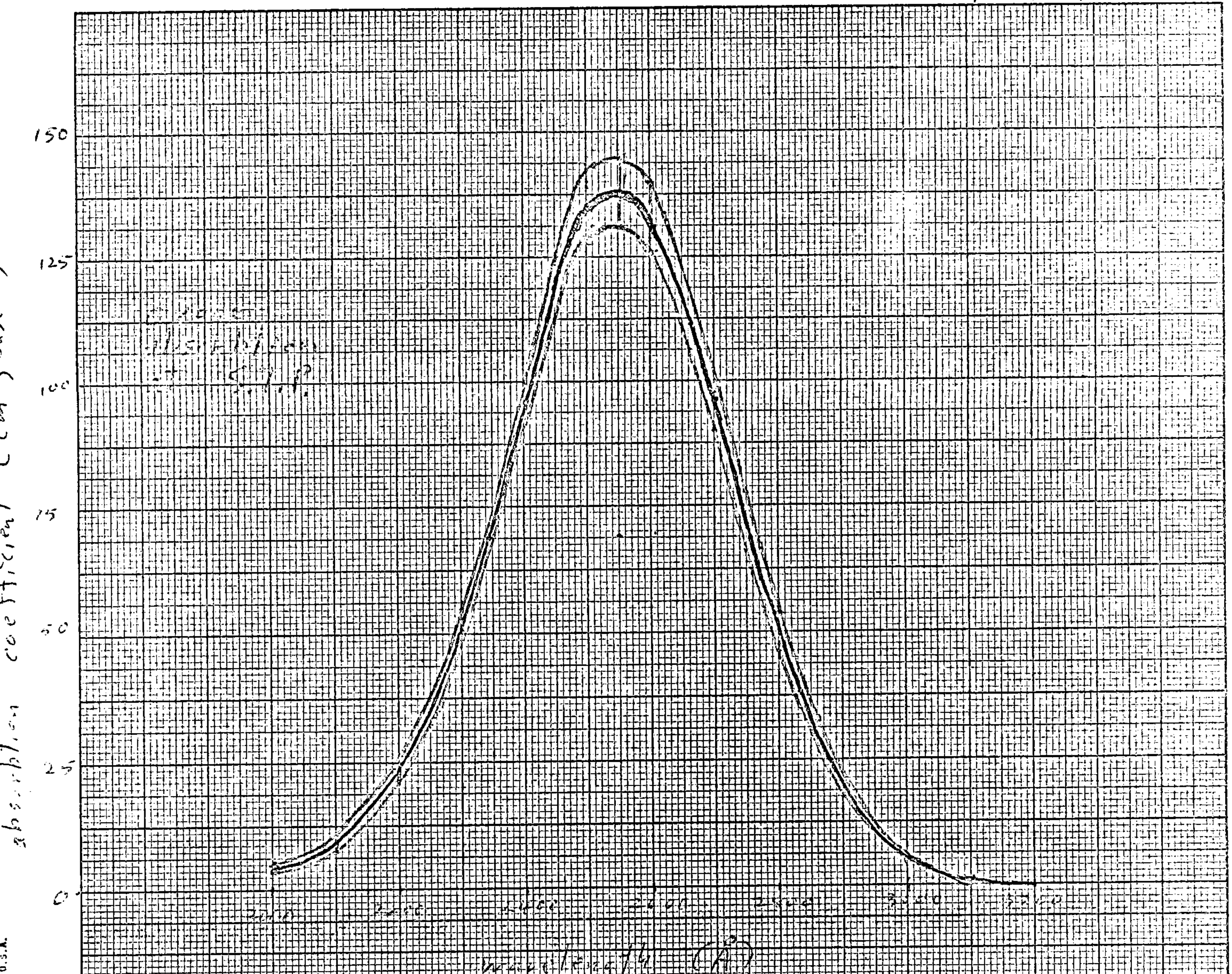

This curve is fairly well represented by

$$A = 138\, e^{-\frac{1}{2}(\lambda - 2550)^2/(170)^2} \quad (\text{cm}^{-1}, \text{base } 10)$$

$$= 318\, e^{-\frac{(\lambda-2550)^2}{2(170)^2}} \quad (\text{cm}^{-1}, \text{base } e)$$

Typical total ozone thickness is about .25 cm

Fig. 4

memo 504 p. 21

April 29, 1964

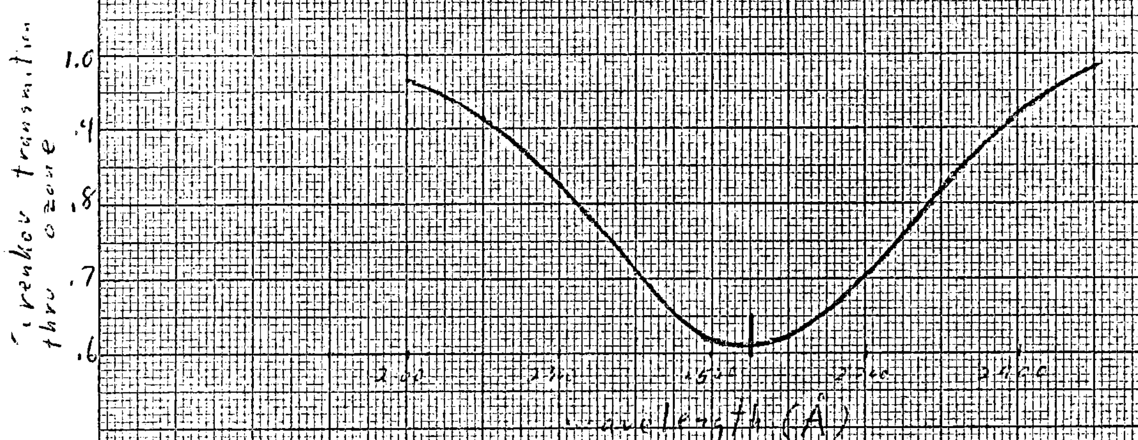

Fig. 5

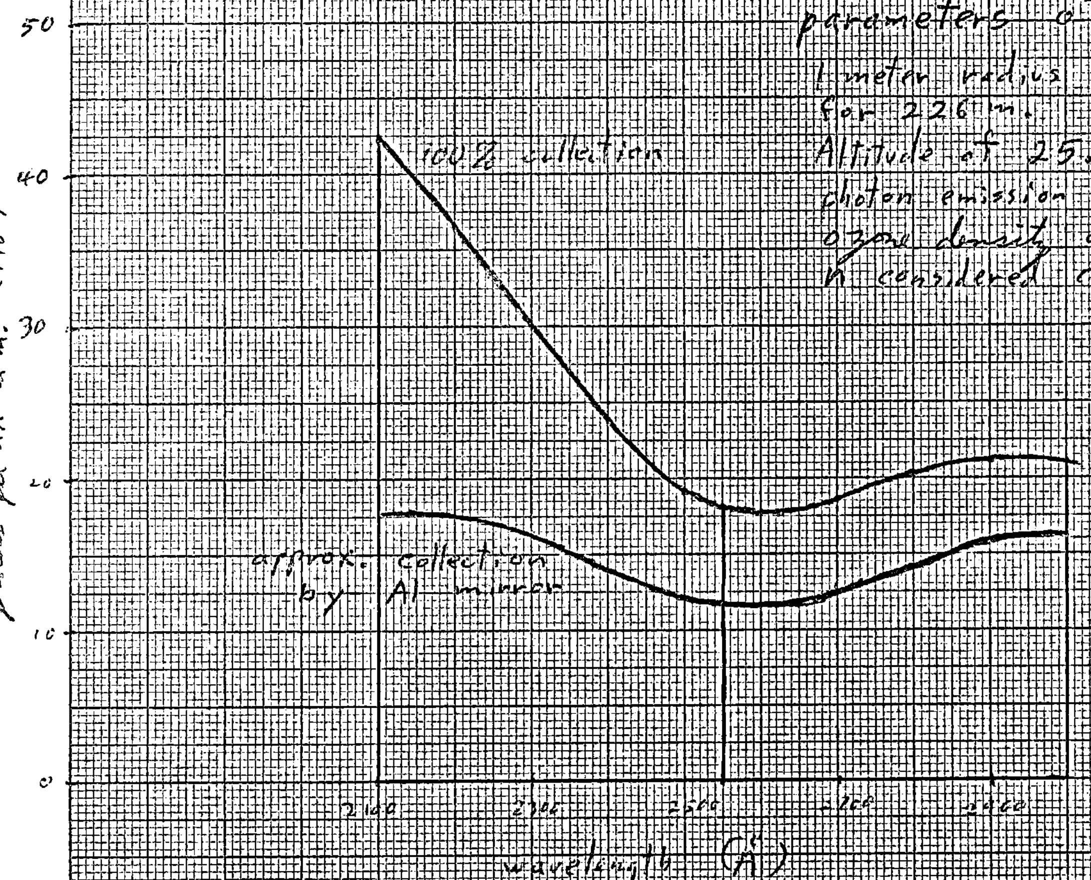

Fig. 6

parameters of calculations:
1 meter radius mirror collecting for 226 m.
Altitude of 25.1 km, $n-1 = 9.8 \times 10^{-6}$
photon emission for 1000 Bev/c p. ($\gamma = 10$
ozone density of 15×10^{-3} cm. per km.
n considered constant (~1% error)

Integrated yield (photons):

	2100 to 2550 Å	2550 to 3000 Å	2100 to 3000 Å
100% collection	131	90	221
Al mirror	69	63	132

Table I

memo 504 p.

May 3 1964

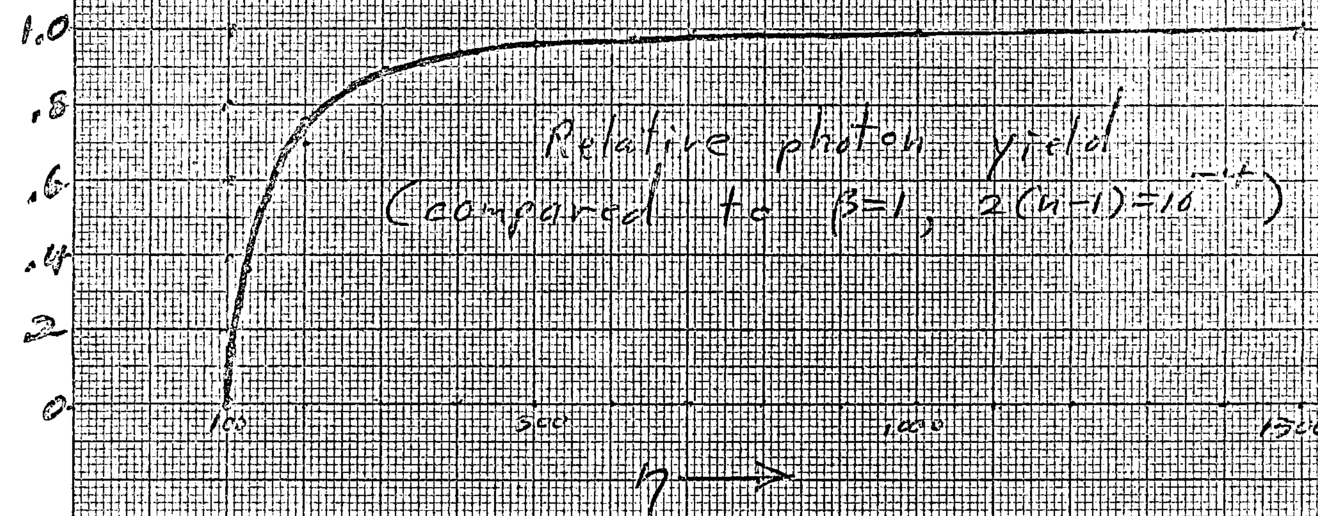

Fig. 7

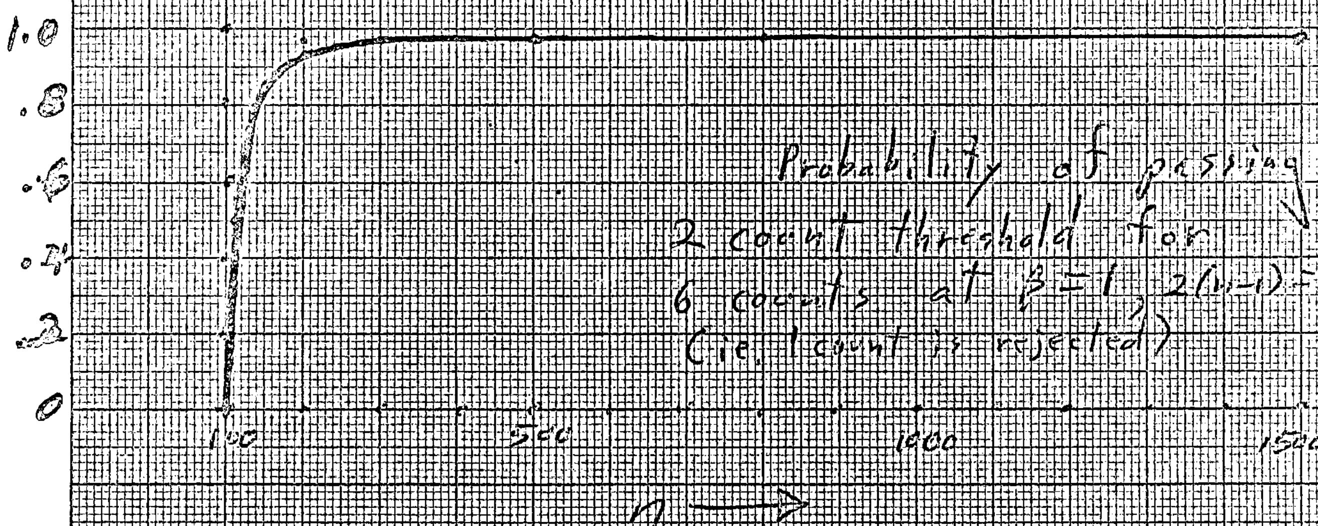

Fig. 8

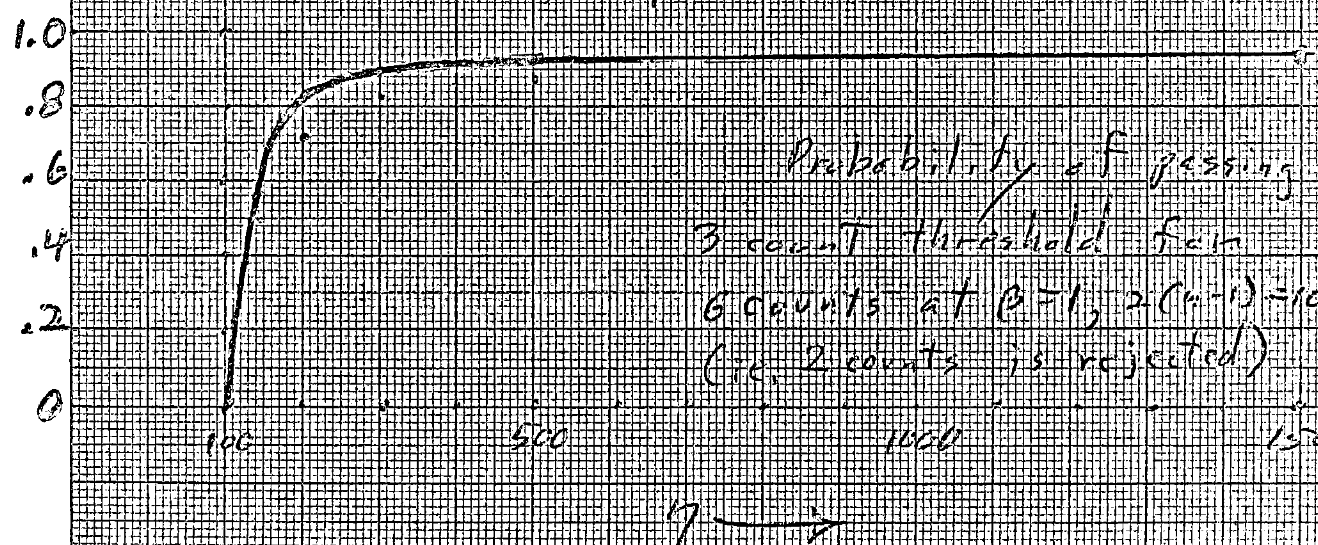

Fig. 9

SUBJECT Is the Parity of the K^o meson imaginary?
A proposed analysis of K_1^o-K_2^o mass difference experiments.

NAME A. Natapoff

DATE May 5, 1964

If all parity conserving reactions conserve strangeness, the title question is meaningless. The parity of the K^o relative to the vacuum is, in that case, unmeasurable in principle. If, on the other hand, as R. Spitzer suggests [1,2], there is a sequence of parity-conserving reactions* (A) $K^o \rightarrow K^o + \gamma \rightarrow K^o + \gamma + \gamma' \rightarrow \bar{K}^o + \gamma' + \gamma'' \rightarrow \bar{K}^o + \gamma' + F \rightarrow \bar{K}^o$ that involves only gamma rays and an external field, F, the question becomes meaningful.

The sequence (A) carries K^o into $\bar{K}^o$, competes with the weak $K^o \rightarrow \bar{K}^o$ transition and contributes, if present, a term depending on the external field to the measured K_1^o-K_2^o mass difference. In particular, if we start with a pure K^o state at time t = 0, at time t the fraction of $\bar{K}^o$ present is $P(\bar{K}_o; t) = 1/4 \times (e^{-\gamma_1 t} + e^{-\gamma_2 t} - 2e^{-\gamma t}\cos\omega t)$. where γ_1, γ_2 are the inverse lifetimes of the K_1, K_2, γ is the average of these, $\gamma = 1/2(\gamma_1 + \gamma_2)$, and ω is the K_1^o - K_2^o mass difference in appropriate units,

Given a Spitzer-type reaction, ω will not be constant but will depend linearly on the external magnetic field as

$$\omega = (\alpha_0 + \alpha_1 \hat{K}\cdot H + \alpha_2 E\cdot H)\gamma_1$$

where $\hat{k}$ is a unit vector in the direction of the original K^o trajectory and E and H are the external electric and magnetic fields.

In bubble chambers, K^o's are commonly produced in secondary reactions and emitted at different angles relative to an external magnetic field. We suggest, therefore, that since $\hat{K}\cdot H$ will be different for each observed event, that the proposed dependence of the K_1^o - K_2^o mass difference, ω, on $\hat{K}\cdot H$ be investigated. In particular, the bubble chamber experiments measuring ω, assuming it to be constant, should be scrutinized for a linear term in $\hat{K}\cdot H$. An appropriate calculation for these purposes is given in the appendix.

The pseudoscalar character of the $\hat{K}\cdot H$ and $E\cdot H$ terms determines (if the reaction occurs) that the relative intrinsic parity of K^0 and $\bar{K}^0$ is negative. If we assume space inversion to be a local transformation, then the product of the intrinsic parity of a spin zero particle and that of its anti-particle is +1.

$$\eta(K^0) \quad \eta(\bar{K}^0) = 1$$

The experimental conclusion that

$$\eta(K^0) = -\eta(K^0)$$

would imply then, that the intrinsic parity of the K^0 is imaginary.

$$\eta(K^0) \quad \eta(\bar{K}^0) = 1 = -\eta(K^0) \quad \eta(K^0)$$

$$\eta^2(K^0) = -1$$

The intrinsic parities of the Λ and Σ must also be imaginary, in this case, relative to that of a nucleon of appropriate charge to achieve consistency with experiment. Starting with imaginary parities for the K, Λ, Σ it follows that parity-conserving reactions of pions and nucleons must produce such particles in pairs. Further, the decay of such a particle into states of pions and nucleons alone, cannot conserve parity.

From this point of view, then

(1) The conservation of strangeness in associated production reactions is explained by parity conservation alone.

(2) Failures of strangeness conservation by odd numbers, in parity conserving reactions, are forbidden by parity conservation alone.

(3) Conversely, failure of parity conservation in the decay for example of a K-meson into pi-mesons is attributed to the imaginary parity of the former and the real parity of the latter and is thus almost a tautology under these assumptions.

(4) The non-occurrence of reactions having even strangeness changes remains unexplained (e.g. $\pi^- + p \rightarrow \Sigma^+ + K^-$).

NAME A. Matapoff

DATE May 5, 1964

Apart from the experimental and statistical difficulties in determining if a significant result, not attributable to fluctuations has been found there are two other complications.

First, there may be a real $\hat{K}\cdot H$ dependence that does not have the implications of the one postulated by Spitzer. The essential feature is the absence of scalar terms like $\hat{K}\cdot E$. Whatever the parity-conserving mechanism, the presence of pseudoscalar and the absence of scalar terms lead to the same conclusion. If a $\hat{K}\cdot H$ dependence is found, the absence of $K\cdot E$ term should be checked separately.

Second, the coefficient α_1 contains a complicated kinematic dependence on p^2, p'^2 and $p\,p'$ whose form has not yet been calculated, where the unprimed variable reters to the K^o and the primed, to the $\bar{K}^o$. Specifically, the matrix element for process (A) is proportional to

$$\beta_2 = \epsilon_{\mu\nu\rho\sigma} f_{\rho\sigma} p'_\mu p_\nu C_2 \approx -2i\, C_2 \left[p_0 H\cdot(\bar{p}-\bar{p}') + (\bar{p}'\times\bar{p})\cdot E \right] .$$

Since we examine only $\bar{K}^o$'s emitted in the forward direction, only the first term on the right survives. The complicated kinematic dependence mentioned above is contained in C_2 and $\hat{K}$ is a unit vector in the direction $\bar{p} - \bar{p}'$. The strength of the coupling associated with reaction (A) might be poorly estimated from α_1 because of this radical averaging over kinematic quantities.

APPENDIX:

Calculation of dependence of $K_1^o - K_2^o$ mass difference on external magnetic field using the maximum likelihood method.

We perform the calculation using the MINFUN computer program [3], as specialized to the particular calculation given below. (The calculations are programmed in Fortran IV language and will be made available on request).

Assume the probability that a $\bar{K}^o$ will undergo a detectable identifying reaction in the proper time interval t, t + dt is $\lambda(t)\,dt$. Then an unbiased likelihood function for a given event is proportional to

$$\mathcal{L}_i' = P(\bar{K}_o; t_i) \Big/ \int_0^{T_i} P(\bar{K}_o; t)\,\lambda(t)\,dt$$

where t_i = proper time at which the $\bar{K}^o$ is detected.

T_i = latest proper time at which the $\bar{K}^o$ could have been detected.

If $\lambda(t)$ is independent of time (assume $\bar{K}^o$ momentum is constant) the likelihood functions $\mathcal{L}_i'$ will achieve maxima for the same values of α_0, α_1 and α_2, independent of λ. Thus we can ignore λ and work with

$$\mathcal{L}_i = P(\bar{K}_o; t_i) \Big/ \int_0^{T_i} P(\bar{K}_o; t)\,dt$$

SUBJECT

NAME A. Natapoff

DATE May 5, 1964

$$\mathcal{L}_i = \frac{e^{-\gamma_1 t_i} + e^{-\gamma_2 t_i} - 2e^{-\gamma t_i}\cos\omega_i t_i}{1/\gamma_1(1-e^{-\gamma_1 T_i}) + 1/\gamma_2(1-e^{-\gamma_2 T_i}) - (2/(\gamma^2+\omega_i^2))(\gamma + e^{-\gamma T_i}[\omega_i \sin\omega_i T_i - \gamma\cos\omega_i T_i])}$$

$$= \frac{N_i}{D_i} \quad \text{where} \quad G_i = \gamma + e^{-\gamma T_i}(\omega_i \sin\omega_i T_i - \gamma\cos\omega_i T_i)$$

$$D_i = 1/\gamma_1\,(1-e^{-\gamma_1 T_i}) + 1/\gamma_2\,(1-e^{-\gamma_2 T_i}) - 2G_i/(\gamma^2+\omega_i^2)$$

The total likelihood function is $\mathcal{L} = \prod_i \mathcal{L}_i$; and the function we treat is f $f = -2\log\mathcal{L}$, which has a minimum where $\mathcal{L}$ has a maximum (enabling us to use MINFUN, a program which seeks function minima) and corresponds to the chi square parameter. For calculating such minima, the derivatives of f are needed.

$$\frac{\partial f}{\partial \alpha_j} = -2\sum_i \frac{\partial \omega_i}{\partial \alpha_j}\left(T_i^{(1)} + T_i^{(2)}\right)$$

$$T_i^{(1)} = (1/N_i)\,(t_i \sin\omega_i t_i\; e^{-\gamma t_i})$$

$$T_i^{(2)} = \left[2/(D_i(\gamma^2+\omega_i^2)^2)\right]\left[(\gamma^2+\omega_i^2)e^{-\gamma T_i}(\sin\omega_i T_i(1+\gamma T_i) + \omega_i T_i\cos\omega_i T_i - 2G_i\omega_i\right]$$

$$\omega_i = \gamma_1\left(\alpha_0 + \alpha_1(\hat{k}\cdot H)_i + \alpha_2(E.H)_i\right)$$

References

1. R. Spitzer, Nuc. Phys. 21, 681 (1961)
2. R. Spitzer, Nuc Phys. 47, 367 (1963)
3. W. E. Humphrey, MINFUN; Alvarez Group Programmer Note P6, Lawrence Radiation laboratory, Berkeley, California (unpublished)

Acknowledgements

The author wishes to thank Dr. Richard Spitzer for useful discussions over a period of several years.

NAME P. Eberhard
DATE May 26, 1964

SUBJECT A HIGH SENSITIVITY MONOPOLE DETECTOR

This note is to propose an apparatus which could detect a monopole of a charge of the order of the charge of the electron. Only classical physics arguments are used. No discussion about quantification of angular momentum for a system of monopole and charge and very little consideration has been made about the quantification of flux through a supra conductor coil.

Furthermore, I do not claim any originality in this proposal because I have not looked up the literature and it may be that someone has already proposed such a device. Anyway, my major source of information is Luis' Note 479 where, among other things, the electromotive force induced by a monopole is exposed.

Principle

Consider the same kind of equipment that Luis has used. A ball is travelling along an orbit inside and outside of a coil. (Fig. 1)

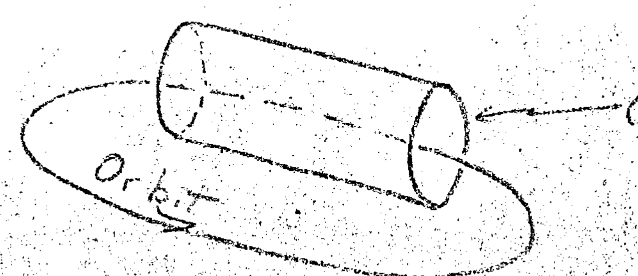

Fig 1

If the ball contains a monopole of charge

$$q = g \times \text{charge of electron} \quad (1)$$

an electronmotive force $\mathcal{E}$ is induced from the variation of the flux as a function of time.

When the monopole has made one turn, if we measure $\mathcal{E}$ in 10^{-8} Volts and the time in seconds,

$$\int \mathcal{E}\, dt = \frac{g}{137} \times 8.3 \times 10^{-7} \text{ gauss cm}^2 \quad (2)$$

If the coil is closed on itself (for instance if the "coil" is just a cylinder), the electromotive force $\mathcal{E}$ is the source of a current i

$$\mathcal{E} = \mathcal{L}\frac{di}{dt} + Ri \qquad (3)$$

where $\mathcal{L}$ is the coefficient of self induction

R is the resistance

If the "coil" is just a cylinder of good conductor, $R \simeq 0$, therefore, from (2) and (3) we get, for one turn of the monopole

$$\mathcal{L}\Delta i = \frac{g}{137} \times 8.3 \times 10^{-7} \text{ gauss cm}^2 \qquad (4)$$

$\mathcal{L}i$ is just equal to the flux of magnetic field produced by the "coil" through the coil itself. So equation (4) shows that a conductor cylinder obliges the field lines to be squeezed in the cylinder after the monopole has passed through it, that property looks pretty obvious if one assumes that a conductor material refuees any electric field in it, therefore no curl $E = -\frac{dB}{dt}$ (Fig. a, b and c)

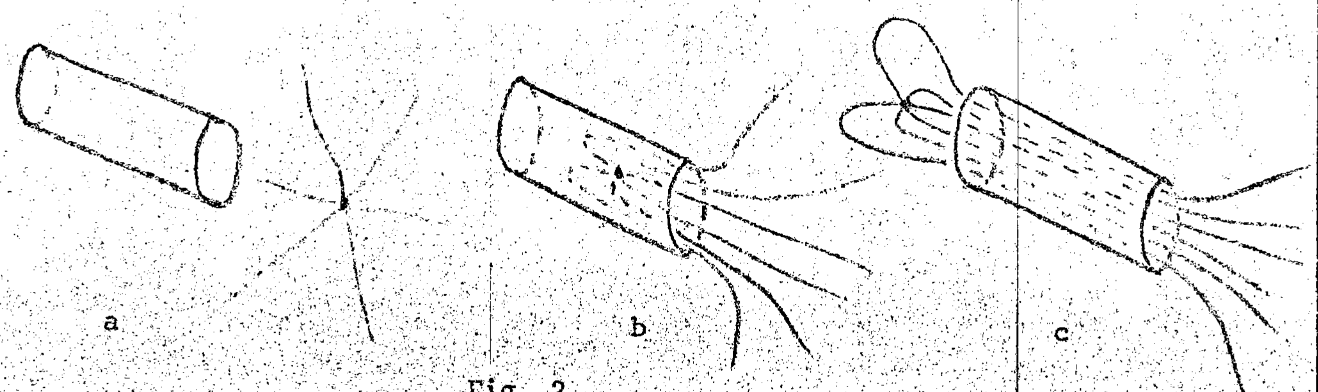

Fig. 2

If we repeat the operation we will each time increase the flux through the cylinder, such as the lines of flux are sowed into the cylinder.

If n is the number of turns made by the monopole per second there will be a flux ϕ circulating in and out of the cylinder (after Δt second)

$$\phi = n\Delta t \frac{g}{137} \times 8.3 \times 10^{-7} \text{ gauss cm}^2 \qquad (5)$$

Let's consider the ball circulating on its orbit with a frequency of 10^2

turns/sec. After 1000 seconds (15 to 20 min), the circulating flux will be $\Phi = 0.083 \frac{g}{137}$ Gauss cm^2 which should be not too difficult to be detected. Moreover, because we just use 10^5 times the property that only a monopole has, we must expect the noise to be small.

Practical Design

The flux given by equation (5), circulating inside and outside the cylinder, is much easier detectable if it is located. Therefore, we wish to place a metal bar to locate it and direct it on a flux meter. Fig. 3 represents the cut of the equipment

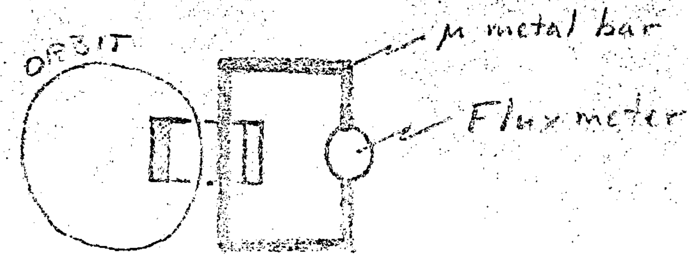

Fig. 3

It is clear that all those sowed flux forces will end up in the μ metal bar if its magnetic reluctance is low. Typical dimensions could be, for the coil, diameter 10cm and length 10cm. The μ metal bar can have about 3cm x 3cm $\cong$ 10 cm^2, therefore, even with a length of 1m, the ratio of the reluctances $\frac{r_{\mu\ metal}}{r_{air}}$ would be

$$\frac{10^{-5} \times \frac{100\,cm}{10\,cm^2}}{1 \times \frac{10\,cm}{100\,cm}} \cong 10^{-3}$$

We have used 10^5 for the value of permeability of μ metal. As long as no part of the fluxmeter presents a reluctance comparable to 0.1 cm^{-1}, the whole flux can be considered travelling through the metal circuit.

Several kinds of fluxmeter could be designed. Let us just describe one (Fig. 4)

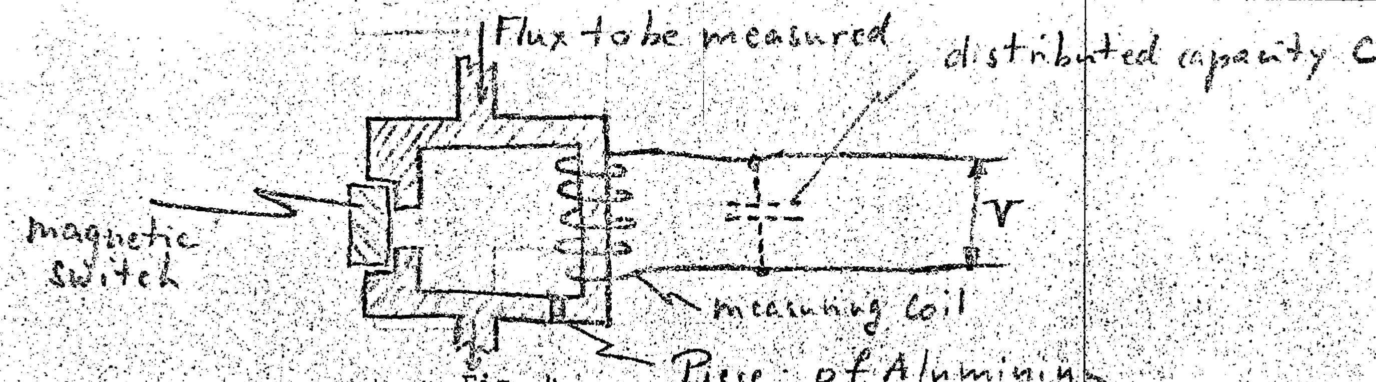

Fig. 4

Two magnetic circuits are interposed in parallel on the path of the magnetic flux. The flux Φ to be measured either traverses the coil when the magnetic switch is off and takes the other path when the switch is on because the piece of Al presents a reluctance much bigger than the other path. Therefore, each time one turns the switch off, a pulse V is produced across the coil and has to be measured.

The magnetic switch is on almost all the time. I believe that one can make contacts for that switch better than 1/10mm on surfaces of the order of $10cm^2$. Therefore, the reluctance $\mathcal{R}_{on}$ is inferior to 10^{-3} cm^{-1} when switch is on. We will use that figure which must however be pessimistic.

If the piece of Aluminium is $10cm^2 \times 1mm$, it has a reluctance $\mathcal{R}_{Al}$ $= 10^{-2}$ cm^{-1}, 10 times superior to $\mathcal{R}_{on}$. Therefore, 90% of the flux does not traverse the coil.

When the switch is open, the reluctance of the circuit through the coil is $\mathcal{R}_{Al}$ while the reluctance everywhere else is $\mathcal{R}_{off}$ of the order of 10^{-1} cm^{-1}. Therefore, most of the flux wants to go through the coil.

Equations of the Apparatus

a) Switch on

i = current in the cylinder

R = resistance of the cylinder

Φ = Flux through the cylinder

$\mathcal{E}$ = electromotrix force due to monopole

$$\Phi = 4\pi\mu_0\, i / \mathcal{R}_{on}$$

$$\varepsilon - \frac{d\phi}{dt} = Ri = \frac{R\,\mathcal{R}_{on}}{4\pi\mu_0}\,\Phi = \frac{1}{\tau}\,\Phi \qquad (6)$$

$$\phi = \varepsilon\tau\left(1 - e^{-\frac{t}{\tau}}\right) \qquad (7)$$

For a copper cylinder 10cm long, 10cm diameter 3cm thick, at temperature -259°, R is

$$R = 0.014 \times 10^{-6} \times \frac{\pi \times 10}{3 \times 10} = 1.4 \times 10^{-8}\ \text{ohms}$$

$$\tau = \frac{4\pi\mu_0}{R\,\mathcal{R}_{on}} = \frac{4\pi \times 10^{-7}}{1.4 \times 10^{-8}\ \text{ohm} \times 10\, m^{-1}\ (= 10^{-3} cm^{-1})} = 8 \cdot 10^{3}\ \text{sec}$$

Of course, a supra conductor looks a priori even better, but one must think more about flux quantization in a supraoonductor loop in presence of a monopole before proposing such a device to detect monopoles of charge inferior to $\frac{137}{4}$ charge of the electron.

Furthermore, even with ordinary conductors at low temperature, one can certainly do better than what I compute here (which has to be considered as a pessimistic estimation).

In (7), we get an asymptotic value for Φ, using as an average for the value given by (2) divided by a period of 10^{-2} sec for the revolution of the monopole $\Phi = 0.07\,\frac{g}{137}$ gauss cm^2 (8).

b) Switch off

i_{coil} is the current in the coil

R_{coil} is the resistance of the coil

N is the number of turns of the coil

Φ coil is the flux through the coil

We have the following equations:

V is the potential across the coil

C the distributed capacity

$$\Phi - \Phi_{coil} = 4\pi\mu_0 i / \mathcal{R}_{off}$$

$$\Phi_{coil} = \frac{4\pi\mu_0}{\mathcal{R}_{Al}} (i + N i_{coil})$$

$$R i = - \frac{d\Phi}{dt}$$

because we can neglect the monopole action when we turn the switch off.

$$R_{coil}\, i_{coil} = -N \frac{d\Phi_{coil}}{dt} - V$$

$$i_{coil} = C \frac{dV}{dt}$$

Eliminating i and i_{coil} in the above equations

$$\frac{d}{dt} \begin{vmatrix} \Phi \\ \Phi_{coil} \\ V \end{vmatrix} = \begin{vmatrix} -\frac{\mathcal{R}_{off} R}{4\pi\mu_0} & \frac{\mathcal{R}_{off} R}{4\pi\mu_0} & 0 \\ +\frac{\mathcal{R}_{off} R_{coil}}{4\pi\mu_0 N^{-2}} & -\frac{(\mathcal{R}_{off} + \mathcal{R}_{Al}) R_{coil}}{4\pi\mu_0 N^2} & -\frac{1}{N} \\ -\frac{\mathcal{R}_{off}}{4\pi\mu_0 C N} & \frac{\mathcal{R}_{off} + \mathcal{R}_{Al}}{4\pi\mu_0 C N} & 0 \end{vmatrix} \begin{vmatrix} \Phi \\ \Phi_{coil} \\ V \end{vmatrix} \qquad (9)$$

Neglecting $\mathcal{R}_{Al}$ versus $\mathcal{R}_{off}$, and calling

$$\lambda = \sqrt{\frac{\mathcal{R}_{off}}{4\pi\mu_0 C}}$$

$$\frac{d}{dt}\begin{vmatrix}\Phi\\ \Phi_{coil}\\ V/\lambda\end{vmatrix} = \lambda\begin{vmatrix}-RC\lambda & RC\lambda & 0\\ \frac{R_{coil}C\lambda}{N^2} & -\frac{R_{coil}C\lambda}{N^2} & -\frac{1}{N}\\ -\frac{1}{N} & \frac{1}{N} & 0\end{vmatrix}\begin{vmatrix}\Phi\\ \Phi_{coil}\\ V/\lambda\end{vmatrix} \qquad (10)$$

$\mathcal{R}_{off}$ being of the order of 10^{-1} cm^{-1} = $10m^{-1}$, we will probably not obtain C bigger than 0.01 μF (=10^{-8} Farad) therefore

$$\lambda \geq 3 \cdot 10^{7}\ sec^{-1}$$

$$RC\lambda \leq 0.5 \quad 10^{-8}$$

Therefore $(RC\lambda)$ can be neglected in (10) for time much shorter than $\lambda^2 RC =$ = 10 sec.

Furthermore $\frac{R_{coil}}{N^2}$ depends on the size of the coil, if it has the same dimensions as the cylinder, but is kept at room temperature

$$\frac{R_{coil}\lambda^2 C}{N^2} = \frac{1}{T} \simeq 17 \text{ second}^{-1}$$

Equations (10) become therefore,

$$\Phi = \text{constant in time (given by (8))}$$

$$\frac{d(\varphi_{coil}-\phi)}{dt} = -\frac{(\varphi_{coil}-\phi)}{T} - \frac{V}{N} \qquad (11)$$

$$\frac{dV}{dt} = \frac{\lambda^2}{N}\left(\Phi_{coil} - \Phi\right)$$

For V, equations (11) is an oscillation circuit equations and we know that, when the switch is just turned off, V = 0 and $\Phi_{coil} = 0$

$$V = \frac{\lambda^2}{N\omega} \Phi e^{-\frac{t}{3T}} \sin\omega t$$

$$\omega^2 = \frac{\lambda^2}{N^2} - \frac{1}{4T^2} \quad (12)$$

We want $2\pi/\omega$ big with respect to the time of rupture of the switch. Therefore, N should be big, let's set it at 2×10^5 turns

$$\omega = 50 \sec^{-1}$$

The switch should then operate in $\sim 10^{-2}$ sec, requiring forces of the order of one pound on a 10 gram switch.

Then (12) gives

$$V_{max} \cong \lambda \Phi = 3 \times 10^7 \times \Phi \text{ (Weber)} \quad (13)$$

Plugging (8) into (13)

$$V_{max} \cong g \times 0.2 \text{ millivolt} \quad (14)$$

Conclusion

Using all those numbers that I believe pessimistic, we get as an output of the equipment, a pulse 1/15 sec long and as big as 0.2 mV/unit charge of electron as soon as one turns off the switch.

With that, we should be able to measure monopoles of the order of the charge of an electron.

Important questions not discussed here

1) The μ metal bar has some conductivity, it may be necessary to make it out of sheets so that loop currents be small compared to the cylinder current.

2) A zeroing system is needed for the measuring coil, and this system can be used also to calibrate the apparatus.

3) The whole apparatus must be shielded so that leakage flux through the switch does not change within 1/4 hour more than 0.005 gauss cm^2.

4) To avoid background, we may have to stop the ball always at the same place before opening the switch.

SUBJECT

PI-63 SCANNING INSTRUCTIONS

0 D

NAME Uhl, Koellner, Miller ~~Starr, Strong~~

DATE 5/14/64

TABLE OF CONTENTS

SUBJECT: PI-63 SCANNING INSTRUCTIONS
NAME: Dahl, Koellner, Miller, Starr, Strong
DATE: 5/14/64

PROCEDURE

A list of rolls to be scanned is in Room 305. Put your initials by the roll number when you begin, and the date finished when you are done.

Make sure that your scanning table is working properly. Call a maintenance man if it is not.

Sign the log in Room 305 each day when you have finished scanning.

If you have any questions about these instructions or the experiment, please see one of the authors or Cathy Bowers. See your shift supervisor if you have a question about a particular event.

THE SCAN SHEET

Record events on scan sheets as you come across them. Beam track assignment begins with the beam track to the left at the window in view 2. Use black lead pencil only, since other colors are used by the library. Please be careful since these sheets are punched by people who know little or nothing about the experiment. Put completed scan sheets in the binder in Room 305. Scan sheets are kept in Room 336 after they are key punched.

An example of the correct scan sheet format follows. Most columns are self-explanatory.

LAWRENCE RADIATION LABORATORY • UNIVERSITY OF CALIFORNIA PHYSICS NOTES	NFD	MEMO NO. 507	PAGE 2

SUBJECT: FI-63 SCANNING INSTRUCTIONS

NAME: Dahl, Koellner, Miller, Starr, Strong

DATE: 5/14/64

K72 S

Roll # (1–4)	Frame # (5–7)	Scan # (8)	Beam Track (9–10)	Exp. # (11–12)	Interpretation (13)	Year (14–15)	Vertices (16)	Month (17–18)	Primary Event Type (19–21)	X (22)	Y (23–24)	F_1 (25)	F_2 (26)	Day / Unmeasurable (27–28)	Secondary Event Type (29–31)	X (32)	Y (33–34)	F_1 (35)	F_2 (36)	Scanner (37–39)
6471	001		01						32	E	21									
	3								32	C	22				$e^{\pm}$ associated					
	26								92	D	12									
	31								32	D	23									
	48								30	D	32			1						
	65		1						32	D	25									
			2						34	E	07									
	102		1						34	D	22									
	107								30	E	27									
	120								30	D	19									

Comments →

INIT. - NO.
DATE
ROLL

SCAN SHEET

Not Scanned: frame (40–42)	reason (43–47)	Junk: frame (48–50)	loc. (51–55)	Binary Switches 1–10 (56–60)	11–20 (61–65)	21–30 (66–70)	Decimal Switches (71–80)
22	BAD	40	F09	Zoom	$K^0 p$ →	$\Sigma^+ \pi^0$	start 001
827 }	BAD						end 588
86 }							skipped -15
101	TTD						total 573
115	NT						

NAME Dahl, Koellner, Miller
Starr, Strong
SUBJECT

PI-63 SCANNING INSTRUCTIONS

DATE 5/14/64

Columns 5-10 Use leading zeros in the first row on each sheet only. (Keypunch has requested this.)

Column 28 Whenever an event is unmeasurable, place a one (1) in this column.

Columns 44-47 List here the reason a frame was not scanned.

These reasons are:

NT	No valid tracks
TTD	Tracks too dense
BAD	Film quality poor, view missing or bad, etc.

On the first page record the first and last frames scanned, the number of frames not scanned, and the total number of frames scanned.

GENERAL INSTRUCTIONS

Do not scan frames where:

1. The tracks are so dense the frame cannot be scanned accurately (TTD).
2. There are no valid beam tracks (NT).
3. The film quality is poor (BAD).
4. One or more views are missing or bad (BAD).

List all unscanned frames and note the reason.

Scan all events in three views in order to find small angle kinks and difficult events.

Do not scan events where the production vertex is:

1. less than one centimeter from the window in view 2.
2. above rake 15 in view 2.
3. within two centimeters of the sides (the sides are not at the rake) in all three views. (One view is not sufficient.)
4. not the primary event. The primary event is the first interaction of the beam track, even if this is a small angle scatter.
5. from a non-beam track. A non-beam track makes an angle greater than 5^{o} or has a momentum more than 15% different from the majority of the incoming tracks.

An event is unmeasurable if:

1. it is obscured by the rakes or the flare.
2. any vertex is obscured or unclear to the degree that superimposing would not help the measurer and guessing would be quite inaccurate in measuring.
3. there are so many beam tracks in the vicinity that the direction of the beam track is impossible to tell.

4. one of the tracks is unmeasurable (stereo is bad or can't be seen).

5. both tracks of vee are less than 2 centimeters in all three views.

The following should be recorded under comments when they are associated with a valid event:

1. stopping protons

2. gamma conversion pairs

3. Dalitz pairs, including mid-air Dalitz pairs. All electron pairs at the vertex are Dalitz pairs. All mid-air electron pairs with a non-zero opening angle are mid-air Dalitz pairs. (Both prongs should be identified as electrons; if only one is an electron, it could be a leptonic decay.)

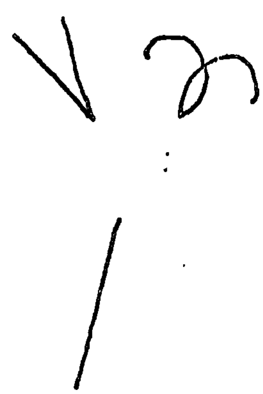

E.T. 30 with mid-air Dalitz pair associated

E.T. 30 with gamma conversion pair associated

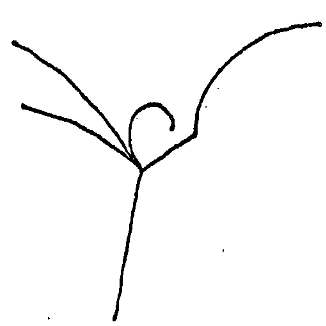

E.T. 92 with Dalitz pair at the vertex

E.T. 30 with Dalitz pair at the vertex

4. positive decays with valid negative decays (i.e., Σ^- K^+ is ET 92.)

5. neutron stars

6. possible Ξ event. Ξ's may be identified by:

a. Ξ^-

(1) A valid negative decay and a Λ^o decay (E.T. 72, 74).

(2) A valid negative decay, a K^o decay, and a K^+ at the vertex (by ionization and/or decay).

(3) A valid negative decay with a vee where the vee points to the decay point.

(4) E.T. 02, 12.

b. Ξ^o

(1) An E.T. 40 where the Λ^o doesn't point directly back to the vertex.

(2) E.T. 50.

(3) An E.T. 42 with a K^+ at the production vertex (by ionization and/or decay.

7. Zoon associated.

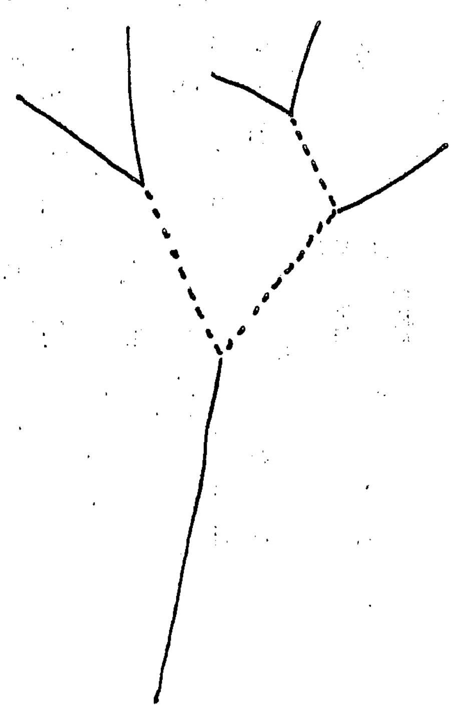

E.T. 30 with Zoon assoc.

(List in "junk" as Zoon E.T. 30 with a neutral recoil and decay.)

8. unmeasurable decay associated. If one decay vertex of a multiple decay vertex (either neutral or charge) event is partially unmeasurable, assign the event type by the measurable part, and note the other decay associated.

The following should be recorded in the "junk" column with the proper frame and location:

1. Zoons
2. Unassociated vees. These are vees with no associated production vertex. There are two types:
   a. Window vees are vees below rake 0 which cannot possibly be associated with any interaction.
   b. All other unassociated vees are wall vees.

EVENT TYPES

Event types are assigned by topological characteristics. Generally, these are:

00's	three vees and a negative decay
10's	two vees and a negative decay
20's	no charged decays or vees
30's	one vee
40's	two vees
50's	three vees
60's	one vee and a positive decay
70's	one vee and a negative decay
80's	a positive decay
90's	a negative decay

SUBJECT
NAME Dahl, Koellner, Miller Starr, Strong
DATE 5/14/64

The units digit tells the number of charged prongs at the primary vertex. Regular events on this experiment are 02, 12, 30, 32, 34, 40, 42, 50, 62, 64, 72, 74, 82, 84, 92, and 94. Events in the 20's are not of interest except for special scans. Regular events with additional prongs (e.g., 44, 76, 96) are zoons as regular programs will not handle them.

VEES

A vee is the decay of a neutral particle in the chamber into a positive and negative track. Any vee should be put on the scan sheet unless it can be eliminated by one of the following:

1. The vertex is within one centimeter of the window.
2. It is definitely not a neutral decay. This can be shown if one of the prongs is actually coming into the vertex instead of leaving it. Two common examples of this are:
   a. The "vee" is an obvious $\pi\mu e$ with the π loosing momentum as it comes into the vertex.
   b. The track is incoming since there is at least one obvious delta ray on the track which shows the direction.

SUBJECT

NAME Dahl, Koellner, Miller Starr, Strong
DATE 5/14/64

3. A two prong with a gap on the beam track at the vertex can look like a zero prong and a vee. Call it a vee if the vertex lies outside the 1 x 3 mm box shown below. Call it a two prong if the vertex lies inside. (This applies only to E.T. 30 and 40.)

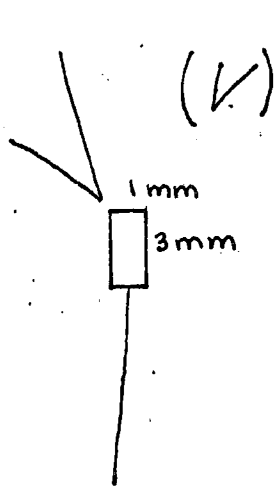

E.T. 30 (or 40)

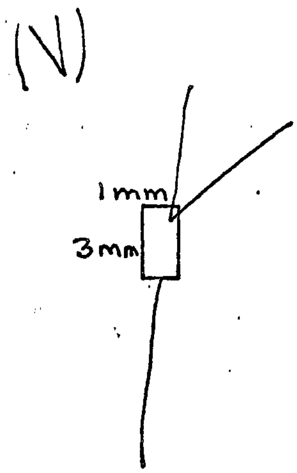

E.T. 22 (or 32)

4. It is definitely a gamma ray pair. This may be established if it meets all of the following criteria.

   a. The angle between the two tracks is 0° in all three views.

   b. Both tracks are minimum ionizing.

   c. Both tracks are less than 800 Mev/c (36" at 17.95 kgauss) or one track is less than 110 Mev/c (5" at 17.95), or is an obvious electron.

Use curvature templates when there is any doubt, and remember that dipping tracks are more strongly curved than flat ones.

SUBJECT
NAME Dahl, Koellner, Miller Starr, Strong
DATE 5/14/64

DECAYS

A charged decay is characterized by either one or both of the following at one specific point.

1. Change in ionization.
2. Change in momentum. Since momentum is a vector, this can be either the direction or the absolute value (as determined by the radius of curvature) or both.

Any event which meets these qualifications should be recorded unless it can be eliminated as one of the following:

1. The decaying particle is definitely a π meson. This may be established:
   a. It goes to an obvious μe and the momentum is clearly less than that of a stopping K.
   b. It's momentum is less than 300 Mev/c (13" at 17.95 kgauss) and it is still minimum ionizing.
   c. It is not dipping much, but it's momentum is obviously less than that of a stopping K.
2. It is a scatter.
   a. There is a proton at the decay point. (Make sure it is not a small delta ray.) In addition, neither the change in momentum nor ionization should be larger than the size of the proton produced warrants.
   b. If the particle "decays" to an obvious proton, call it a scatter if:
      (1) The production angle of the decaying particle is greater than 60°.
      (2) The decay angle is less than 2°. (The decay angle of $\Sigma^+ \rightarrow p + \pi^0$ can be less than 2°, but there is too much

SUBJECT
NAME Dahl, Koellner, Miller
Starr, Strong
DATE 5/14/64

ambiguity with p-p scatters. For this reason, make sure that there is no discernable change in ionization.)

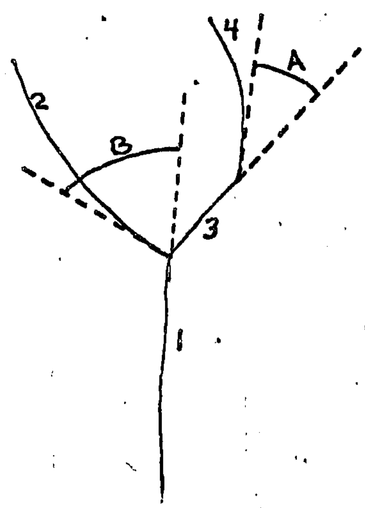

"A" is the decay angle between tracks 3 and 4.

"B" is the production angle of track 2.

SUBJECT

NAME Kuhl, Koellner, Miller ~~Starr, Strong~~
DATE 5/14/64

SCANNING INSTRUCTIONS

VEE ORIGINS

Draw tangents to each track at the vertex as shown below. The origin of the vee will lie within an extension of these tangents.

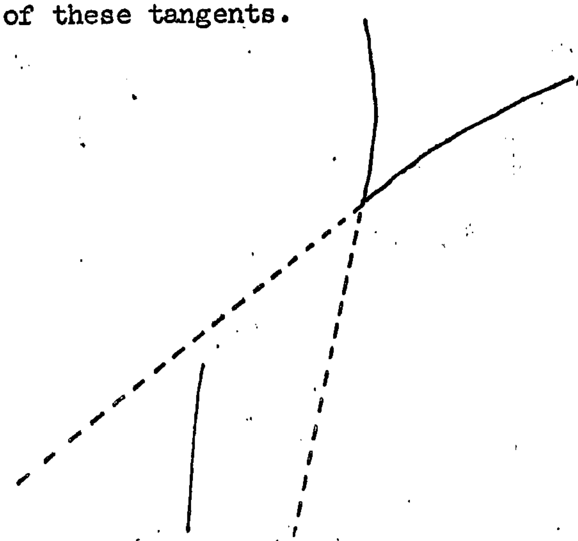

If the two prongs of the vee intersect (or can be made to intersect by extension with a template), the origin of the vee will lie along an extension of the line which joins the vertex and the intersection. (This method is not too accurate where one prong is losing momentum rapidly or is steeply dipping.)

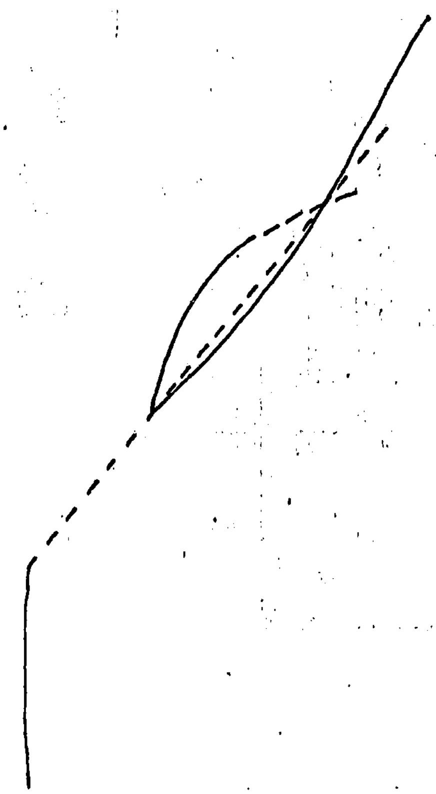

In cases where there are several possible origins, the line of flight lies closer to the track with the larger momentum. More accurately

$$\rho_1/\rho_2 = \theta_2/\theta_1$$

where ρ is the radius of curvature and θ_1 and θ_2 are shown below. (This is not exact for large angles; it is $\rho_1/\rho_2 = \sin\theta_2/\sin\theta_1$.)

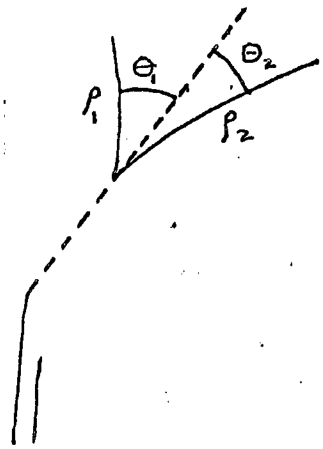

In cases where the origin is still ambiguous, use conservation of momentum and baryons where possible. Where this does not help, choose the closest vertex.

SIGMAS

Charged Σ's, being short lived, often decay close to the vertex (< 1 cm). For this reason our scanning efficiency is low, particularly for Σ^+ decays into $p\pi^0$ where the darkly ionizing proton makes it difficult to distinguish a kink. Carefully check for charged Σ decays.

MISCELLANEOUS

Be sure to check the full length of all prongs for long decays (especially K^+ or K^-), particularly where there is a vee associated.

SUBJECT
NAME Dahl, Koellner, Miller Starr, Strong
DATE 5/14/64

Be sure to check the length of the chamber for long neutral decays (especially K_2^o), particularly when there is an event with a charged decay on the frame.

If there are both a negative and a positive decay, assign the event type using the negative decay and note the positive decay under comments.

IONIZATION

Normally, a track will begin to ionize more than minimum when the momentum of the particle is about equal to its rest mass. This is particularly useful when trying to tell a K from a π. Things to watch out for:

1. Gaps are a more valid criteria than darkness for judging ionization, particularly when a track is dipping.
2. Ionization above rake 12 and near the sides is not too reliable.
3. Whenever possible, compare the ionization of the track in question with that of other tracks in the vicinity.

ZOONS

Record zoons under "junk" and in the correct section in the zoon book.
Zoons in π63 fit into one of five categories:

1. Events where charge is not conserved which do not have a strange particle decay (i.e., E.T. 23).
2. Events where charge is not conserved which have a strange particle decay associated (E.T. 31, 91, 83).
3. Events where:
   a. a K^o, Λ^o, or Σ interacts with a proton to give a visible strange particle decay.

SUBJECT
NAME Dahl, Koellner, Miller Starr, Strong
DATE 5/14/64

b. a K^{o} or Λ^{o} decays via a leptonic or three body mode.

4. Recognizable event types not defined by the scanning instructions (E.T. 44, 96, 36, etc.).

5. Others.

Under 3. would be such things as:

a.

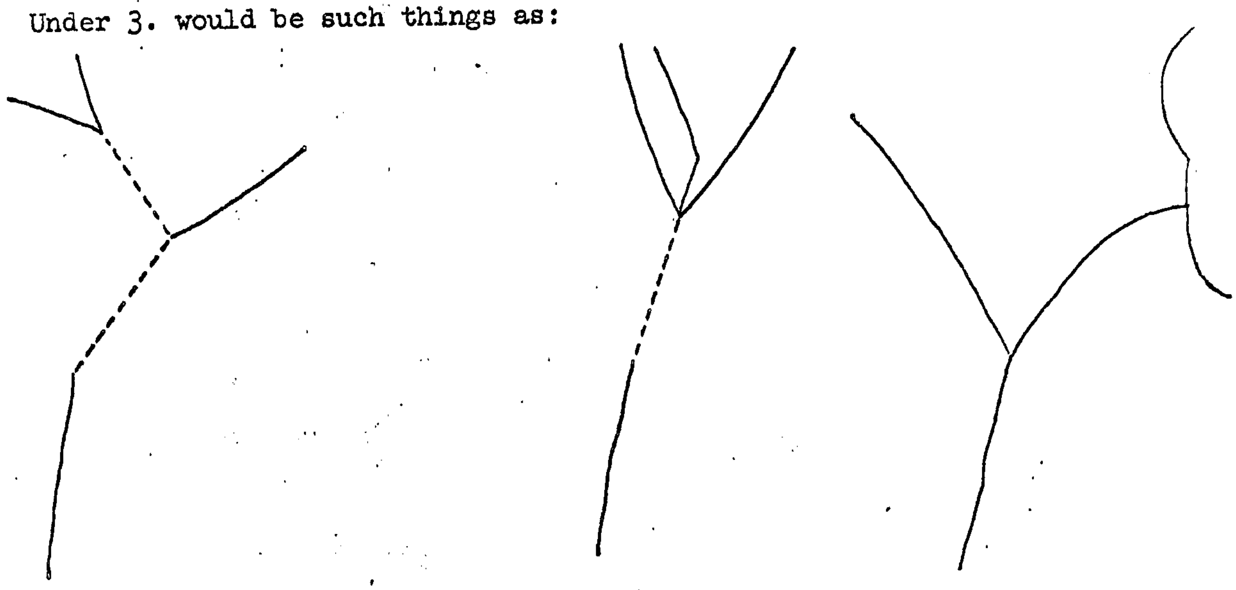

$\Lambda^{o} + p \rightarrow \Lambda^{o} + \pi^{+} + n$

$\Lambda^{o} + p \rightarrow \Lambda^{o} + p$

$\overline{K}^{o} + p \rightarrow \Lambda^{o} + \pi^{+}$

$K^{o} + p \rightarrow K^{o} + p$

$\overline{K}^{o} + p \rightarrow \Sigma^{+} + \pi^{+} + \pi^{-}$

$\Lambda^{o} + p \rightarrow \Sigma^{+} + p + \pi^{-}$

obvious $K^{-} + p$ $\rightarrow \Sigma^{-} + \pi^{+}$

b.

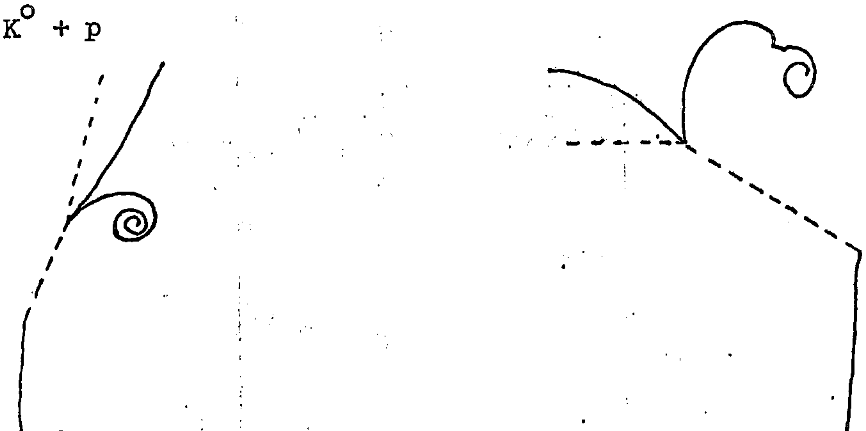

$\Lambda^{o} \rightarrow p + \left\{ \begin{matrix} \mu^{-} \\ e^{-} \end{matrix} \right\} + \overline{\nu}$

$K^{o} \rightarrow \pi + \left\{ \begin{matrix} \mu \\ e \end{matrix} \right\} + \nu$

$K^{o} \rightarrow \pi^{+} + \pi^{-} + \pi^{o}$

(Note that these may not point back to the production vertex.)

SUBJECT
NAME Dahl, Koellner, Miller
Starr, Strong
DATE 5/14/64

EVENT TYPE PAGES

The following 16 event type pages can be summarized as follows:

1. A sketch of the event is given with track numbering for measuring purposes.
2. CPM stands for "check point mark", which represents a specific fit done in the computer program for the stated production or decay hypothesis.
3. "mm" stands for missing mass and represents the energy-momentum unbalance in the overall reaction.
4. Pang is a program which does the geometric reconstruction of the event in three dimensions from the measured points. This program requires that each track be given a "track" number and that each mass assignment for a given track have a different "track bank" number.

The track numbering scheme also follows a simple convention. The incident track is track 1. Next come the charged tracks in the final state of the primary vertex; if there is a charged decay, first the tracks with charge opposite to that of the decay, then non-decaying tracks of the same charge, then the track that decays, and finally its decay; if there is no charged decay, first negative and then positive tracks. Finally each V is numbered in the order neutral, negative, positive. Missing neutrals are called track 31 if they are a part of the primary interaction and track 30 if they are not a part of the primary interaction.

All CPM's are written with the tracks in a standard order.

1. Incident track at vertex I.
2. Missing particle in final state at vertex II (in 2V fits only)

SUBJECT

NAME Dahl, Koellner, Miller Starr, Strong
DATE 5/14/64

3. Particles in final state at vertex I

4. Measured particles in final state at vertex II (in 2V fits only)

Within each group all particles are ordered by the mass of their multiplet (heaviest first). Within a multiplet the order is positive, neutral, negative.

For each event type involving strange particles we have written CPM's for final states up to and including $YK3\pi$ and $NK\bar{K}2\pi$. In the type 20's, where final states not involving strange particles are possible, we have ignored strange particle final states.

NAME Dahl, Koellner, Miller
Starr, Strong
DATE 5/14/64

SUBJECT

EVENT TYPE 02

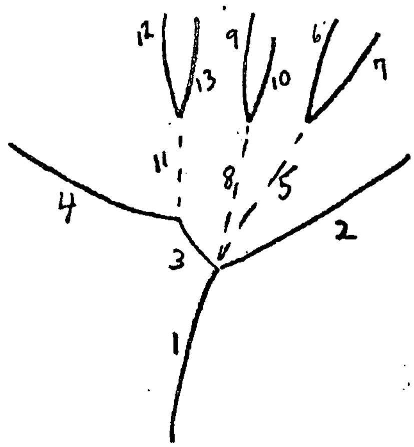

SUBJECT

NAME Dahl, Koellner, Miller
Starr, Strong

DATE 5/14/64

EVENT TYPE 12

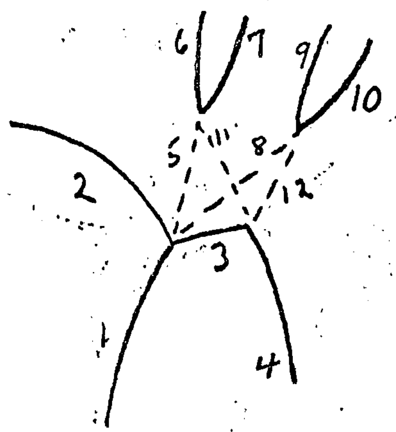

EVENT TYPE 22

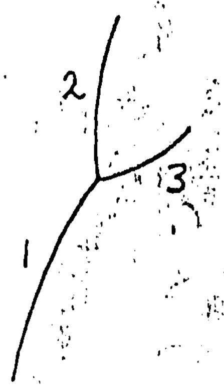

PANG DATA

TRACK BANK	TRACK NUMBER	MASS
1	1	π^-
2	2	π^-
3	3	π^+
4		p

CPM

1 $\pi^-(1) + p \longrightarrow p(3) + \pi^-(2) + mm$

2 $\pi^- + p \longrightarrow \pi^+(3) + \pi^-(2) + mm$

3 $\pi^- + p \longrightarrow p(3) + \pi^-(2)$

4 $\pi^- + p \longrightarrow p(3) + \pi^0(31) + \pi^-(2)$

5 $\pi^- + p \longrightarrow n(31) + \pi^+(3) + \pi^{0-}(2)$

SUBJECT

NAME Lühl, Koellner, Miller
Starr, Stron

DATE 5/14/64

EVENT TYPE 24

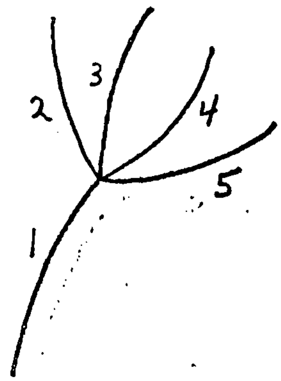

PANG DATA

TRACK BANK	TRACK NUMBER	MASS
1	1	π^-
2	2	π^-
3	3	π^-
4	4	π^+
5		p
6	5	π^+
7		p

CPM

1 $\pi^-(1) + p \longrightarrow p(4) + \pi^+(5) + \pi^-(2) + \pi^-(3)$ + mm

2 $\pi^- + p \longrightarrow p(5) + \pi^+(4) + \pi^-(2) + \pi^-(3)$ + mm

3 $\pi^- + p \longrightarrow \pi^+(4) + \pi^+(5) + \pi^-(2) + \pi^-(3)$ + mm

4 $\pi^- + p \longrightarrow p(4) + \pi^+(5) + \pi^-(2) + \pi^-(3)$

5 $\pi^- + p \longrightarrow p(5) + \pi^+(4) + \pi^-(2) + \pi^-(3)$

6 $\pi^- + p \longrightarrow p(4) + \pi^+(5) + \pi^0(31) + \pi^-(2) + \pi^-(3)$

7 $\pi^- + p \longrightarrow p(5) + \pi^+(4) + \pi^0(31) + \pi^-(2) + \pi^-(3)$

8 $\pi^- + p \longrightarrow n(31) + \pi^+(4) + \pi^+(5) + \pi^-(2) + \pi^-(3)$

NAME Uhl, Koellner, Miller, Starr, Strong

SUBJECT

DATE 5/14/64

EVENT TYPE 26

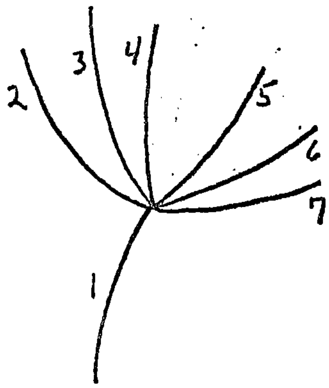

PANG DATA

TRACK BANK	TRACK NUMBER	MASS
1	1	π^-
2	2	π^-
3	3	π^-
4	4	π^-
5	5	π^+
6		p
7	6	π^+
10_8		p
11_8	7	π^+
12_8		p

CPM

1 $\pi^-(1) + p \longrightarrow p(5) + \pi^+(6) + \pi^+(7) + \pi^-(2) + \pi^-(3) + \pi^-(4) + mm$

2 $\pi^- + p \longrightarrow p(6) + \pi^+(5) + \pi^+(7) + \pi^-(2) + \pi^-(3) + \pi^-(4) + mm$

3 $\pi^- + p \longrightarrow p(7) + \pi^+(5) + \pi^+(6) + \pi^-(2) + \pi^-(3) + \pi^-(4) + mm$

4 $\pi^- + p \longrightarrow \pi^+(5) + \pi^+(6) + \pi^+(7) + \pi^-(2) + \pi^-(3) + \pi^-(4) + mm$

5 $\pi^- + p \longrightarrow p(5) + \pi^+(6) + \pi^+(7) + \pi^-(2) + \pi^-(3) + \pi^-(4)$

6 $\pi^- + p \longrightarrow p(6) + \pi^+(5) + \pi^+(7) + \pi^-(2) + \pi^-(3) + \pi^-(4)$

7 $\pi^- + p \longrightarrow p(7) + \pi^+(5) + \pi^+(6) + \pi^-(2) + \pi^-(3) + \pi^-(4)$

NAME Dahl, Koellner, Miller
~~Starr, Strong~~

DATE 5/14/64

SUBJECT

EVENT TYPE 30

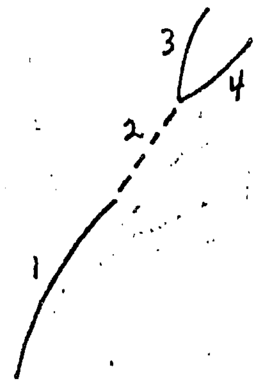

PANG DATA

TRACK BANK	TRACK NUMBER	MASS
1	1	π^-
2	2	K^0
3		Λ
4	3	π^-
5	4	π^+
6		p

CPM

1	$\Lambda(2) \longrightarrow p(4) + \pi^-(3)$	SAVE $\Lambda(2)$
2	$K^0(2) \longrightarrow \pi^+(4) + \pi^-(3)$	SAVE $K^0(2)$
3	$\pi^-(1) + p \longrightarrow \Lambda(2) + K^0(31)$	USE CPM 1
4	$\pi^- + p \longrightarrow \Lambda(2) + mm$	"
5	$\pi^- + p \longrightarrow \Lambda(31) + K^0(2)$	USE CPM 2
6	$\pi^- + p \longrightarrow \Sigma^0(31) + K^0(2)$	"
7	$\pi^- + p \longrightarrow K^0(2) + mm$	"

SUBJECT

NAME Dahl, Koellner, Miller ~~Starr, Strong~~

DATE 5/14/64

EVENT TYPE 32

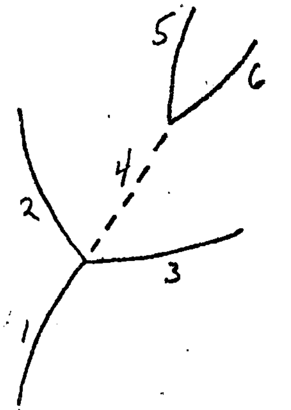

PANG DATA

TRACK BANK	TRACK NUMBER	MASS
1	1	π^-
2	2	π^-
3		K^-
4	3	π^+
5		K^+
6		p
7	4	K^0
10_8		Λ
11_8	5	π^-
12_8	6	π^+
13_8		p

CPM

1 $\Lambda(4) \longrightarrow p(6) + \pi^-(5)$ SAVE $\Lambda(4)$

2 $K^0(4) \longrightarrow \pi^+(6) + \pi^-(5)$ SAVE $K^0(4)$

3 $\pi^-(1) + p \longrightarrow \Lambda(4) + K^+(3) + \pi^-(2)$ USE CPM 1

4 $\pi^- + p \longrightarrow \Sigma^0(31) + K^+(3) + \pi^-(2);\ \Sigma^0 \to \Lambda(4) + \gamma(30)$ "

5 $\pi^- + p \longrightarrow \Lambda(4) + K^+(3) + \pi^0(31) + \pi^-(2)$ "

6 $\pi^- + p \longrightarrow \Lambda(4) + K^0(31) + \pi^+(3) + \pi^-(2)$ "

7 $\pi^- + p \longrightarrow \Lambda(31) + K^0(4) + \pi^+(3) + \pi^-(2)$ USE CPM 2

8 $\pi^- + p \longrightarrow \Sigma^0(31) + K^0(4) + \pi^+(3) + \pi^-(2)$ "

9 $\pi^- + p \longrightarrow \Lambda(4) + K^+(3) + \pi^-(2) + mm$ USE CPM 1

10 $\pi^- + p \longrightarrow \Lambda(4) + \pi^+(3) + \pi^-(2) + mm$ "

11 $\pi^- + p \longrightarrow K^0(4) + \pi^+(3) + \pi^-(2) + mm$ USE CPM 2

12 $\pi^- + p \longrightarrow p(3) + K^0(4) + K^-(2)$ "

13 $\pi^- + p \longrightarrow p(3) + K^0(4) + K^0(31) + \pi^-(2)$ "

14 $\pi^- + p \longrightarrow p(3) + K^0(4) + K^-(2) + \pi^0(31)$ "

15 $\pi^- + p \longrightarrow n(31) + K^+(3) + K^0(4) + \pi^-(2)$ "

16 $\pi^- + p \longrightarrow n(31) + K^0(4) + K^-(2) + \pi^+(3)$ "

17 $\pi^- + p \longrightarrow p(3) + K^0(4) + \pi^-(2) + mm$ "

18 $\pi^- + p \longrightarrow p(3) + K^0(4) + K^-(2) + mm$ "

19 $\pi^- + p \longrightarrow K^+(3) + K^0(4) + \pi^-(2) + mm$ "

20 $\pi^- + p \longrightarrow K^0(4) + K^-(2) + \pi^+(3) + mm$ "

SUBJECT
NAME Dahl, Koellner, Miller
Starr, Strong
DATE 5/14/64

EVENT TYPE 34

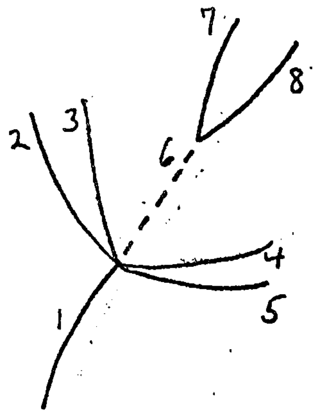

PANG DATA

TRACK BANK	TRACK NUMBER	MASS
1	1	π^-
2	2	π^-
3		K^-
4	3	π^-
5		K^-
6	4	π^+
7		K^+
10_8		p
11_8	5	π^+
12_8		K^+
13_8		p
14_8	6	K^0
15_8		Λ
16_8	7	π^-
17_8	8	π^+
20_8		p

CPM

1 $\Lambda(6) \longrightarrow p(8)+\pi^-(7)$ SAVE $\Lambda(6)$

2 $K^0(6) \longrightarrow \pi^+(8)+\pi^-(7)$ SAVE $K^0(6)$

3 $\pi^-(1)+p \longrightarrow \Lambda(6)+K^+(4)+\pi^+(5)+\pi^-(2)+\pi^-(3)$ USE CPM 1

4 $\pi^- +p \longrightarrow \Lambda(6)+K^+(5)+\pi^+(4)+\pi^-(2)+\pi^-(3)$ "

5 $\pi^- +p \longrightarrow \Sigma^0(31)+K^+(4)+\pi^+(5)+\pi^-(2)+\pi^-(3)$ SAVE $\Sigma^0(31)$

6 $\Sigma^0(31) \longrightarrow \Lambda(6)+\gamma(30)$ USE CPMs 1,5

7 $\pi^-(1)+p \longrightarrow \Sigma^0(31)+K^+(5)+\pi^+(4)+\pi^-(2)+\pi^-(3)$ SAVE $\Sigma^0(31)$

8 $\Sigma^0(31) \longrightarrow \Lambda(6)+\gamma(30)$ USE CPMs 1,7

9 $\pi^-(1)+p \longrightarrow p(4)+K^+(5)+K^0(6)+\pi^-(2)+\pi^-(3)$ USE CPM 2

10 $\pi^- +p \longrightarrow p(5)+K^+(4)+K^0(6)+\pi^+(2)+\pi^-(3)$ "

11 $\pi^- +p \longrightarrow p(4)+K^0(6)+K^-(2)+\pi^+(5)+\pi^-(3)$ "

12 $\pi^- +p \longrightarrow p(5)+K^0(6)+K^-(2)+\pi^+(4)+\pi^-(3)$ "

13 $\pi^- +p \longrightarrow p(4)+K^0(6)+K^-(3)+\pi^+(5)+\pi^-(2)$ "

14 $\pi^- +p \longrightarrow p(5)+K^0(6)+K^-(3)+\pi^+(4)+\pi^-(2)$ "

[illegible]

SUBJECT

NAME Dahl, Koellner, Miller ~~Starr, Strong~~

DATE 5/14/64

Event Type 40

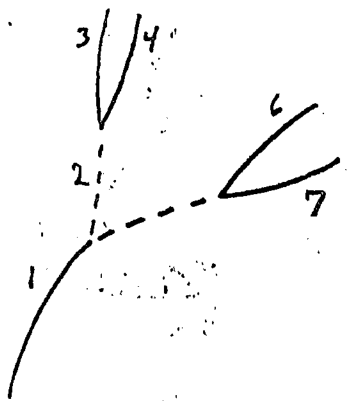

Pang Data

Track Bank	Track Number	Mass
1	1	π^-
2	2	K^0
3		Λ
4	3	π^-
5	4	π^+
6		p
7	5	K^0
10_8		Λ
11_8	6	π^-
12_8	7	π^+
13_8		p

CPM

1 $\Lambda(2) \longrightarrow p(4) + \pi^-(3)$ Save $\Lambda(2)$

2 $K^0(2) \longrightarrow \pi^+(4) + \pi^-(3)$ Save $K^0(2)$

3 $\Lambda(5) \longrightarrow p(7) + \pi^-(6)$ Save $\Lambda(5)$

4 $K^0(5) \longrightarrow \pi^+(7) + \pi^-(6)$ Save $K^0(5)$

5 $\pi^-(1) + p \longrightarrow \Lambda(2) + K^0(5)$ Use CPMs 1,4

6 $\pi^- + p \longrightarrow \Lambda(5) + K^0(2)$ Use CPMs 2,3

7 $\pi^- + p \longrightarrow \Sigma^0(31) + K^0(5)$; $\Sigma^0 \longrightarrow \Lambda(2) + \gamma(30)$ Use CPMs 1,4

8 $\pi^- + p \longrightarrow \Sigma^0(31) + K^0(2)$; $\Sigma^0 \longrightarrow \Lambda(5) + \gamma(30)$ Use CPMs 2,3

9 $\pi^- + p \longrightarrow \Lambda(2) + K^0(5) + \pi^0(31)$ Use CPMs 1,4

10 $\pi^- + p \longrightarrow \Lambda(5) + K^0(2) + \pi^0(31)$ Use CPMs 2,3

11 $\pi^- + p \longrightarrow \Lambda(2) + K^0(5) + mm$ Use CPMs 1,4

12 $\pi^- + p \longrightarrow \Lambda(5) + K^0(2) + mm$ Use CPMs 2,3

13 $\pi^- + p \longrightarrow n(31) + K^0(2) + K^0(5)$ Use CPMs 2,4

14 $\pi^- + p \longrightarrow K^0(2) + K^0(5) + mm$ "

NFD

NAME Dahl, Koellner, Miller Starr, Strong

SUBJECT

DATE 5/14/54

Event Type 42

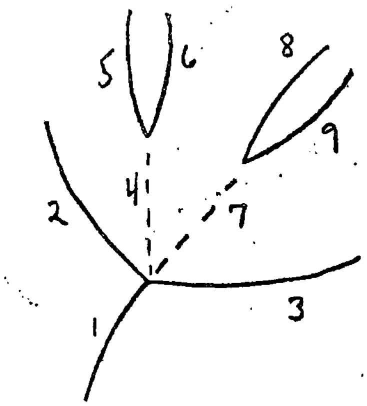

Pang Data

Track Bank	Track Number	Mass
1	1	π^-
2	2	π^-
3	3	π^+
4		p
5	4	K°
6		Λ
7	5	π^-
10_8	6	π^+
11_8		p
12_8	7	K°
13_8		Λ
14_8	8	π^-
15_8	9	π^+
16_8		p

CPM

1 $\Lambda(4) \longrightarrow p(6) + \pi^-(5)$ Save $\Lambda(4)$
2 $K^\circ(4) \longrightarrow \pi^+(6) + \pi^-(5)$ Save $K^\circ(4)$
3 $\Lambda(7) \longrightarrow p(9) + \pi^-(8)$ Save $\Lambda(7)$
4 $K^\circ(7) \longrightarrow \pi^+(9) + \pi^-(8)$ Save $K^\circ(7)$
5 $\pi^-(1) + p \longrightarrow \Lambda(4) + K^\circ(7) + \pi^+(3) + \pi^-(2)$ Use CPMs 1,4
6 $\pi^- + p \longrightarrow \Lambda(7) + K^\circ(4) + \pi^+(3) + \pi^-(2)$ Use CPMs 2,3
7 $\pi^- + p \longrightarrow \Sigma^\circ(31) + K^\circ(7) + \pi^+(3) + \pi^-(2); \Sigma^\circ \longrightarrow \Lambda(4) + \gamma(30)$ Use CPMs 1,4
8 $\pi^- + p \longrightarrow \Sigma^\circ(31) + K^\circ(4) + \pi^+(3) + \pi^-(2); \Sigma^\circ \longrightarrow \Lambda(7) + \gamma(30)$ Use CPMs 2,3
9 $\pi^- + p \longrightarrow \Lambda(4) + K^\circ(7) + \pi^+(3) + \pi^\circ(31) + \pi^-(2)$ Use CPMs 1,4
10 $\pi^- + p \longrightarrow \Lambda(7) + K^\circ(4) + \pi^+(3) + \pi^\circ(31) + \pi^-(2)$ Use CPMs 2,3
11 $\pi^- + p \longrightarrow \Lambda(4) + K^\circ(7) + \pi^+(3) + \pi^-(2) + mm$ Use CPMs 1,4
12 $\pi^- + p \longrightarrow \Lambda(7) + K^\circ(4) + \pi^+(3) + \pi^-(2) + mm$ Use CPMs 2,3
13 $\pi^- + p \longrightarrow p(3) + K^\circ(4) + K^\circ(7) + \pi^-(2)$ Use CPMs 2,4
14 $\pi^- + p \longrightarrow p(3) + K^\circ(4) + K^\circ(7) + \pi^\circ(31) + \pi^-(2)$ "
15 $\pi^- + p \longrightarrow n(31) + K^\circ(4) + K^\circ(7) + \pi^+(3) + \pi^-(2)$ "

LAWRENCE RADIATION LABORATORY - UNIVERSITY OF CALIFORNIA
PHYSICS NOTES

NFD

MEMO NO. 507

PAGE 28

Dahl, Koellner, Miller
Starr, Strong

SUBJECT

DATE 5/14/64

EVENT TYPE 50

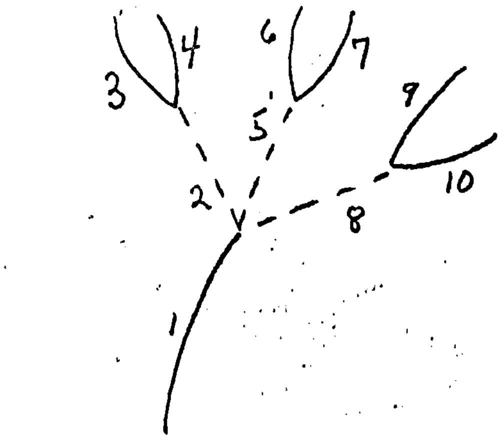

NFD

Dahl, Koellner, Miller
Starr, Strong

SUBJECT

DATE 5/14/64

EVENT TYPE 62

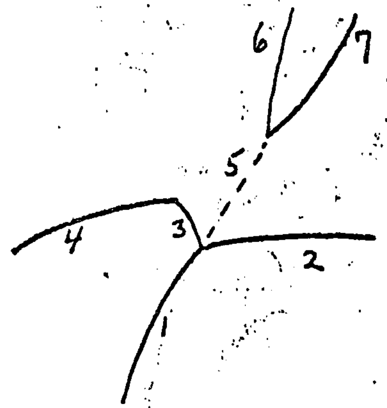

PANG DATA

TRACK BANK	TRACK NUMBER	MASS
1	1	π^-
2	2	π^-
3	3	K^+
4		Σ^+
5	4	π^+
6		p
7	5	K^0
10_8		Λ
11_8	6	π^-
12_8	7	π^+
13_8		p

CPM

1 $K^0(5) \longrightarrow \pi^+(7) + \pi^-(6)$ SAVE $K^0(5)$

2 $\Sigma^+(3) \longrightarrow n(30) + \pi^+(4)$ DAMN + SAVE $\Sigma^+(3)$

3 " DAMN − "

4 $\Sigma^+(3) \longrightarrow p(4) + \pi^0(30)$ DAMN + "

5 " DAMN − "

6 $\pi^-(1) + p \longrightarrow \Sigma^+(3) + K^0(5) + \pi^-(2)$; $\Sigma^+ \rightarrow n(30) + \pi^+(4)$

7 " $\Sigma^+ \rightarrow p(4) + \pi^0(30)$

8 $\pi^-(1) + p \longrightarrow \Sigma^+(3) + K^0(5) + \pi^0(31) + \pi^-(2)$; $\Sigma^+ \rightarrow n(30) + \pi^+(4)$ DAMN + USE CPM 1

9 " " DAMN − "

10 " $\Sigma^+ \rightarrow p(4) + \pi^0(30)$ DAMN + "

11 " " DAMN − "

12 $\pi^-(1) + p \longrightarrow \Sigma^+(3) + K^0(5) + \pi^-(2) + mm$ USE CPMs 1,2

13 " USE CPMs 1,3

14 " USE CPMs 1,4

15 " USE CPMs 1,5

16 $\Lambda(5) \longrightarrow p(7) + \pi^-(6)$ SAVE $\Lambda(5)$

17 $\pi^-(1) + p \longrightarrow \Lambda(5) + K^+(3) + \pi^-(2)$ USE CPM 16

18 $\pi^-(1) + p \longrightarrow \Sigma^0(31) + K^+(3) + \pi^-(2)$; $\Sigma^0 \rightarrow \Lambda(5) + \gamma(30)$ "

19 $\pi^-(1) + p \longrightarrow \Lambda(5) + K^+(3) + \pi^0(31) + \pi^-(2)$ "

20 $\pi^-(1) + p \longrightarrow \Lambda(5) + K^+(3) + \pi^-(2) + mm$ "

21 $\pi^-(1) + p \longrightarrow n(31) + K^+(3) + K^0(5) + \pi^-(2)$ USE CPM 1

22 $\pi^-(1) + p \longrightarrow K^+(3) + K^0(5) + \pi^-(2) + mm$ "

Dahl, Koellner, Miller
Starr, Strong
SUBJECT
DATE 5/14/64

EVENT TYPE 64

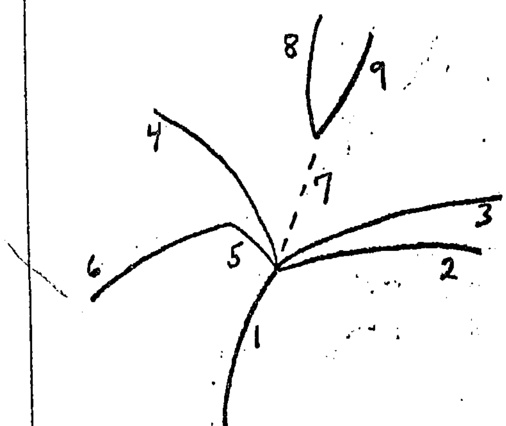

PANG DATA

TRACK BANK	TRACK NUMBER	MASS
1	1	π^-
2	2	π^-
3	3	π^-
4	4	π^+
5		p
6	5	K^+
7		Σ^+
10_8	6	π^+
11_8		p
12_8	7	K^0
13_8		Λ
14_8	8	π^-
15_8	9	π^+
16_8		p

CPM

1 $K^0(7) \longrightarrow \pi^+(9) + \pi^-(8)$ SAVE $K^0(7)$

2 $\pi^-(1) + p \longrightarrow \Sigma^+(5) + K^0(6) + \pi^+(4) + \pi^-(2) + \pi^-(3)$ USE CPM 1, SAVE $\Sigma(5)$

3 $\Sigma^+(5) \longrightarrow n(30) + \pi^+(6)$ USE CPM 2

4 $\Sigma^+(5) \longrightarrow p(6) + \pi^0(30)$ "

5 $\Lambda(7) \longrightarrow p(9) + \pi^-(8)$ SAVE $\Lambda(7)$

6 $\pi^-(1) + p \longrightarrow \Lambda(7) + K^+(5) + \pi^+(4) + \pi^-(2) + \pi^-(3)$ USE CPM 5

7 $\pi^-(1) + p \longrightarrow \Sigma^0(31) + K^+(5) + \pi^+(4) + \pi^-(2) + \pi^-(3)$ SAVE $\Sigma^0(31)$

8 $\Sigma^0(31) \longrightarrow \Lambda(7) + \gamma(30)$ USE CPMs 5, 7

9 $\pi^-(1) + p \longrightarrow p(4) + K^+(5) + K^0(7) + \pi^-(2) + \pi^-(3)$ USE CPM 1

NAME Dahl, Koellner, Miller ~~Starr, Strong~~

SUBJECT

DATE 5/14/64

EVENT TYPE 72

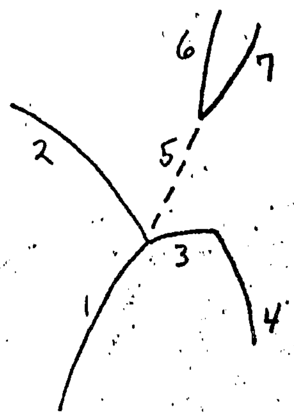

PANG DATA

TRACK BANK	TRACK NUMBER	MASS
1	1	π^-
2	2	π^+
3		p
4	3	K^-
5		Σ^-
6	4	π^-
7	5	K^0
10_8	6	π^-
11_8	7	π^+

CPM

1 $K^0(5) \longrightarrow \pi^+(7) + \pi^-(6)$ SAVE $K^0(5)$

2 $\Sigma^-(3) \longrightarrow n(30) + \pi^-(4)$ DAMN + ; SAVE $\Sigma^-(3)$

3 '' DAMN − ; ''

4 $\pi^-(1) + p \longrightarrow \Sigma^-(3) + K^0(5) + \pi^+(2)$; $\Sigma^- \longrightarrow n(30) + \pi^-(4)$ USE CPM 1

5 $\pi^-(1) + p \longrightarrow \Sigma^-(3) + K^0(5) + \pi^+(2) + \pi^0(31)$; $\Sigma^- \longrightarrow n(30) + \pi^-(4)$ DAMN + , USE CPM 1

6 '' DAMN − ''

7 $\pi^-(1) + p \longrightarrow \Sigma^-(3) + K^0(5) + \pi^+(2) + mm$ USE CPMs 1, 2

8 '' USE CPMs 1, 3

9 $\pi^-(1) + p \longrightarrow p(2) + K^0(5) + K^-(3)$ USE CPM 1

10 $\pi^-(1) + p \longrightarrow p(2) + K^0(5) + K^-(3) + \pi^0(31)$ ''

11 $\pi^-(1) + p \longrightarrow n(31) + K^0(5) + K^-(3) + \pi^+(2)$ ''

12 $\pi^-(1) + p \longrightarrow p(2) + K^0(5) + K^-(3) + mm$ ''

13 $\pi^-(1) + p \longrightarrow K^0(5) + K^-(3) + \pi^+(2) + mm$ ''

Dahl, Koellner, Miller
Starr, Strong

DATE 5/14/64

EVENT TYPE 74

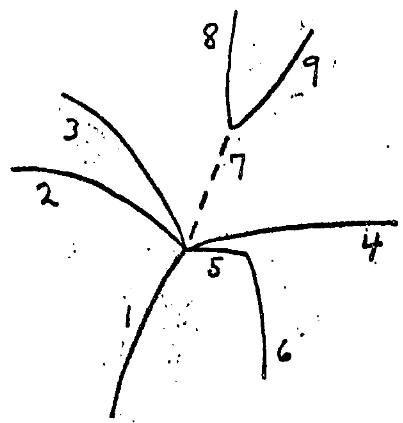

PANG DATA

TRACK BANK	TRACK NUMBER	MASS
1	1	π^-
2	2	π^+
3		p
4	3	π^+
5		p
6	4	π^-
7	5	K^-
10_8		Σ^-
11_8	6	π^-
12_8	7	K^0
13_8	8	π^-
14_8	9	π^+

CPM

1 $K^0(7) \longrightarrow \pi^+(9) + \pi^-(8)$ SAVE $K^0(7)$

2 $\pi^-(1) + p \longrightarrow \Sigma^-(5) + K^0(7) + \pi^+(2) + \pi^+(3) + \pi^-(4)$; USE CPM 1, SAVE $\Sigma^-(5)$

3 $\Sigma^-(5) \longrightarrow n(30) + \pi^-(6)$ USE CPM 2

4 $\pi^-(1) + p \longrightarrow p(2) + K^0(7) + K^-(5) + \pi^+(3) + \pi^-(4)$; USE CPM 1

5 $\pi^-(1) + p \longrightarrow p(3) + K^0(7) + K^-(5) + \pi^+(2) + \pi^-(4)$ "

SUBJECT
~~Dahl~~, Koellner, Miller ~~Starr, Strong~~
DATE 5/14/64

EVENT TYPE 82

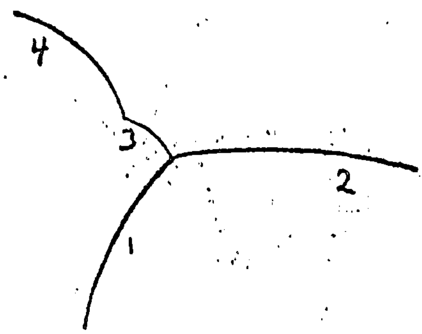

PANG DATA

TRACK BANK	TRACK NUMBER	MASS
1	1	π^-
2	2	π^-
3		K^-
4	3	K^+
5		Σ^+
6	4	π^+
7		p

CPM

1 $\Sigma^+(3) \longrightarrow n(30) + \pi^+(4)$ DAMN + SAVE $\Sigma^+(3)$
2 » DAMN − »
3 $\Sigma^+(3) \longrightarrow p(4) + \pi^0(30)$ DAMN + »
4 » DAMN − »
5 $\pi^-(1) + p \longrightarrow \Sigma^+(3) + K^0(31) + \pi^-(2)$; $\Sigma^+ \to n(30) + \pi^+(4)$ DAMN +
6 » » DAMN −
7 » $\Sigma^+ \to p(4) + \pi^0(30)$ DAMN +
8 » » DAMN −
9 $\pi^-(1) + p \longrightarrow \Sigma^+(3) + \pi^-(2) + mm$ USE CPM 1
10 » USE CPM 2
11 » USE CPM 3
12 » USE CPM 4
13 $\pi^-(1) + p \longrightarrow \Lambda(31) + K^+(3) + \pi^-(2)$
14 $\pi^- + p \longrightarrow \Sigma^0(31) + K^+(3) + \pi^-(2)$
15 $\pi^- + p \longrightarrow K^+(3) + \pi^-(2) + mm$
16 $\pi^- + p \longrightarrow n(31) + K^+(3) + K^-(2)$
17 $\pi^- + p \longrightarrow K^+(3) + K^-(2) + mm$

NAME Dahl, Koellner, Miller ~~Starr, Strong~~

SUBJECT

DATE 5/14/64

EVENT TYPE 84

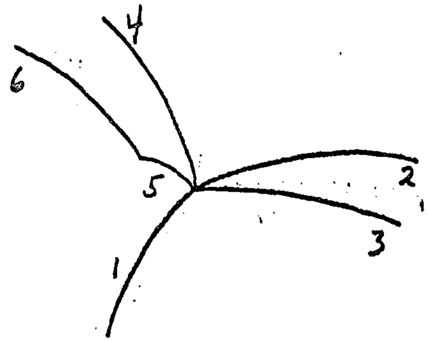

PANG DATA

TRACK BANK	TRACK NUMBER	MASS
1	1	π^-
2	2	π^-
3		K^-
4	3	π^-
5		K^-
6	4	π^+
7		K^+
10_8		p
11_8	5	K^+
12_8		Σ^+
13_8	6	π^+
14_8		p

CPM

1 $\Sigma^+(5) \longrightarrow n(30) + \pi^+(6)$ DAMN + SAVE $\Sigma^+(5)$
2 " DAMN − "
3 $\Sigma^+(5) \longrightarrow p(6) + \pi^0(30)$ DAMN + "
4 " DAMN − "
5 $\pi^-(1) + p \longrightarrow \Sigma^+(5) + K^+(4) + \pi^-(2) + \pi^-(3)$; $\Sigma^+ \longrightarrow n(30) + \pi^+(6)$
6 " $\Sigma^+ \longrightarrow p(6) + \pi^0(30)$
7 $\pi^-(1) + p \longrightarrow \Sigma^+(5) + K^+(4) + \pi^0(31) + \pi^-(2) + \pi^-(3)$ USE CPM 1
8 " USE CPM 2
9 " USE CPM 3
10 " USE CPM 4
11 $\pi^-(1) + p \longrightarrow \Sigma^+(5) + K^0(31) + \pi^+(4) + \pi^-(2) + \pi^-(3)$ USE CPM 1
12 " USE CPM 2
13 " USE CPM 3
14 " USE CPM 4
15 $\pi^-(1) + p \longrightarrow \Lambda(31) + K^+(5) + \pi^+(4) + \pi^-(2) + \pi^-(3)$
16 $\pi^-(1) + p \longrightarrow \Sigma^0(31) + K^+(5) + \pi^+(4) + \pi^-(2) + \pi^-(3)$
17 $\pi^-(1) + p \longrightarrow p(4) + K^+(5) + K^-(2) + \pi^-(3)$
18 $\pi^-(1) + p \longrightarrow p(4) + K^+(5) + K^-(3) + \pi^-(2)$
19 $\pi^-(1) + p \longrightarrow p(4) + K^+(5) + K^-(2) + \pi^0(31) + \pi^-(3)$
20 $\pi^-(1) + p \longrightarrow p(4) + K^+(5) + K^-(3) + \pi^0(31) + \pi^-(2)$
21 $\pi^-(1) + p \longrightarrow p(4) + K^+(5) + K^0(31) + \pi^-(2) + \pi^-(3)$
22 $\pi^-(1) + p \longrightarrow n(31) + K^+(5) + K^-(2) + \pi^+(4) + \pi^-(3)$
23 $\pi^-(1) + p \longrightarrow n(31) + K^+(5) + K^-(3) + \pi^+(4) + \pi^-(2)$

SUBJECT

NAME Dahl, Koellner, Miller, ~~Starr, Stron~~

DATE 5/14/64

EVENT TYPE 92

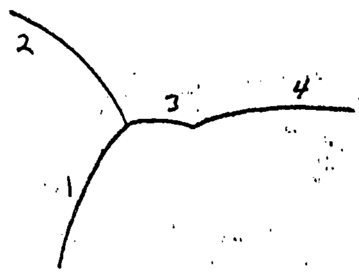

PANG DATA

TRACK BANK	TRACK NUMBER	MASS
1	1	π^-
2	2	π^+
3		K^+
4		p
5	3	K^-
6		Σ^-
7	4	π^-

CPM

1 $\Sigma^-(3) \longrightarrow n(30) + \pi^-(4)$ DAMN + SAVE $\Sigma^-(3)$

2 " DAMN − "

3 $\pi^-(1) + p \longrightarrow \Sigma^-(3) + K^+(2)$; $\Sigma^- \longrightarrow n(30) + \pi^-(4)$

4 $\pi^-(1) + p \longrightarrow \Sigma^-(3) + K^+(2) + \pi^0(31)$; $\Sigma^- \longrightarrow n(30) + \pi^-(4)$ DAMN +

5 " " DAMN −

6 $\pi^-(1) + p \longrightarrow \Sigma^-(3) + K^0(31) + \pi^+(2)$; $\Sigma^- \longrightarrow n(30) + \pi^-(4)$ DAMN +

7 " " DAMN −

8 $\pi^-(1) + p \longrightarrow \Sigma^-(3) + K^+(2) + mm$ USE CPM 1

9 " USE CPM 2

10 $\pi^-(1) + p \longrightarrow \Sigma^-(3) + \pi^+(2) + mm$ USE CPM 1

11 " USE CPM 2

12 $\pi^-(1) + p \longrightarrow n(31) + K^+(2) + K^-(3)$

13 $\pi^-(1) + p \longrightarrow p(2) + K^0(31) + K^-(3)$

14 $\pi^-(1) + p \longrightarrow p(2) + K^-(3) + mm$

15 $\pi^-(1) + p \longrightarrow K^+(2) + K^-(3) + mm$

16 $\pi^-(1) + p \longrightarrow K^-(3) + \pi^+(2) + mm$

Dahl, Koellner, Miller
Starr, Strong

SUBJECT

DATE 5/14/64

EVENT TYPE 94

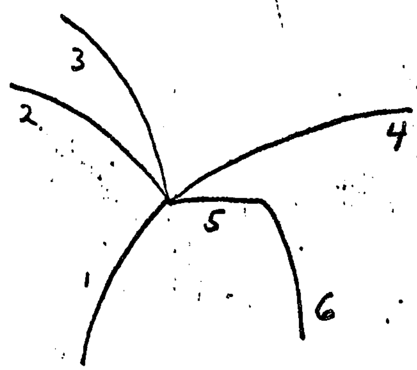

PANG DATA

TRACK BANK	TRACK NUMBER	MASS
1	1	π^-
2	2	π^+
3		K^+
4		P
5	3	π^+
6		K^+
7		P
10 & 8	4	π^-
11 & 9	5	K^-
12 & 10		Σ^-
13 & 11	6	π^-

CPM

1 $\Sigma^-(5) \longrightarrow n(30) + \pi^-(6)$ DAMN + SAVE $\Sigma^-(5)$

2 " DAMN − "

3 $\pi^-(1) + p \longrightarrow \Sigma^-(5) + K^+(2) + \pi^+(3) + \pi^-(4); \Sigma^- \rightarrow n(30) + \pi^-(6)$

4 $\pi^-(1) + p \longrightarrow \Sigma^-(5) + K^+(3) + \pi^+(2) + \pi^-(4); \Sigma^- \longrightarrow n(30) + \pi^-(6)$

5 $\pi^-(1) + p \longrightarrow \Sigma^-(5) + K^+(2) + \pi^+(3) + \pi^0(31) + \pi^-(4)$ USE CPM 1

6 " USE CPM 2

7 $\pi^-(1) + p \longrightarrow \Sigma^-(5) + K^+(3) + \pi^+(2) + \pi^0(31) + \pi^-(4)$ USE CPM 1

8 " USE CPM 2

9 $\pi^-(1) + p \longrightarrow \Sigma^-(5) + K^0(31) + \pi^+(2) + \pi^+(3) + \pi^-(4)$ USE CPM 1

10 " USE CPM 2

11 $\pi^-(1) + p \longrightarrow p(2) + K^+(3) + K^-(5) + \pi^-(4)$

12 $\pi^-(1) + p \longrightarrow p(3) + K^+(2) + K^-(5) + \pi^-(4)$

13 $\pi^-(1) + p \longrightarrow p(2) + K^+(3) + K^-(5) + \pi^0(31) + \pi^-(4)$

14 $\pi^-(1) + p \longrightarrow p(3) + K^+(2) + K^-(5) + \pi^0(31) + \pi^-(4)$

15 $\pi^-(1) + p \longrightarrow p(2) + K^0(31) + K^-(5) + \pi^+(3) + \pi^-(4)$

16 $\pi^-(1) + p \longrightarrow p(3) + K^0(31) + K^-(5) + \pi^+(2) + \pi^-(4)$

17 $\pi^-(1) + p \longrightarrow n(31) + K^+(2) + K^-(5) + \pi^+(3) + \pi^-(4)$

18 $\pi^-(1) + p \longrightarrow n(31) + K^+(3) + K^-(5) + \pi^+(2) + \pi^-(4)$

SUBJECT (K^-p) Interactions from 1-3 BeV/c
INVITED TALK WASHINGTON APS MEETING

NAME J. Button-Shafer

DATE May 15, 1964

D Merrill

I. INTRODUCTION

I shall discuss K^--p interactions yielding final states which contain hyperons and hyperon resonances. The data presented were obtained by the Alvarez Group with the 72-inch hydrogen bubble chamber in two series of runs at the Bevatron. The first, commonly referred to as the "K-72 Experiment," was carried out with a beam designed by Harold K. Ticho (UCLA) with assistance from Berkeley and UCLA physicists; this beam produced film for the Alvarez Group from a momentum of 1.05 BeV/c to 1.75 BeV/c. The second series of runs, called the "K-63 Experiment," is more recent and to date has produced film at 2.45, 2.7 and 2.6 BeV/c. This beam was designed by Joseph J. Murray, with assistance primarily from Shafer, Kadyk and Trilling; it has been used extensively for high-energy π^- as well as K^- running.

Almost the entire Alvarez Group participated in the analysis of film from the K-72 experiment; a slightly smaller number are taking part in the K-63 experiment. As I shall mention those who have participated in various research projects later, I now give the names only of those who are maintaining the K-63 beam at the Bevatron and those who are largely responsible for the bulk processing of K-63 data. The first group includes Shively, Eberhard, Galtieri, Kalbfleisch and Tripp, in addition to Murray and Shafer; the second group directing analysis is comprised of G. Smith, Kalbfleisch and Dahl.

The total K^- tracklength in the K-72 experiment was such as to yield about 12,000 events per mb of cross section (with much of this at 1.5 BeV/c). The tracklength in K-63 to date is equivalent to about 10,000 events per mb, the greater part of this being at 2.6 BeV/c. For the K-63 film, only the analysis at 2.45 BeV/c is near completion.

II. A. CROSS SECTIONS FOR HYPERON FINAL STATES

As I shall be showing data at many different beam momenta, ~~it may~~ be helpful to remark that an incident K^- laboratory momentum of 1.5 BeV/c corresponds to a center-of-mass energy of 2.025 BeV, which is the mass of the J-5/2 Regge recurrence of the Λ_β; further, as a reference figure at higher energy, the K^- momentum of 2.5 BeV/c yields a c.m. energy of nearly 2.5 BeV.

FIGURE 1 displays the momentum-dependence of $\Xi^- K^+$ and $\Xi K \pi$ production from 1.2 to 2.7 BeV/c. Note that the cross sections reach maxima of only 150 and 100 ub, respectively. Thresholds for $\Xi^* K$ and ΞK^* processes are indicated by the arrows. (Analysis of Ξ's in the K-72 experiment has been carried out by Stevenson, Solmitz, and Berge; and in the K-63 experiment, it has been done chiefly by Smith).

FIGURE 2 gives the momentum dependence of the $\Sigma\pi$ production for both charge combinations. Note that the cross section for Σ^+ production is approximately 3 times that for Σ^- production near 1.5 BeV/c. It may be possible to explain this by the fact that K^* exchange is permitted for Σ^+ production, but not for Σ^-. Both cross sections rise toward values of about 2 mb at 1.08 BeV/c; and at this momentum, corresponding to the Λ_α recurrence or Kerth bump, both processes have angular distributions requiring $\cos^5 \theta$. (The work on Σ production has been carried out by Galtieri, Alston, Ferro-Luzzi, Rosenfeld, and Wojcicki and also by Miller and Wohl.)

FIGURE 3 shows the dependence of $\Lambda 2\pi$ and $\Lambda 3\pi$ production on incident K momentum. These cross sections are again of the order of 1 to 2 mb, as in the case of $\Sigma^\pm \pi^\mp$ production. The $\Lambda 2\pi$ process has a cross section of about 4 mb at 1.08 BeV/c (not shown), drops to 2.7 mb at 1.2 BeV/c, and continues dropping as the momentum increases. This $\Lambda 2\pi$ final state is nearly 100% Y_1^* (1385) + π, as we shall see shortly. Production of $\Lambda 3\pi$ increases to a maximum just above 1.5 BeV/c and then falls with momentum. (Analysis of Λ final states has been done by Huwe, Murray and Shafer and also by Stevenson and Wohl in K-72; in K-63, it has been carried out chiefly by Ross.)

II. B. CROSS SECTIONS FOR RESONANCE PRODUCTION

FIGURE 4 displays the dependence on momentum of $Y^{*\pm}\pi^{\mp}$ production in K-72 and gives percentages of various resonance states at 2.45 BeV/c. The predominance of Y^{*-} over Y^{*+} at 1.22 BeV/c (55% & 45%) changes with increasing momentum; work at Brookhaven showed in fact that Y^* production at 2.22 BeV/c in the final state is predominantly Y^{*+}.

The $\Lambda 3\pi$ final state is somewhat more interesting than the $\Lambda 2\pi$ final state at 2.45 BeV/c, not only because of its greater cross section, but also because of the many resonant states which result. In fact, no non-resonant amplitude is required, and besides Y_1^*'s of all three charges, there are appreciable percentages of ρ (with Y_1^*) and ω (with Λ).

FIGURE 5 displays the dependence of $\Lambda\omega$ production on momenta in the K-72 experiment. This reaches a maximum of 0.9 mb around 1.5 BeV/c, where evidently both K and K^* exchange as well as the Λ_β recurrence in the forward channel are necessary to fit the data. (This study has been directed by Stevenson).

FIGURE 6 shows the dependence of $\Xi^* K$ and ΞK^* production on momentum. The maximum cross section was obtained by UCLA in their work at 1.8 and 1.95 BeV/c and has a value of 50 μbarns. (Berkeley has had considerable difficulty in obtaining Ξ^* data! This Ξ-π resonance was orginally predicted at a mass much higher than 1530 MeV and so was not looked for seriously in film at momenta below 1.8 BeV/c; and in the higher-energy experiment now in progress near 2.5 BeV/c, the cross section is very low.)

The $\Sigma 3\pi$ final states show complicated resonant effects which have been interpreted only after extensive study (by Alston, Galtieri, Rosenfeld, and Wojcicki). The 1520-MeV Y_0^* or the 1405 Y_0^* is manifested in a $\Sigma^\pm\pi^\mp$ resonance

SUBJECT

NAME J. B. Shafer

DATE May 15, 1964

in most of the $\Sigma 3\pi$ events. Further, the Y_1^* (1660)$^+$ is clearly observed as a $\Sigma\pi\pi$ combination (and may be the parent state for the 1405 Y_0^*) in an appreciable fraction of the events.

III. ANALYSIS OF THE Y_1^* (1385 MeV) AT VARIOUS ENERGIES

FIGURE 7 displays the events yielding $\Lambda\pi\pi$ (those which were measured and processed) from the K-72 experiment over the range 1.1 to 1.75 BeV/c. At each momentum setting made in 100-MeV/c intervals, the total momentum bite was 5-6%.

FIGURE 8 presents the Dalitz plot of the $\Lambda 2\pi$ events at 1.22 BeV/c incident K momentum, where the Y^{*+} and Y^{*-} bands are very pronounced and fairly well separated. (Zero to 5 percent background is needed to fit the mass spectra.) In FIGURE 9 the so-called "normal" and "magic" components of polarization are shown as functions of the projection of the decay lambda onto the normal (to the production plane of the Y^*). As is well-known, comparison of these data with predicted distributions for various spin-parity hypotheses established $P_{3/2}$ as the Y^* state, provided spin greater than 3/2 were not considered. (The "magic" direction is that direction assumed by the normal if it is rotated about the lambda direction by 180 deg.) An equivalent way of studying these two polarization components is to consider their sum/cos θ (called the "longitudinal polarization," as it is the polarization in the direction of the lambda) and also their difference/sin θ (one of the "transverse polarization" components). Longitudinal polarization ($IP_{\parallel}$) of the lambda from Y^* decay obviously will contain cos θ and $\cos^3\theta$ terms, while the transverse polarization (IP_x) will contain even functions of cos θ. (See sketch ~~to~~ below)

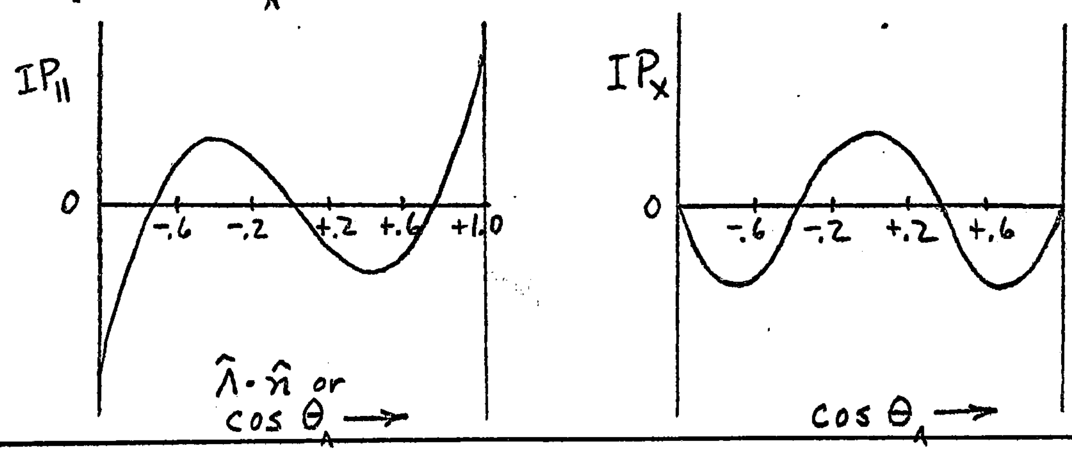

I turn now to more powerful formalism, a major conclusion of which is that the highest power of cos θ allowed is 2J+1 (with J the spin of the resonance) in any angular distribution or polarization distribution of decay products; a further consequence is that the coefficients of certain functions describing the transverse polarization are completely given in magnitude once the longitudinal polarization is known, and are determined in relative sign by the parity of the resonance. This formalism I shall call the method of "moment analysis" of spin and of transition amplitudes suggested by Byers and Fenster (Phys. Rev. Letters 11, 52 (1963)). It is applicable to strong and to weak decays; and as I shall be describing the results of treating not only Y*'s, but also the Ξ^-, and the Ξ^*, I will digress for a few moments to describe the theoretical framework.

The original state of interest (say the Y*) is completely described by $\frac{1}{2}(2J+1)^2$ independent parameters; these may be chosen as the expectation values of certain operators in spin space which we call "irreducible tensors." [These T_{LM} tensors have the same form in spin space (in S_x, S_y, etc.) that the Y_{LM} have in coordinate space.] The density matrix describing the particular collection of Y*'s may be written

$$\rho_{Y^*} = \frac{1}{2J+1} \sum_{L,M}^{L=2J} (2L+1) \langle T_{LM} \rangle^* T_{LM} .$$

Now, if the Y*'s undergo decay into a spin-1/2 particle (e.g., a Λ) and a spin-zero boson, a simple transition operator M (equal to A or to B $\vec{\sigma}\cdot\hat{\Lambda}$)may be used to describe the spin states of the Λ after Y* decay. The Λ density matrix is $\rho_\Lambda = M \rho_{Y^*} M^\dagger$; but after rotation* this is also $\rho_\Lambda = \frac{I}{2}\begin{pmatrix} 1+P_\parallel & P_\perp^* \\ P_\perp & 1-P_\parallel \end{pmatrix}$ where diagonal terms give the longitudinal polarization and off-diagonal terms give the x and y components of transverse polarization (relative to the Λ direction).

*This "helicity-state" representation of the Λ spin was derived by Byers and Fenster through the inclusion of a rotation operator with the transition matrix to take the original normal or z axis into the lambda direction.)

FIGURE 10 shows the expressions for angular distribution of the decay lambda and also for the three components of polarization. (The forms of these expressions are predictable also from invariance arguments.) In applying these to our data, we obtain information not sought in the original normal-magic polarization analysis in that we study a third component of polarization ($P_\perp$ being $P_x + iP_y$) and also the Ø-dependence of the distributions.

The coordinate system used for the analysis of Y*'s and other "particles" is shown at the bottom left of FIGURE 10. It is based solely on the Y* production kinematics; the normal is chosen as the Z axis, since in such a system all odd-M T_{LM}'s must have zero expectation value because of parity conservation in production.

Evaluation of "moments" is made as shown in FIGURE 11. "Moment" means the average value of a particular spherical harmonic (similar to the multipole moments of low-energy physics); and the $\langle T_{LM} \rangle$ or t_{LM} values, which we shall loosely call "moments" are found from these by dividing by the appropriate $n_{L0}(J)$ or $n_{L1}(J)$ found from Clebsch-Gordan coefficients. Then the problem is to ask the right question to test for spin or parity. The expression for the "parity" χ^2 is given in FIGURE 11; it compares each t_{LM} from longitudinal polarization with the same $t_{LM} \times \gamma$ from transverse polarization (where γ is + 1 or -1 depending on the parity). A χ^2 to test spin asks whether the moments not allowed for a given hypothesis are consistent with zero. As it is difficult by this technique to establish a low-order spin, the equation at the bottom of FIGURE 11 has been applied; it follows from the relation between n_{L0} and n_{L1}, containing a (2J + 1) factor (in FIGURE 10). (This evaluation of the 2J+1 quantity is non-Gaussian because of being proportional to a ratio of experimental data, so must be interpreted with care.)

FIGURE 12 gives the various t_{LM} values found for the data at 1.22 BeV/c incident K momentum. Note that there is only 1 interesting moment for J = 1/2; there are 7 moments for J = 3/2; and there are 17 for J = 5/2, with Re and Im parts counted separately.

FIGURE 13 displays the more significant moments as functions of momentum from 1.2 through 1.7 BeV/c. FIGURE 14 shows the variation of the "spin χ^2" with momentum; obviously the assignment J = 1/2 is ruled out. FIGURE 15 gives the variation of the "parity χ^2" with momentum, both for J = 3/2 and J = 5/2. The $P_{3/2}$ hypothesis looks very good at all momenta; however, the $D_{5/2}$ hypothesis (not ruled out at 1.22 BeV/c) has confidence limits less than 2% at two of the momenta. Thus, with consideration of spins through 5/2, the $P_{3/2}$ assignment is certainly the best.

FIGURE 16 reinforces the selection of J = 3/2 through the evaluation of the (2J+1) quantity from the ratio of transverse to longitudinal moments. Results are for data from 1.2 through 1.4 BeV/c and are plotted as if they were contributions for an ideogram. Since the expected distribution of the 2J+1 quantity is non-Gaussian (and in fact is skewed slightly toward low values), the central values are to be taken more seriously than the errors. These are closer to 4 than to 6 (i.e., to J = 3/2 rather than 5/2).

IV. STUDY OF THE Y_1^* (1660- MeV)

From the data at 1.51 BeV/c it was found that a resonance decaying into a Λ or a Σ hyperon with one or two pions existed at 1660 MeV. To date the spin and parity of this resonance have not been firmly established. I have applied the moment analysis to the approximately 80 events lying in the right half of the horizontal Y_1^*(1660-MeV) band, seen in the $\Lambda\pi\pi$ Dalitz plot (FIGURE 17). The left half of the band is useless because of the predominance of the Y^*(1385); but only one-half the band is necessary to analyze for even-M moments. The results support spin $\geq 3/2$, but are inconclusive on parity. This study is being extended to the more numerous and much cleaner sample of events $Y^*_{1660} \rightarrow \Sigma^0 + \pi$.

V. THE Ξ^- HYPERON

FIGURE 18 shows a rather photogenic example of Ξ^- production and decay (and includes about 2/5 of the useful volume of the 72-inch bubble chamber); the K^+ produced with the Ξ^- decays (atypically) into three pions.

The next graph FIGURE 19 displays the dependence of Ξ^- polarization on the momentum of the incident K^- beam. This polarization, an average over all production angles, passes through zero close to 1.5 BeV/c; nevertheless, at certain production angles the data at 1.5 BeV/c show rather large polarization.

Here we return to the moment method of analysis, but with twice as many measurable parameters to be determined for each spin hypothesis as before. FIGURE 20 presents the expressions for angular distribution of the Λ from Ξ^- decay and also of the various polarization distributions. Because the Ξ decays with parity violation, there are odd-L terms in $I(\theta,\phi)$ and even-L terms in $IP_{\parallel}(\theta, \phi)$ which were zero for the Y^*_1 case of strong decay; these are multiplied by the quantity α_{Ξ} (the usual decay parameter). Further, there is an additional β_{Ξ} parameter in the transverse polarization, which is now modified by $(\gamma_{\Xi} + i\beta_{\Xi})$. Both the projection technique (averaging as in Fig. 11) and the maximum-likelihood method have been used with the Byers-Fenster moment language, the general expression for the latter being given toward the bottom of the figure. (A likelihood approach has also been applied to Ξ^- decay with a different formulation of parameters by P. Eberhard, The early work on K-72 Ξ^- analysis, by Stevenson, Solmitz, and Berge, used a likelihood treatment of production and decay under the assumption that the Ξ^- had spin 1/2.)

To establish that a spin has low value is difficult. The relation giving $(2J+1)^2$ in FIGURE 20 proves to be rather useful; it is the exact analog for weak decay of the relation used earlier for Y* decay, as it represents the magnitude squared of an $IP_\perp$ moment divided by the square of the $IP_\parallel$ moment.**

FIGURE 21 presents results for the various parameters of Ξ^- decay for spin 1/2 and spin 3/2, as obtained by the moment formulation of the likelihood function. (These are not the complete set of results, but are fairly representative.) The ordinate represents the parameter $\alpha_\Xi \equiv \frac{2\,\mathrm{Re}\,s^*p}{|s|^2+|p|^2}$ and the abscissa is the inverse tangent of β_Ξ/γ_Ξ (where $\beta \equiv \frac{2\,\mathrm{Im}\,s^*p}{|s|^2+|p|^2}$ and $\gamma \equiv \frac{|s|^2-|p|^2}{|s|^2+|p|^2}$).* The log of the likelihood is given to the right of the plotted results. Some secondary maxima of the likelihood are indicated to the far left. Obviously α is between -0.3 and -0.4; and β is very close to 0.0. The values given are from both the K-72 and the K-63 experiment; the former yielded a total of 750 Ξ^- events and the latter has given to date about 180 Ξ^-'s.

FIGURE 22 shows the evaluations of the quantity 2J+1 obtained by the projection technique of finding moments; the t_{10} moment (or vector polarization) was used with the last equation of FIGURE 20. (Data yielding abnormal values for the α, β, and γ parameters were not used.) Because of the non-Gaussian nature of the 2J+1 quantity, the distribution of central values is possibly the most reliable information. A few of the results plotted would be negative if sign information were retained. Evidently the best answers are $2J+1 \leq 2$, though consistent with zero, so the J is most likely 1/2. (The higher moments expected for spin 3/2 were

---

* Amplitudes s and p are those appearing in the transition matrix $M = s + p\,\vec{\sigma}\cdot\hat{\Lambda}$ which gives $\psi_{final} = M\,\psi_{init}$. The parameter β is positive if the polarization along $\hat{n}\times\hat{\Lambda}$ is positive.

** Though very similar to the Byers-Fenster relation used for Y* spin evaluation, the $(2J+1)^2$ relation was explicitly proposed for study of weak decay by Ademollo and Gatto (preprint from Frascati Laboratory, Sept. 1963). It has been used by H. K. Ticho et al on UCLA data (see Phys. Rev. Letters, 12, 482 (1964)). The evaluation of 2J+1 by moment comparison is discussed (for Y*'s) in a paper by Shafer and Huwe to appear in Phys. Rev., June 8, 1964.

also treated, but gave very large errors and thus further substantiated the spin 1/2 conclusion).

VI. K-63 BEAM

The K-63 separated K^- beam still in operation at the Bevatron is the highest-energy K^- experiment ever attempted at this accelerator. Because of the relatively small yield of K^-'s from the 6.2 BeV Bevatron, decay loss greater than that in a 200-ft. long path from target to bubble chamber would be intolerable. However, the lengths of separator (crossed E and B field devices used to separate K's from π's) accommodated in a 200-ft. beam are barely adequate to eliminate pions. Twenty feet of separator are used in the first stage and 30 feet of separator are in the second stage of the K-63 beam; these achieve ~~an~~ angles of separation between K's and π's of about 0.5 mrad. In contrast, the vertical acceptance of the beam channel is a total of 5 mrad; and the horizontal acceptance is a total of 20 mrad. To maintain beams of 2.5 BeV/c with about 90 percent K's it is necessary to hold the voltage over the 2-in. separator gap to $\leq$ 0.3 kV/in 500 kV error. The rejection of π's relative to K's is 7,000 to 10,000. A unique feature of Joe Murray's design is the use of a mass slit which is cocked to the beam at a very acute angle (in the horizontal plane) to accommodate the chromatically aberrated horizontal and vertical images; i.e., cocked mass slits are used instead of sextupole magnets or special shimming to handle chromatic effects. The beam has been operated with a momentum acceptance of 2 to 4 percent. The average of K's per picture (with approx. 1.5×10^{11} protons on target) has been 6 to 10.

FIGURE 23 shows the ray diagram for the first stage of the K-63 beam, as obtained with Dr. Murray's electronic analogue computer. With each sweep of a beam trajectory requiring a second, optimization of magnet settings could be made in minutes to an accuracy of better than 1%. Matrix language was used; and the lines diverging symmetrically from a point target at the left represent unit θ input. Vertical plane is at the top of the figure, and horizontal at the bottom.

VII. $\Xi K\pi$ STUDY FROM K-63 DATA

FIGURES 24 through 27 show some of the Dalitz plots for the $\Xi K\pi$ system obtained at 2.45, 2.6 and 2.7 BeV/c. In FIGURE 26, the 1530-MeV Ξ^* is especially prominent for the $\Xi^-\pi^+$ combination. FIGURE 28 is the $\Xi\pi$ mass spectrum obtained by CERN groups (including Norwegian, French and English collaborators) from 3.5 GeV/c K^- interactions yielding $\Xi K\pi$ and $\Xi K\pi\pi$ in the 1.15m freon bubble chamber; the higher peak at $\sim$1750 MeV was estimated to be a 2.4 to 3.0 standard-deviation effect (depending on the background estimate). FIGURE 29 presents the $\Xi\pi$ mass spectrum from K-63; no significant enhancement is seen except the established 1530-MeV Ξ^*.†

The same moment analysis described above has been carried out for the Ξ^* (1530) events in K-63 data. Spin 1/2 is definitely ruled out; spin 5/2 is not required; and parity for J = 3/2 is + rather than -. Our confidence limits are similar to those of UCLA, but the interference of the K^* tends to weaken them.

VIII. THE 959-MeV MULTI-PION RESONANCE IN K-63 DATA

In analysis work on K-63 $\Lambda n\pi$ data carried out chiefly by Kalbfleisch, a resonance was found at 959 MeV which manifested itself in a rather beautiful, narrow peak in the 5π mass spectrum (FIGURE 30). The observed width was 20 MeV and indicates a true width of $\leq$ 12 MeV. Other mass spectra have exhibited a less prominent peak: that of the neutral mass and of the ($(\pi^+\pi^-$ neutral) mass produced with a Λ (FIGURE 31).

† Note in proof: Since this talk was given, it has been fairly well established that there exists an S = -2 resonance at 1810 MeV which decays principally into $\Xi^*(1530)+\pi$ and $\Lambda+\bar{K}$. (G. Smith - See UCRL-11456)

However, the 3π mass spectrum and the 2π and 4π mass spectra exhibit no distinguishable peak at 959 MeV. (Evidence was found in the neutral mass spectrum by Samios, Leitner, et al in 2.2 BeV/c data at Brookhaven.) The resonance seems to decay predominantly into 2 pions plus an eta. The ratio of neutral ($\pi^0\pi^0\eta$) to charged ($\pi^+\pi^-\eta$) events indicates that T = 0. The 61 events of the 5π and the $\pi^+\pi^-$neutral type have been used to make a Dalitz plot of the $\pi^+\pi^-\eta$ system. Because the Dalitz plot is very nearly uniform and because $\hat{\pi}^+ \cdot \hat{\eta}$ is isotropic (FIGURE 32), the probable quantum numbers are $J^{PG} = 0^{-+}$. Such a particle could be the pseudoscalar singlet meson which Gell-Mann has suggested.

FIG. (1)

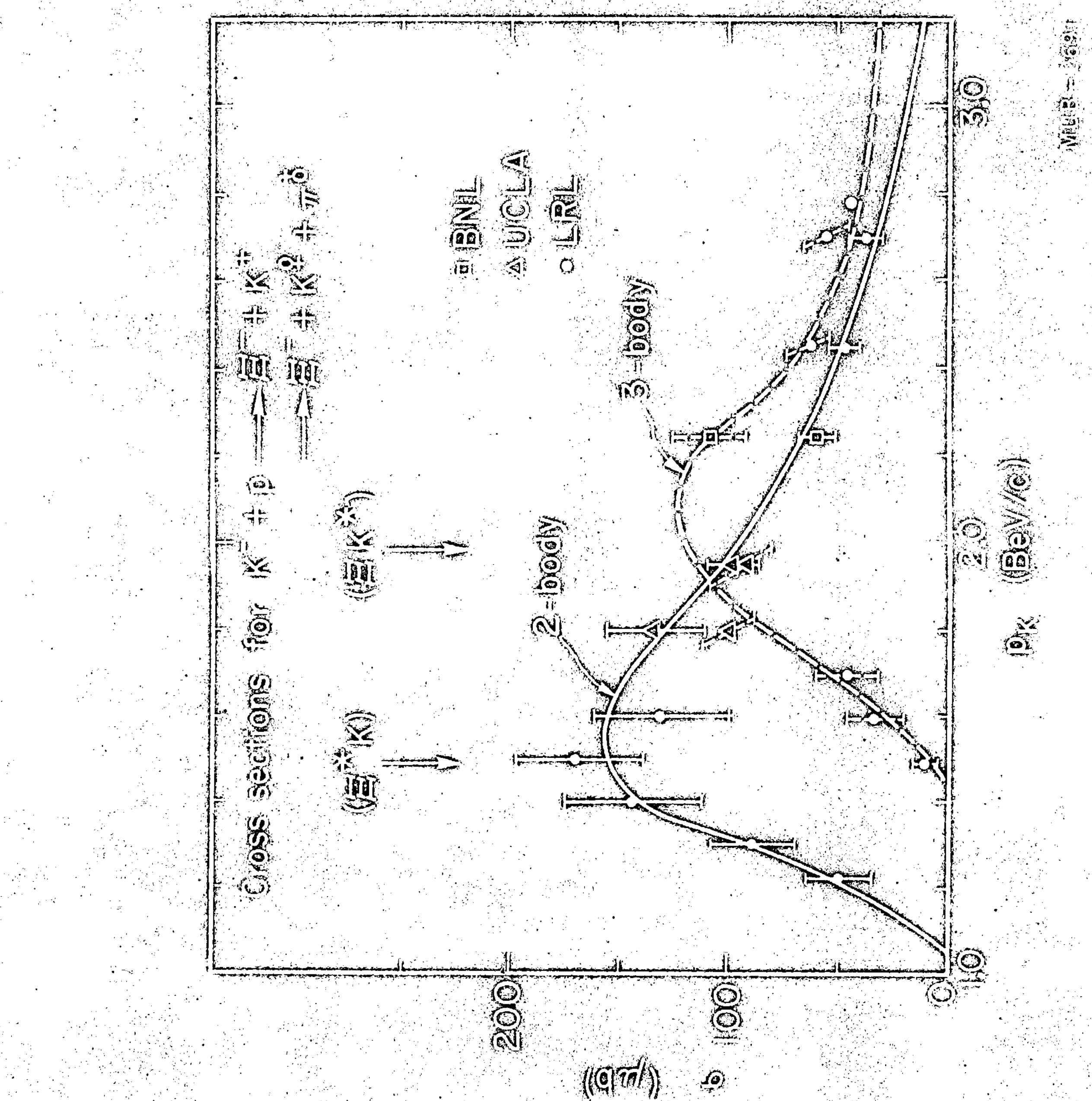

Cross sections for K⁻ + p → Ξ⁻ + K⁺
→ Ξ⁻ + K⁰ + π⁰
(Ξ*K)
(ΞK*)
2-body
3-body
▫ BNL
△ UCLA
○ LRL
σ (μb)
200
100
0
1.0
2.0
3.0
p_K (BeV/c)

FIG. 2

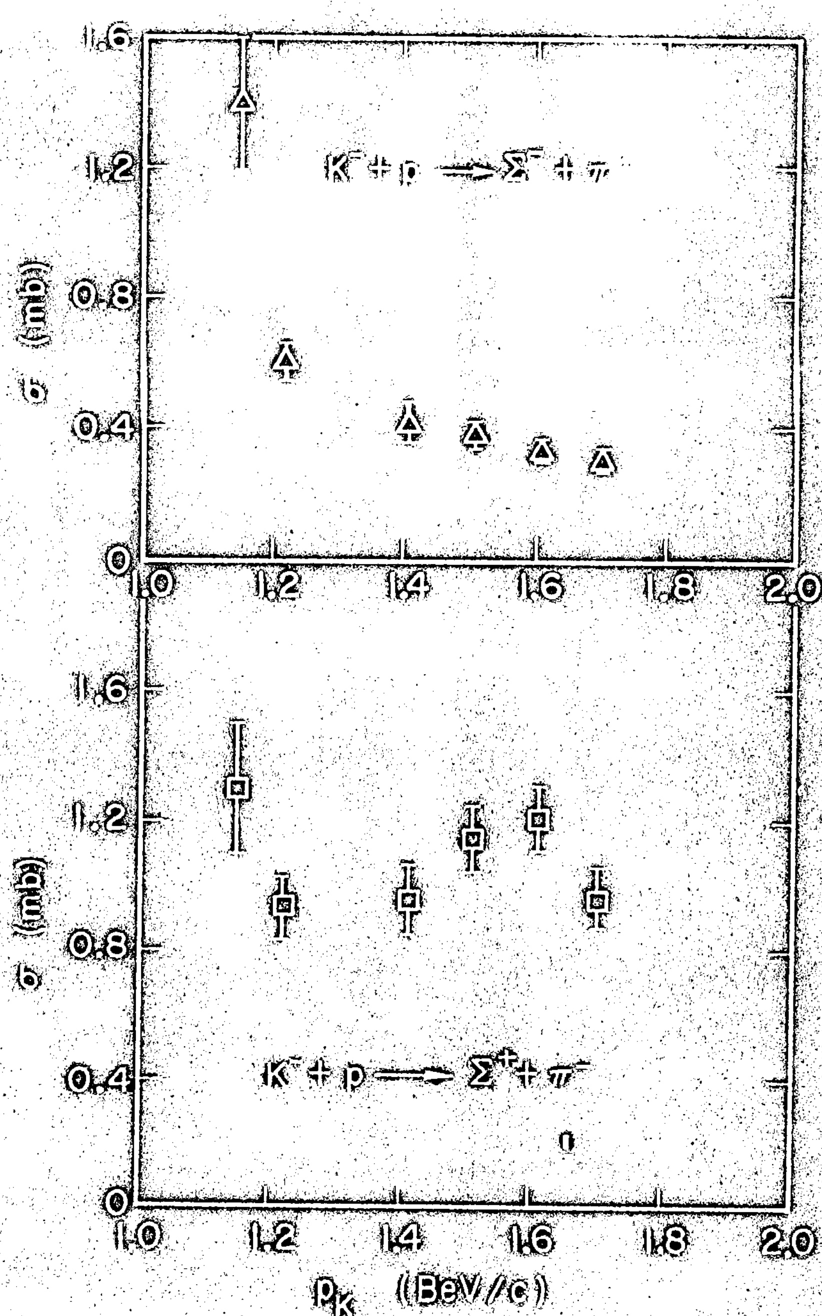

MUB-2690

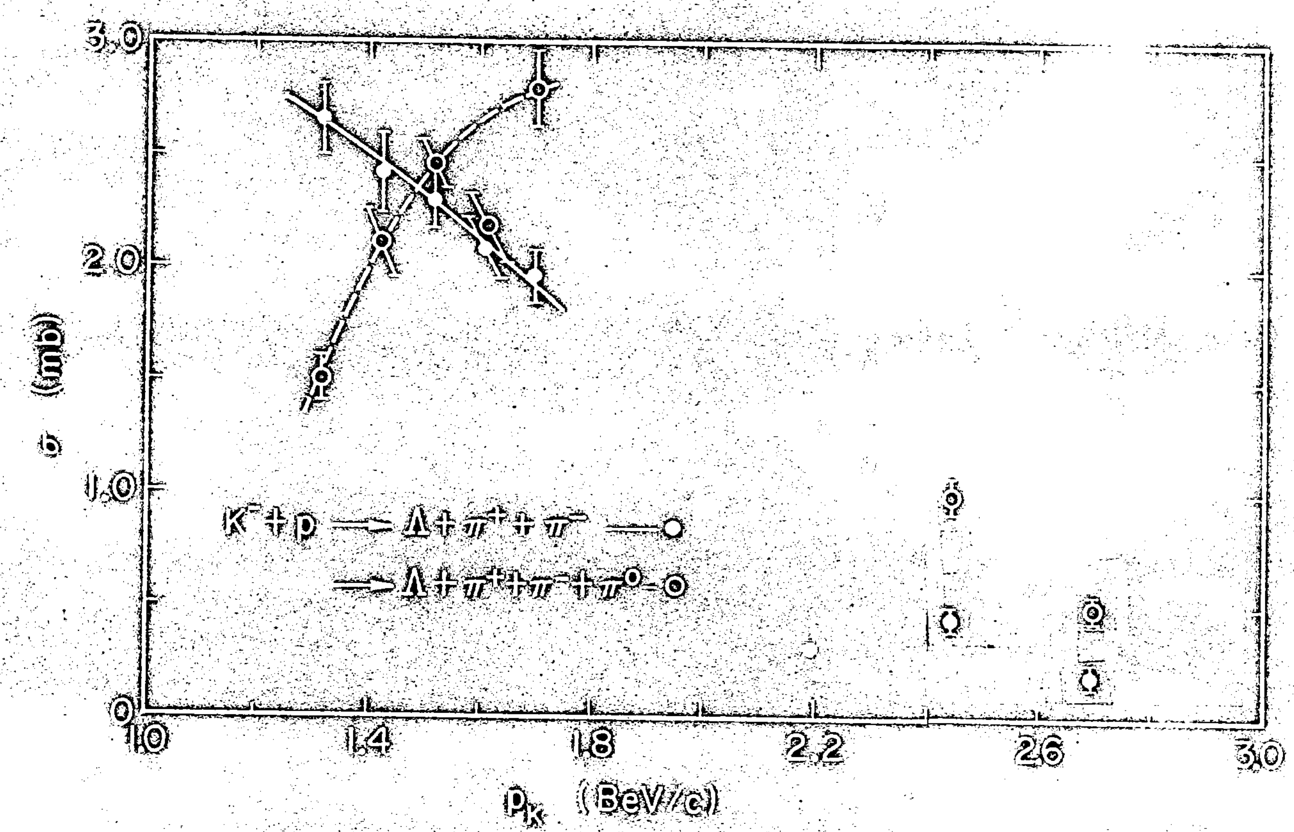

FIG. 3

FIG. ④

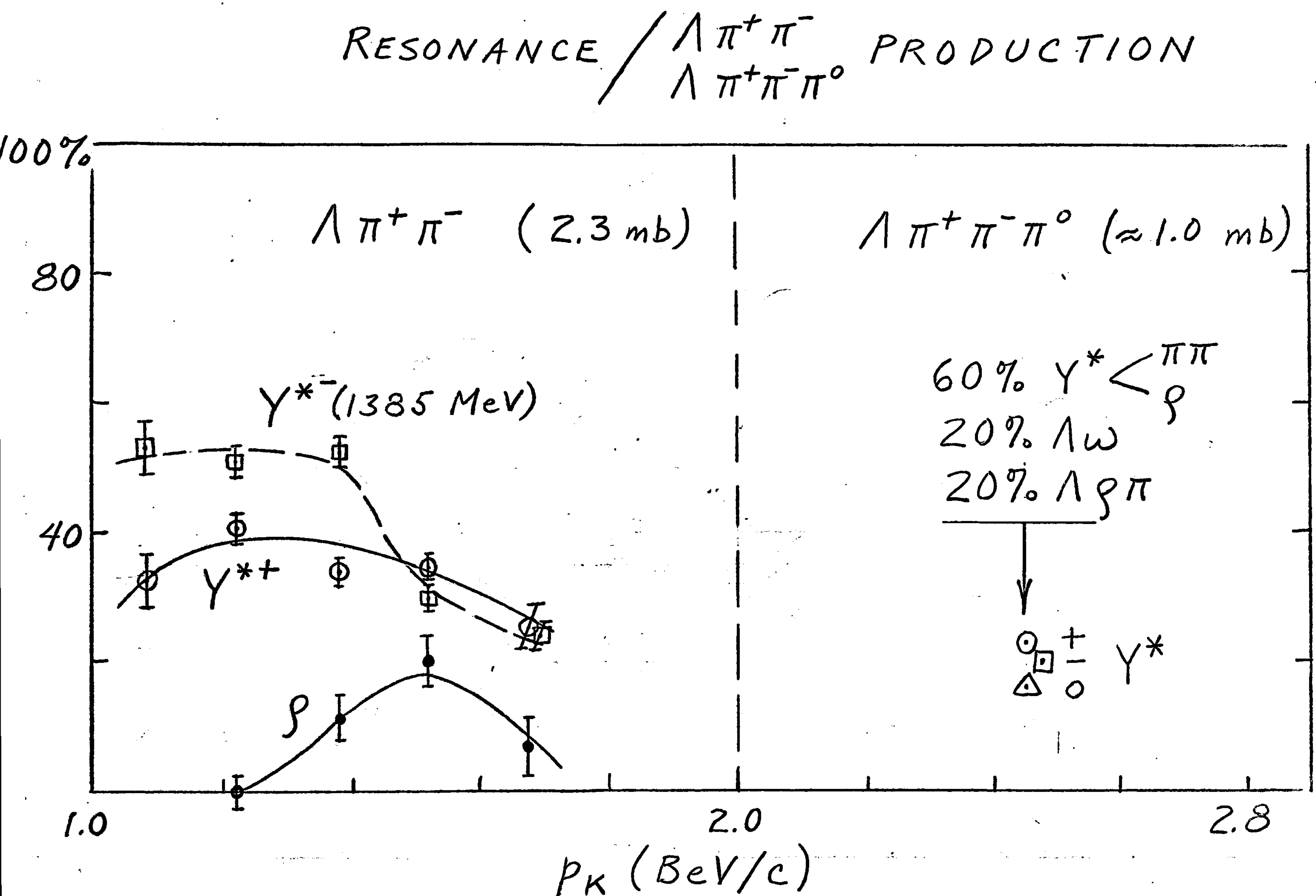

RESONANCE / $\Lambda\pi^+\pi^-$, $\Lambda\pi^+\pi^-\pi^0$ PRODUCTION
100%
80
40
$\Lambda\pi^+\pi^-$ (2.3 mb)
$\Lambda\pi^+\pi^-\pi^0$ (≈1.0 mb)
Y^{*-}(1385 MeV)
Y^{*+}
ρ
60% Y^* < ππ, ρ
20% Λω
20% Λρπ
Y^{*} +, −, 0
1.0
2.0
2.8
P_K (BeV/c)

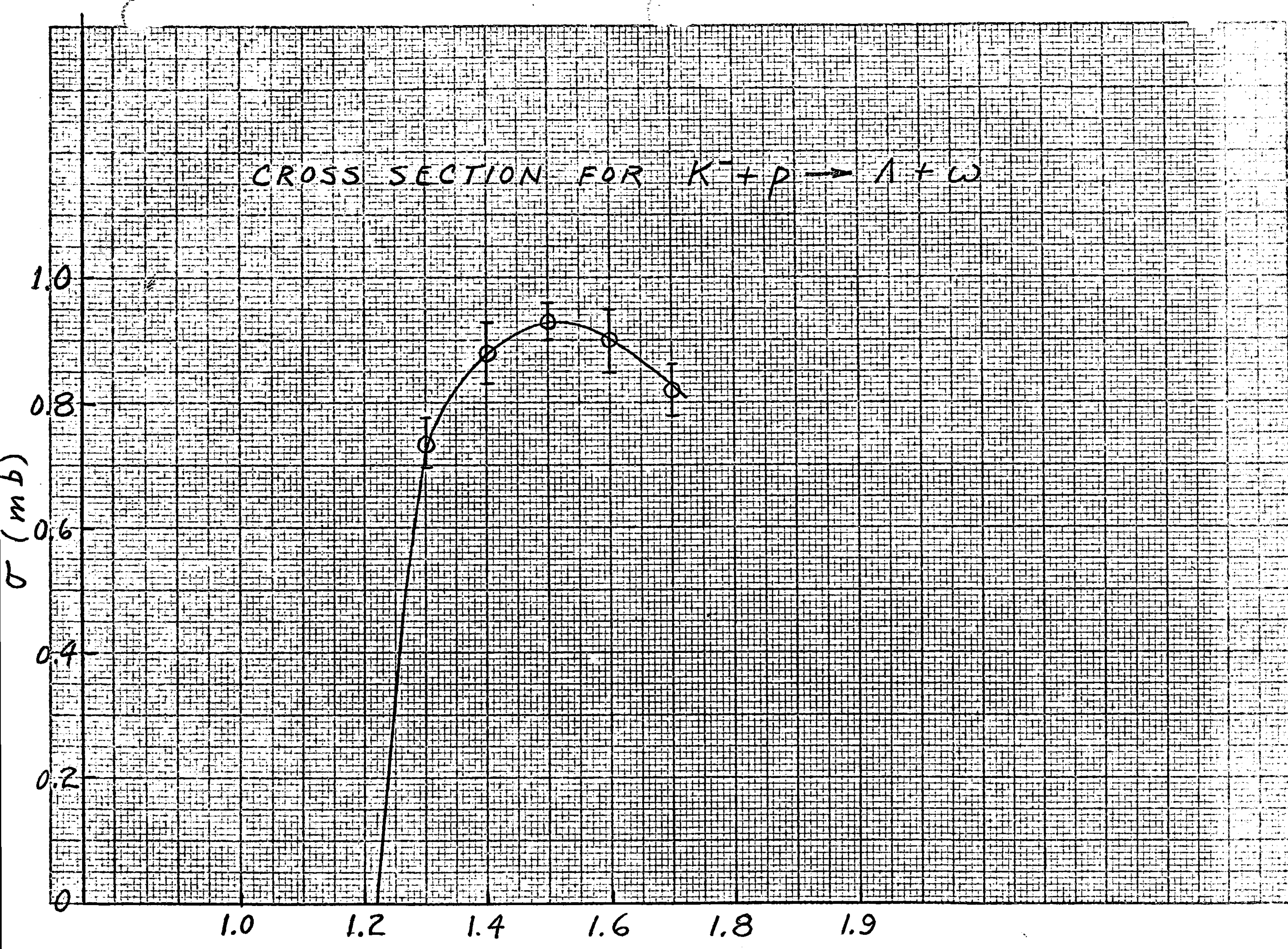
CROSS SECTION FOR $K^- + p \rightarrow \Lambda + \omega$
σ (mb)
1.0
0.8
0.6
0.4
0.2
0
1.0
1.2
1.4
1.6
1.8
1.9
P_{K^-} (BeV/c)

FIG. 5

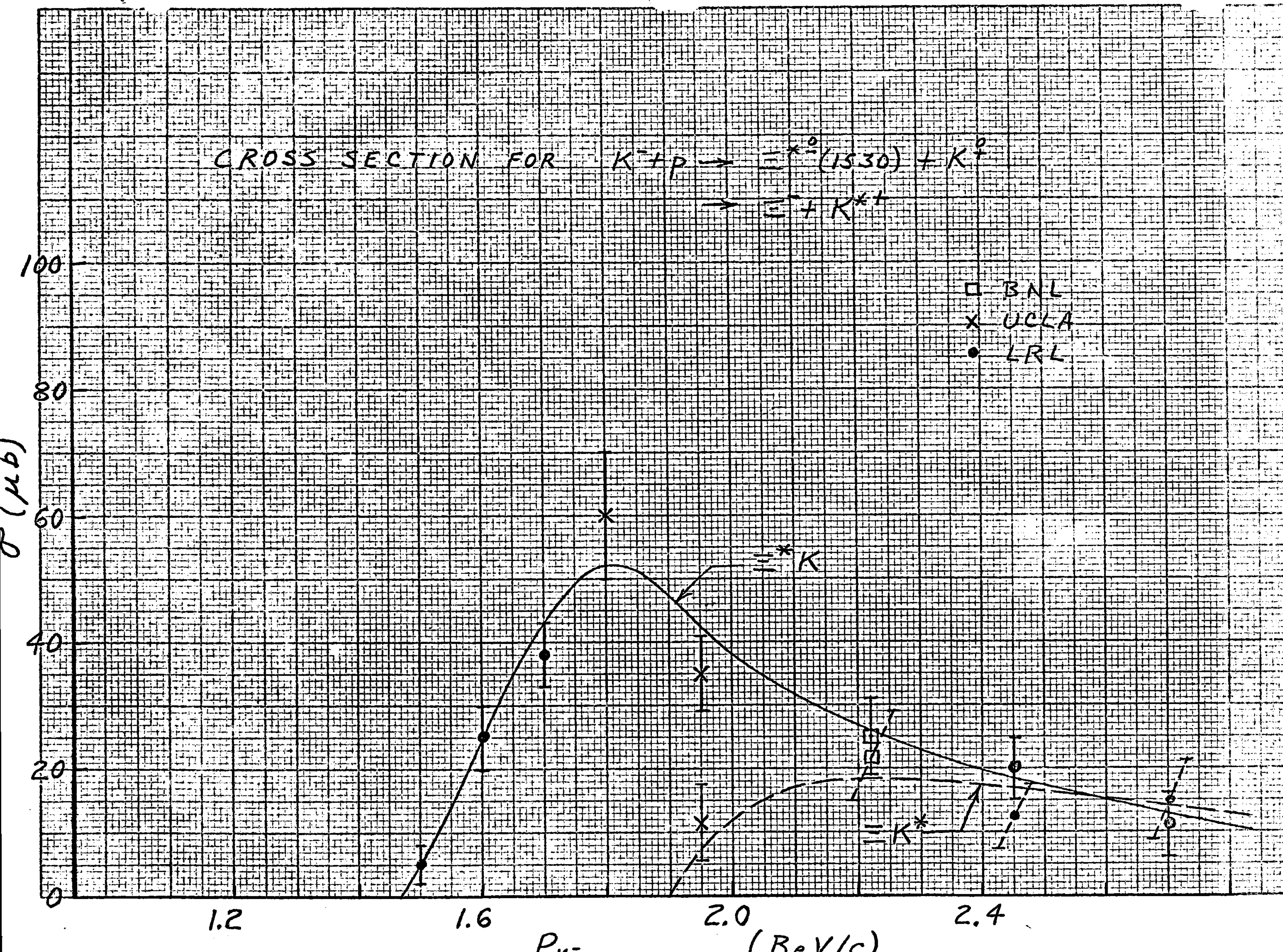
CROSS SECTION FOR $K^- + p \rightarrow \Xi^{*0}(1530) + K^0$
$\rightarrow \Xi^- + K^{*+}$
□ BNL
× UCLA
● LRL
$\Xi^* K$
ΞK^*
σ (μb)
100
80
60
40
20
0
1.2
1.6
2.0
2.4
P_{K^-} (BeV/c)

FIG. 6

FIG. 7

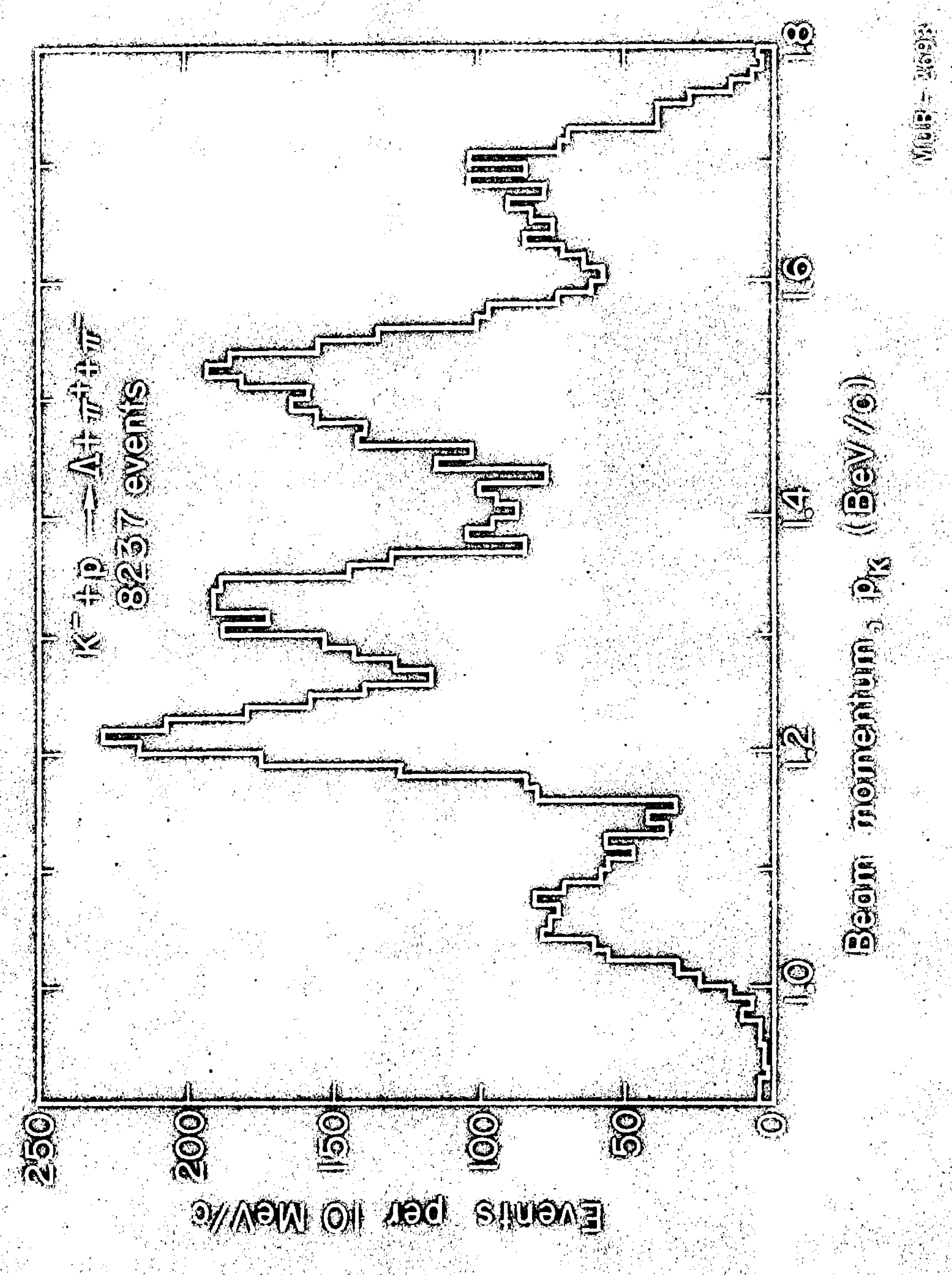

$K^- + p \rightarrow \Lambda + \pi^+ + \pi^-$
8237 events
Events per 10 MeV/c
0
50
100
150
200
250
1.0
1.2
1.4
1.6
1.8
Beam momentum, p_K (BeV/c)

FIG. 8

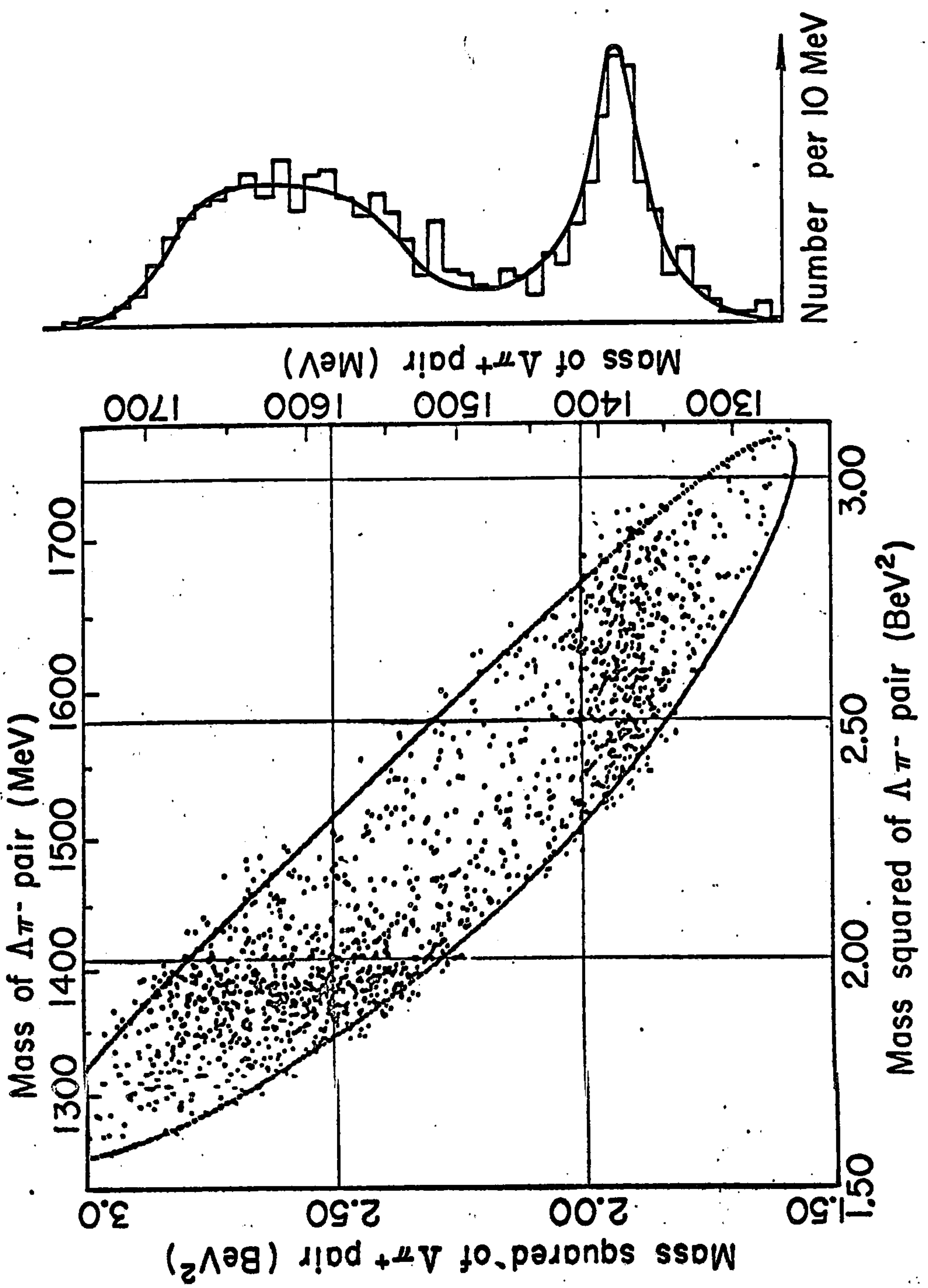

MUB-1576

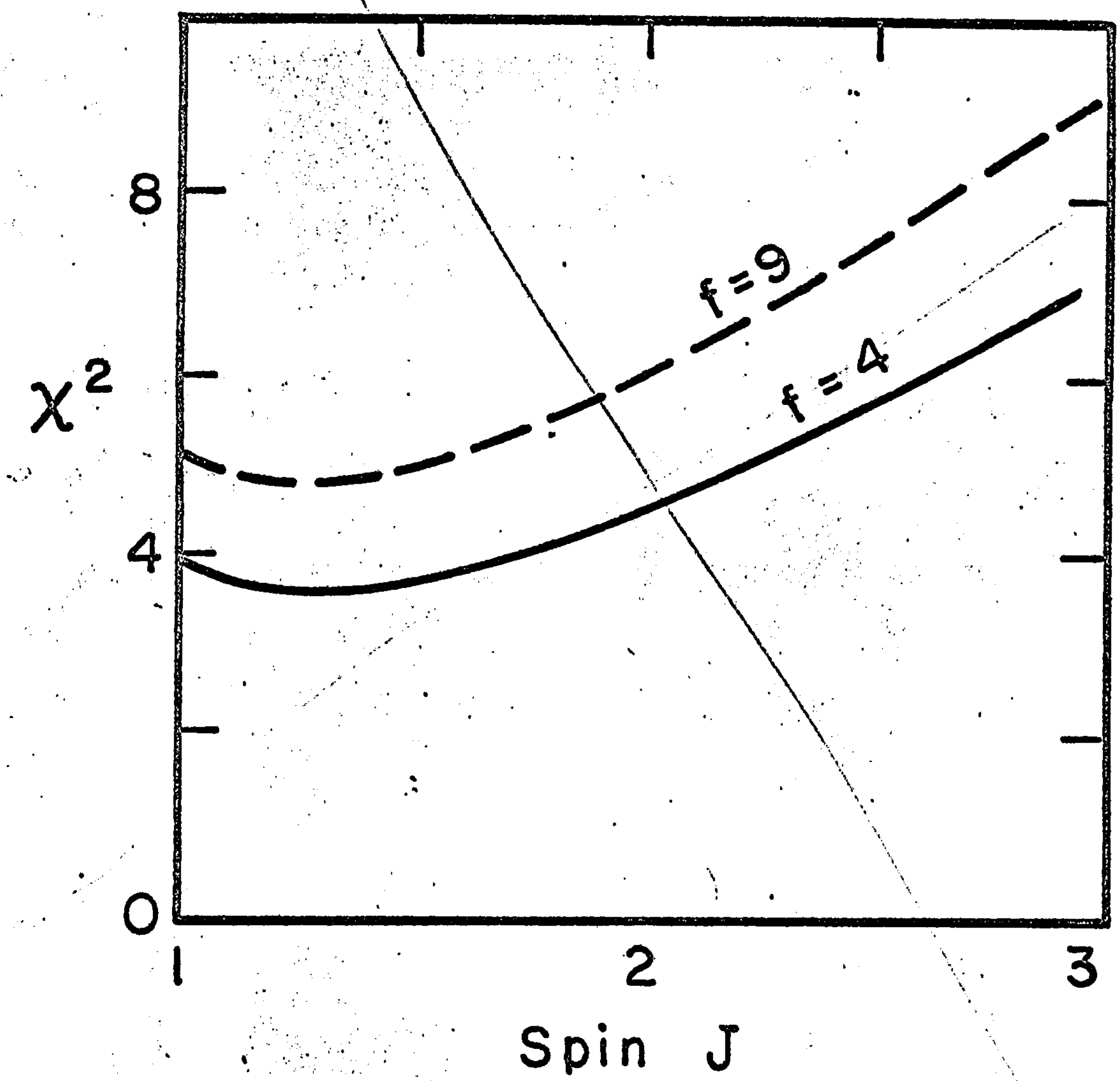

MU-32798

FIG. 9

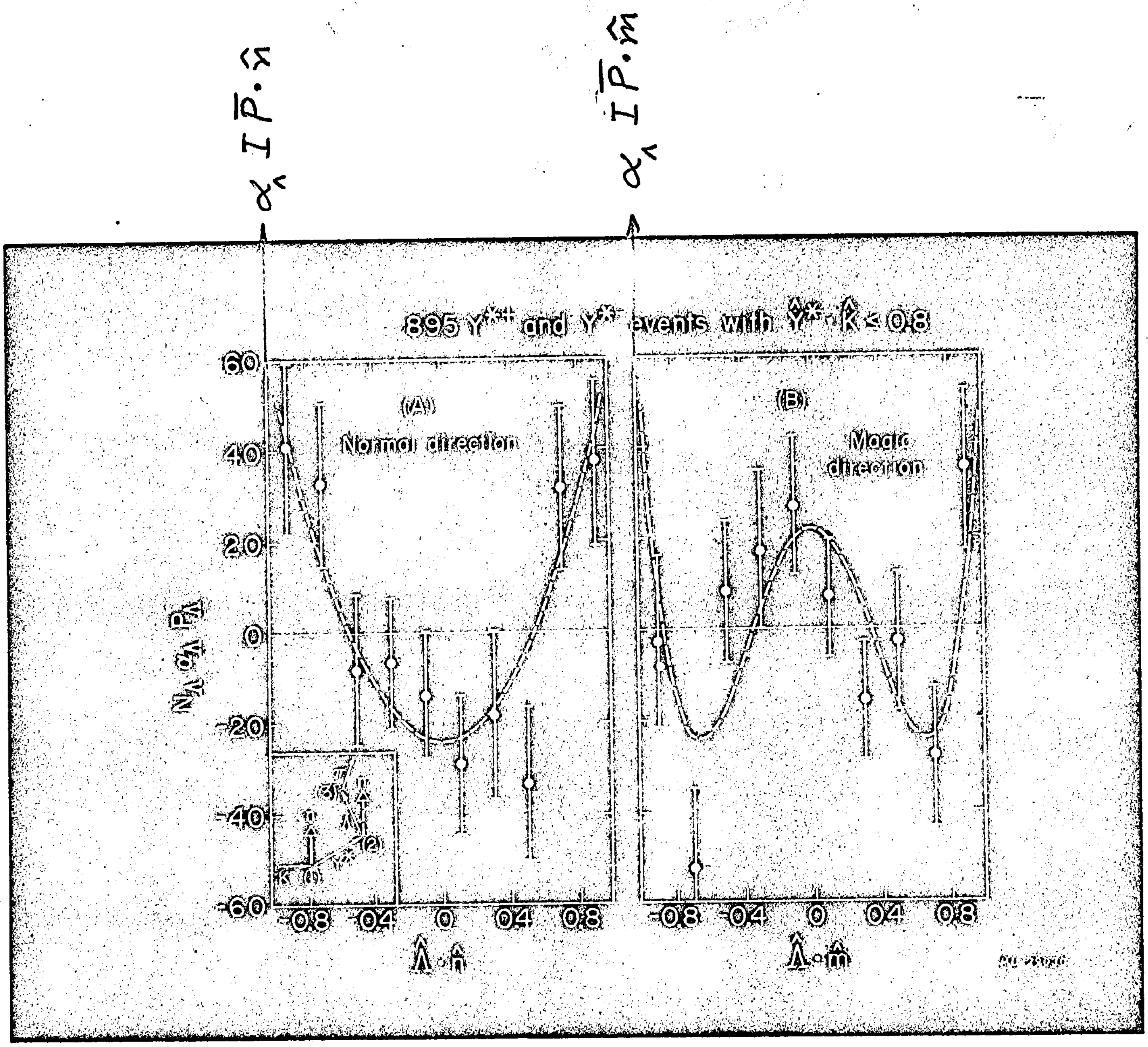

895 Y*+ and Y*- events with Ŷ*·K̂ < 0.8
(A)
Normal direction
(B)
Magic
direction
$N_\Lambda \alpha_\Lambda P_\Lambda$
60
40
20
0
-20
-40
-60
-0.8
-0.4
0
0.4
0.8
$\hat{\Lambda}\cdot\hat{n}$
$\hat{\Lambda}\cdot\hat{m}$
$\alpha_\Lambda I \bar{P}\cdot\hat{n}$
$\alpha_\Lambda I \bar{P}\cdot\hat{m}$

BYERS-FENSTER MOMENT EXPRESSIONS

Strong Decay

$$I(\theta,\phi) = \sum_{L,M} n_{L0}\, t_{LM}\, Y^*_{LM}(\theta,\phi) \text{ — } L \text{ even}$$

$$IP_{\parallel}(\theta,\phi) = \sum_{L,M} n_{L0}\, t_{LM}\, Y^*_{LM}(\theta,\phi) \text{ — } L \text{ odd}$$

M even

$$IP_x + i\,IP_y \equiv IP_{\perp}(\theta,\phi) = -\sum_{L,M} n_{L1} \sqrt{\frac{2L+1}{4\pi}}\, \gamma\, t_{LM}\, \mathcal{D}^{L}_{M1}$$

L odd

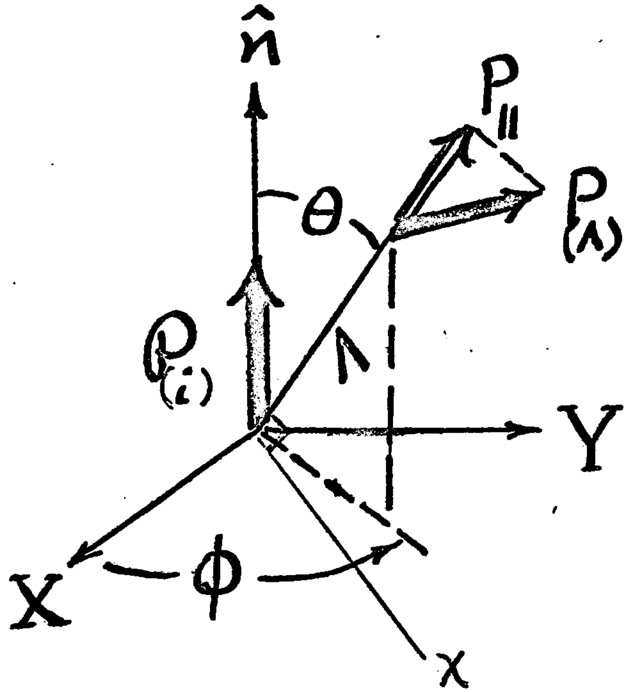

$$n_{L0} = (-)^{J-1/2} \sqrt{\frac{2J+1}{4\pi}}\; C(J,J,L;\tfrac{1}{2},-\tfrac{1}{2})$$

$$n_{L1} = \frac{2J+1}{\sqrt{L(L+1)}}\, n_{L0}$$

FIG. (10)

Error: $\delta(\mathrm{Re}\, t_{LM}) = \frac{1}{n_{L0}} \left\{ \sum_{k=1}^{N} (\mathrm{Re}\, Y_{LM})_k^2 (p \cdot \Lambda)_k^2 - \left(\Sigma \frac{\mathrm{Re}\, Y_{2M}\, p}{N} \cdot \Lambda \right)^2 \right\}^{1/2} \left(\frac{3}{\alpha_\Lambda N} \right)$

MOMENTS FROM EXPERIMENT

$$I(\theta,\phi) \Longrightarrow n_{L0}\,{}^{Re}t_{LM} = \left[\sum_{k=1}^{N} Re\,Y_{LM}(\theta_k,\phi_k)\right]\left(\tfrac{1}{N}\right)$$

$$I P_{\parallel}(\theta,\phi) \Longrightarrow n_{L0}\,{}^{Re}_{Im}t_{LM} = \left[\sum_{k=1}^{N} {}^{Re}_{Im}Y_{LM}(\ \ )\ \hat{p}_k \cdot \hat{\Lambda}_k\right]\left(\frac{3}{\hat{\alpha} N}\right)$$

$$I P_{\perp}(\theta,\phi) \Longrightarrow \gamma\, n_{L1}\,{}^{Re}_{Im}t_{LM} =$$

$$\sqrt{\frac{2L+1}{4\pi}}\left[\sum_{k=1}^{N} {}^{Re}_{Im}\mathcal{D}^{L^*}_{M1}(\phi_k,\theta_k,0)\ P_{\perp}(\theta_k,\phi_k)\right]\left(\frac{1}{N}\right)$$

$$= \frac{1}{\sqrt{2L+1}}\left[\sum_{m}\sum_{k=1} A_L\ {}^{Re}_{Im}Y^{M-m}_{L-1}(\theta_k\phi_k)\ Y^{m}_{1}(\Theta_k,\Phi_k) + \sum\sum_{k}\cdots\ Y_{L+1}\ \cdots\ Y^{m}_{1}\ \right]\left(\frac{3}{\alpha N}\right)$$

↑ (Λ)   ↑ (P)

$$\chi^2 = \sum_{i,j}\left(t^{\parallel}_i - \frac{\gamma t^{\perp}_i}{\gamma'}\right) G^{-1}_{ij}\left(t^{\parallel}_j - \frac{\gamma t^{\perp}_j}{\gamma'}\right)$$

$$\gamma(2J+1) = \sqrt{L(L+1)}\ \frac{(n_{L1}\,\gamma\, t_{LM})}{(n_{L0}\, t_{LM})}$$

FIG. (11)

FIG. 12

Table I. t_L^M moments.

A. from $I(\theta, \phi)$

J	L	M	Re t_L^M	Im t_L^M
1/2, 3/2, 5/2	0	0	1.0000	
3/2	2	+2	-0.018±0.022	-0.028±0.023
	2	0	-0.118±0.034	
5/2	2	+2	-0.017±0.021	-0.026±0.021
	2	0	-0.110±0.032	
	4	+4	-0.025±0.024	-0.011±0.024
	4	+2	0.014±0.025	0.042±0.025
	4	0	0.027±0.037	

B. from $I\overline{P}(\theta, \phi)$ - Longitudinal component

J	L	M	Re t_L^M	Im t_L^M
1/2	1	0	-0.019±0.100	
3/2	1	0	-0.043±0.225	
	3	+2	-0.134±0.048	-0.066±0.051
	3	0	0.247±0.073	
5/2	1	0	-0.066±0.343	
	3	+2	-0.246±0.088	-0.121±0.094
	3	0	0.454±0.134	
	5	+4	0.046±0.042	0.025±0.043
	5	+2	0.045±0.044	0.008±0.046
	5	0	0.030±0.065	

C. from $I\overline{P}(\theta, \phi)$ - Transverse component

J	L	M	γ Re t_L^M	γ Im t_L^M
1/2	1	0	-0.051±0.061	
3/2	1	0	-0.056±0.068	
	3	+2	-0.077±0.041	0.040±0.041
	3	0	0.272±0.058	
5/2	1	0	-0.057±0.070	
	3	+2	-0.095±0.050	0.048±0.050
	3	0	0.332±0.071	
	5	+4	0.026±0.037	-0.029±0.038
	5	+2	0.012±0.038	
	5	0	0.015±0.055	

FIG. 13

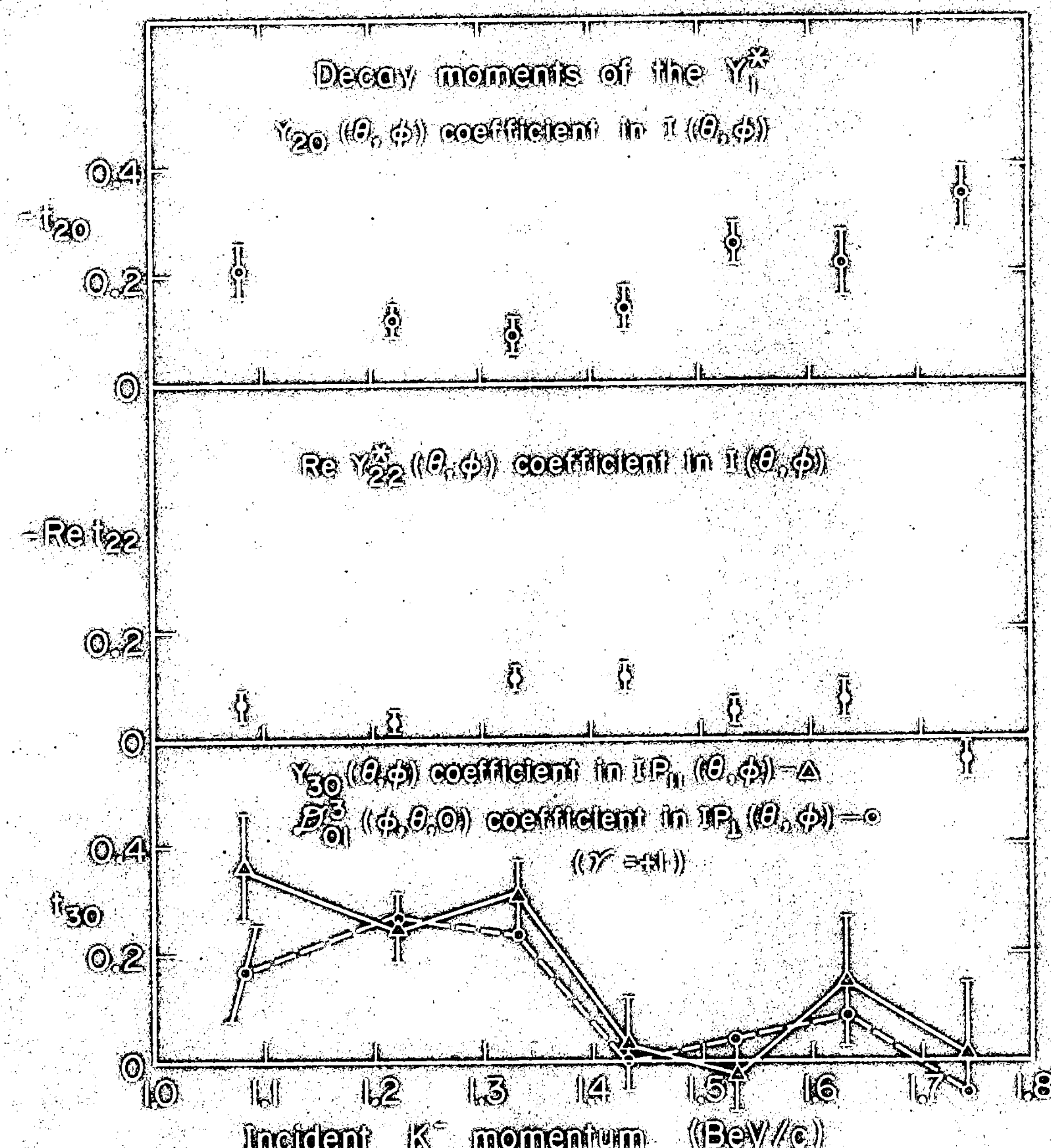

MUB-2696

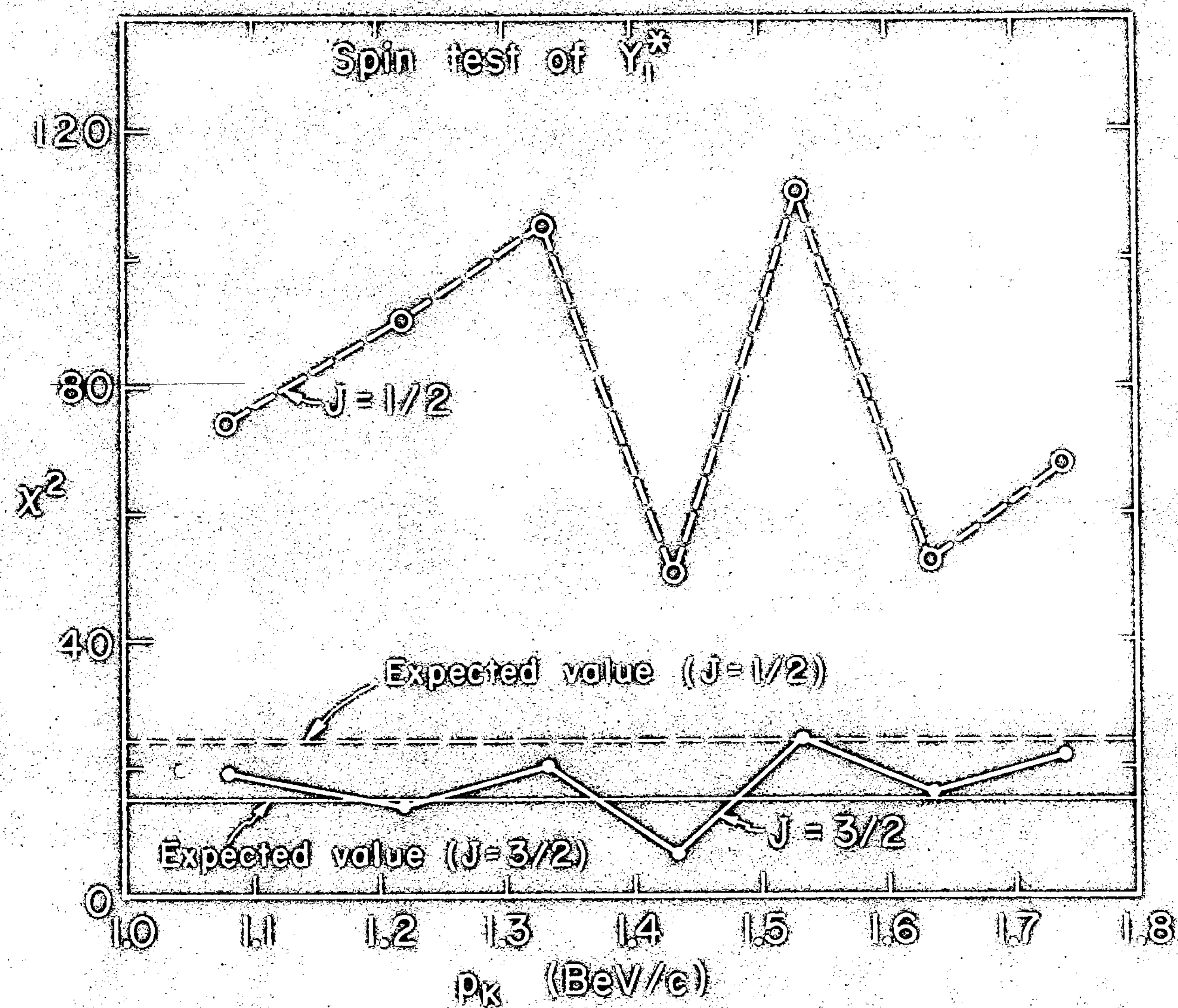

MUB - 2694

FIG. 14

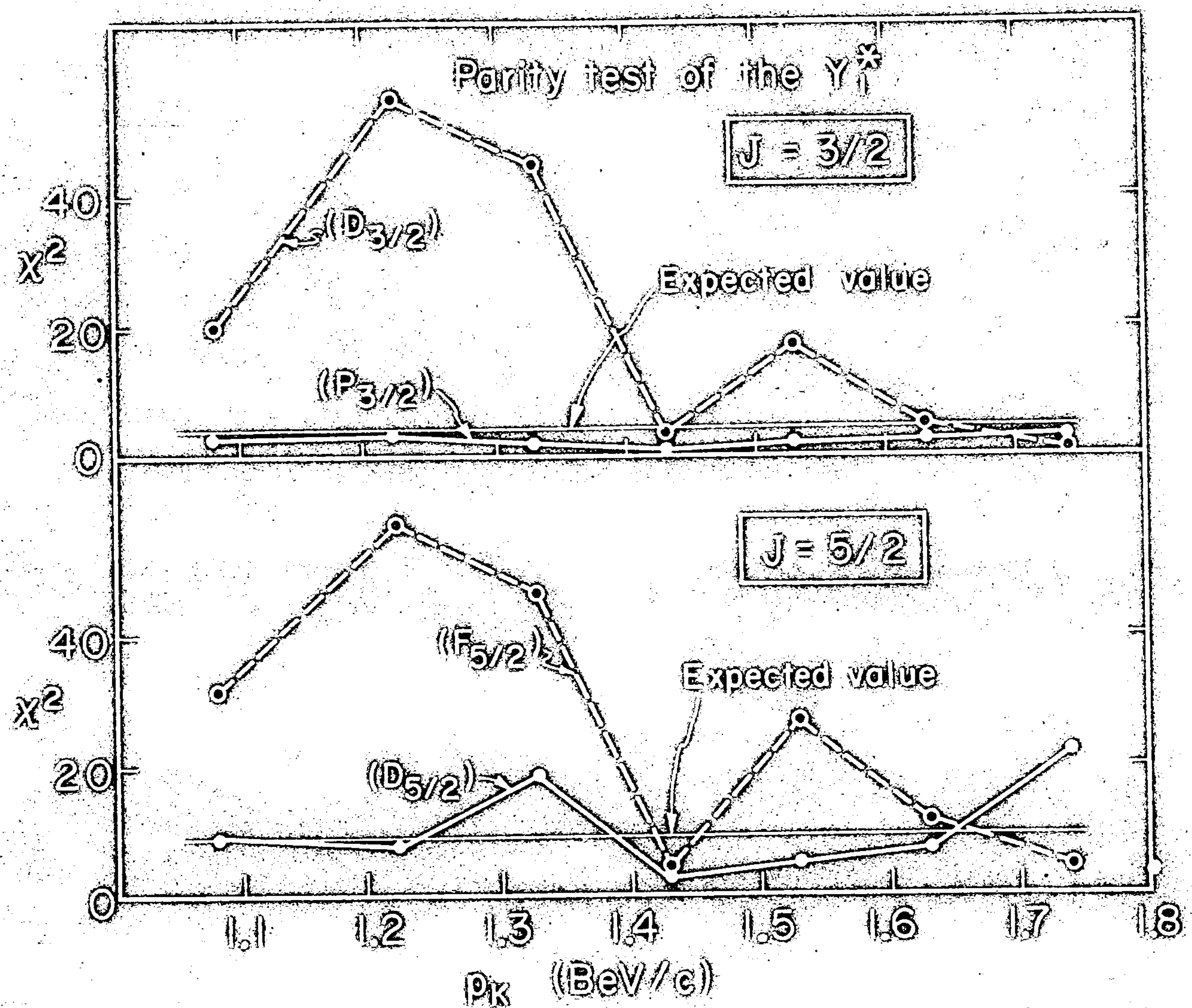

MUB - 2695

FIG. 15

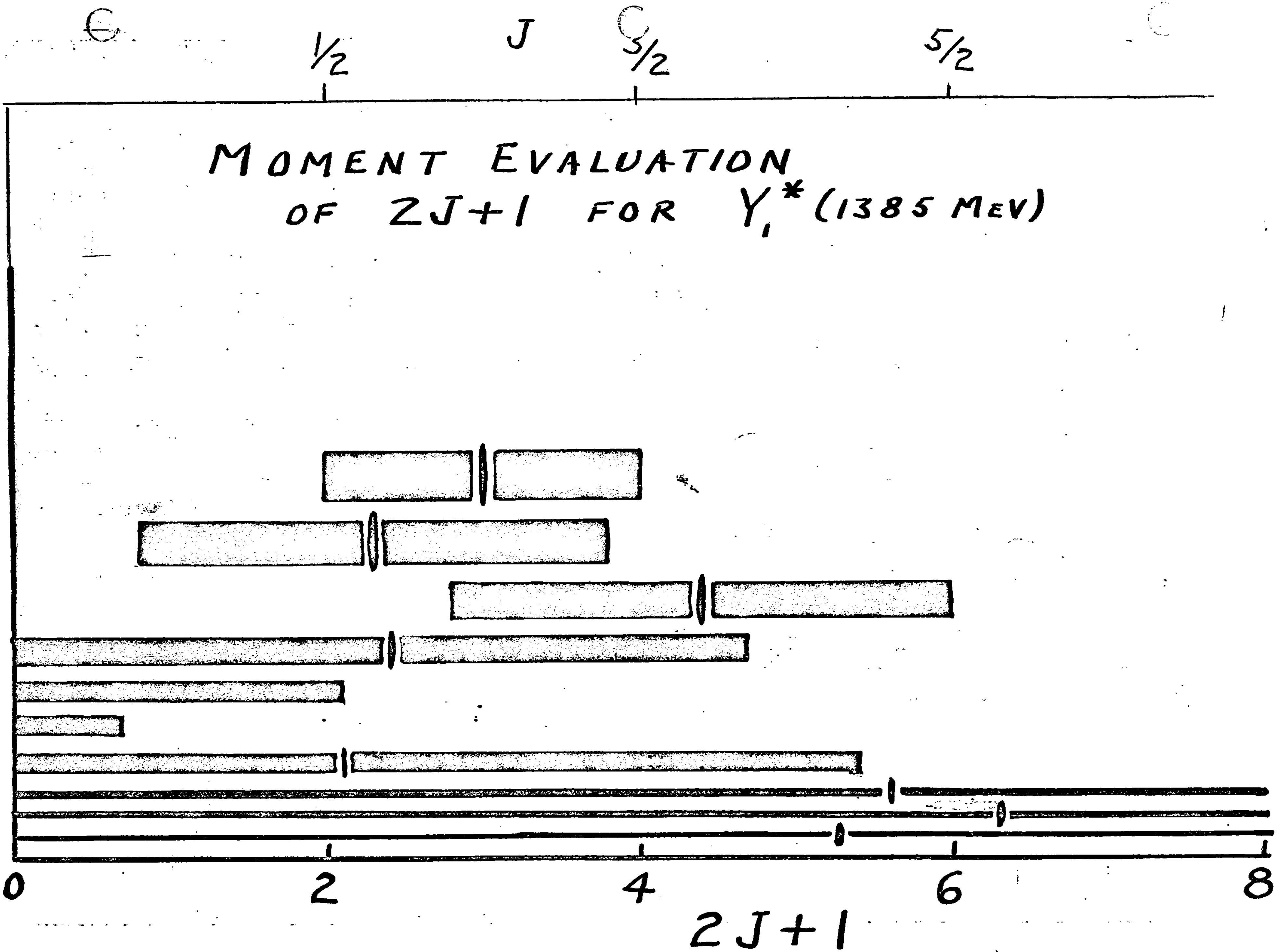

FIG. (16)

FIG. 17

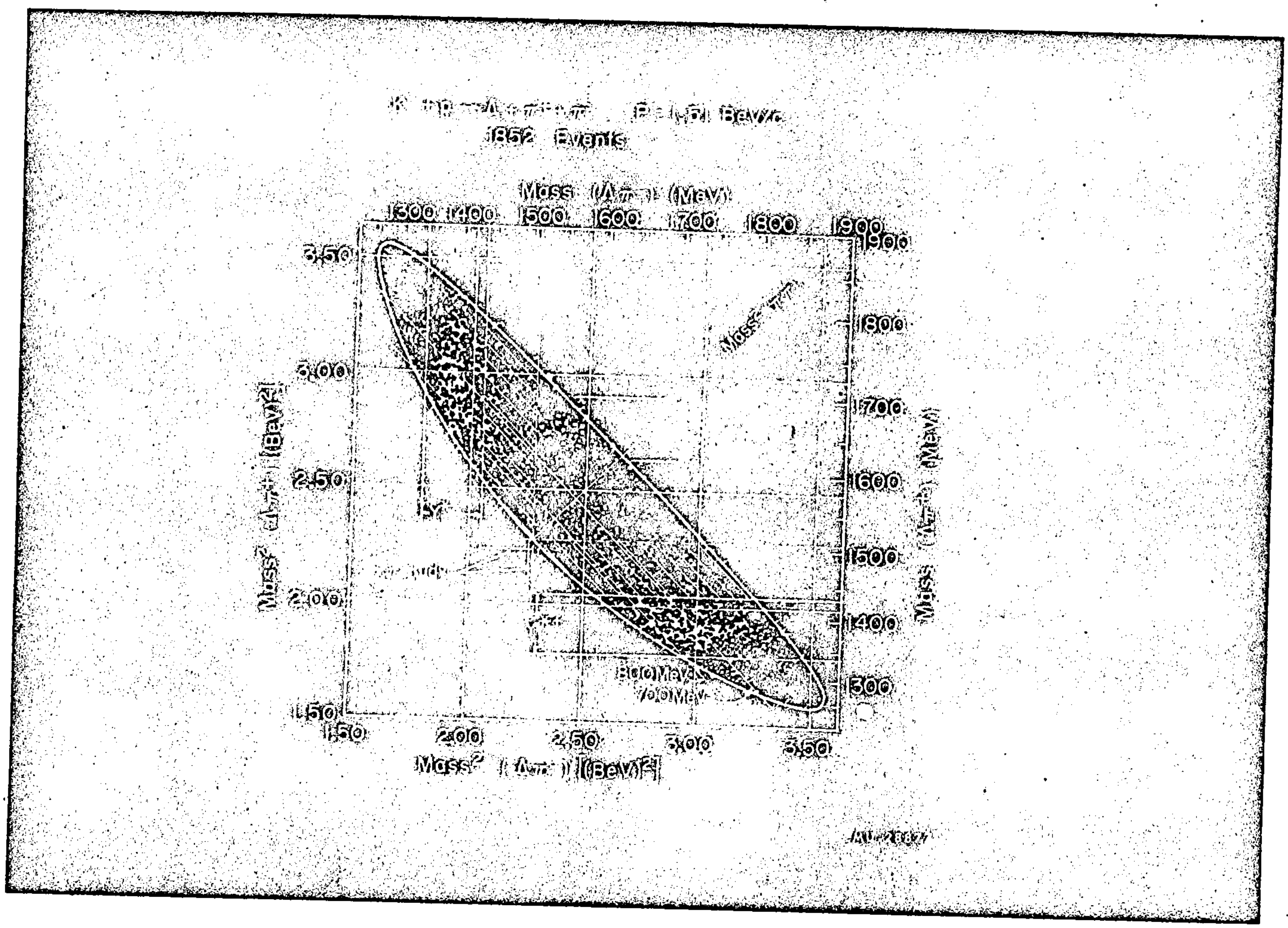

1852 Events
1300 1400 1500 1600 1700 1800 1900
1900
1800
1700
1600
1500
1400
1300
3.50
3.00
2.50
2.00
1.50
1.50 2.00 2.50 3.00 3.50
800MeV
700MeV

FIG. 18

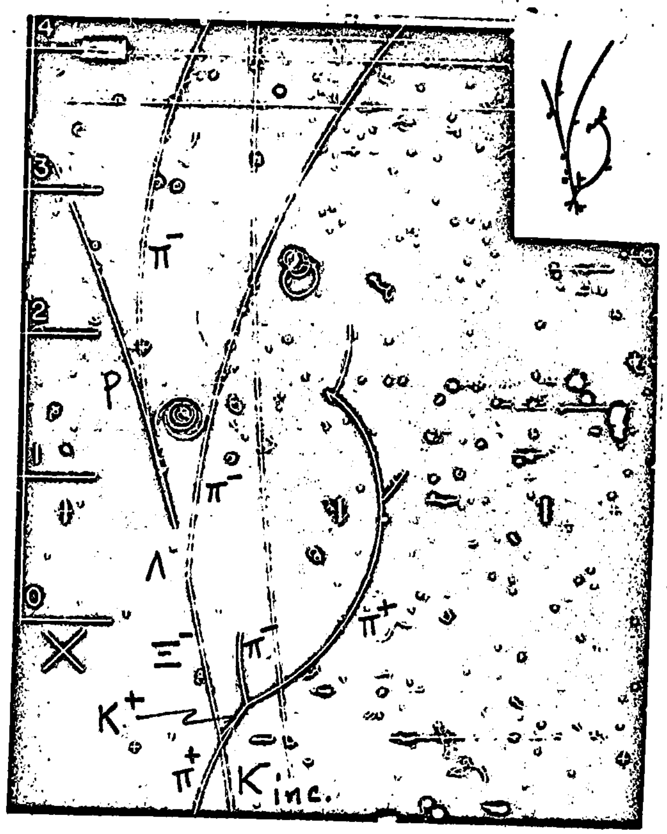

PRODUCTION AND DECAY OF A XI MINUS AND A K PLUS TAU DECAY

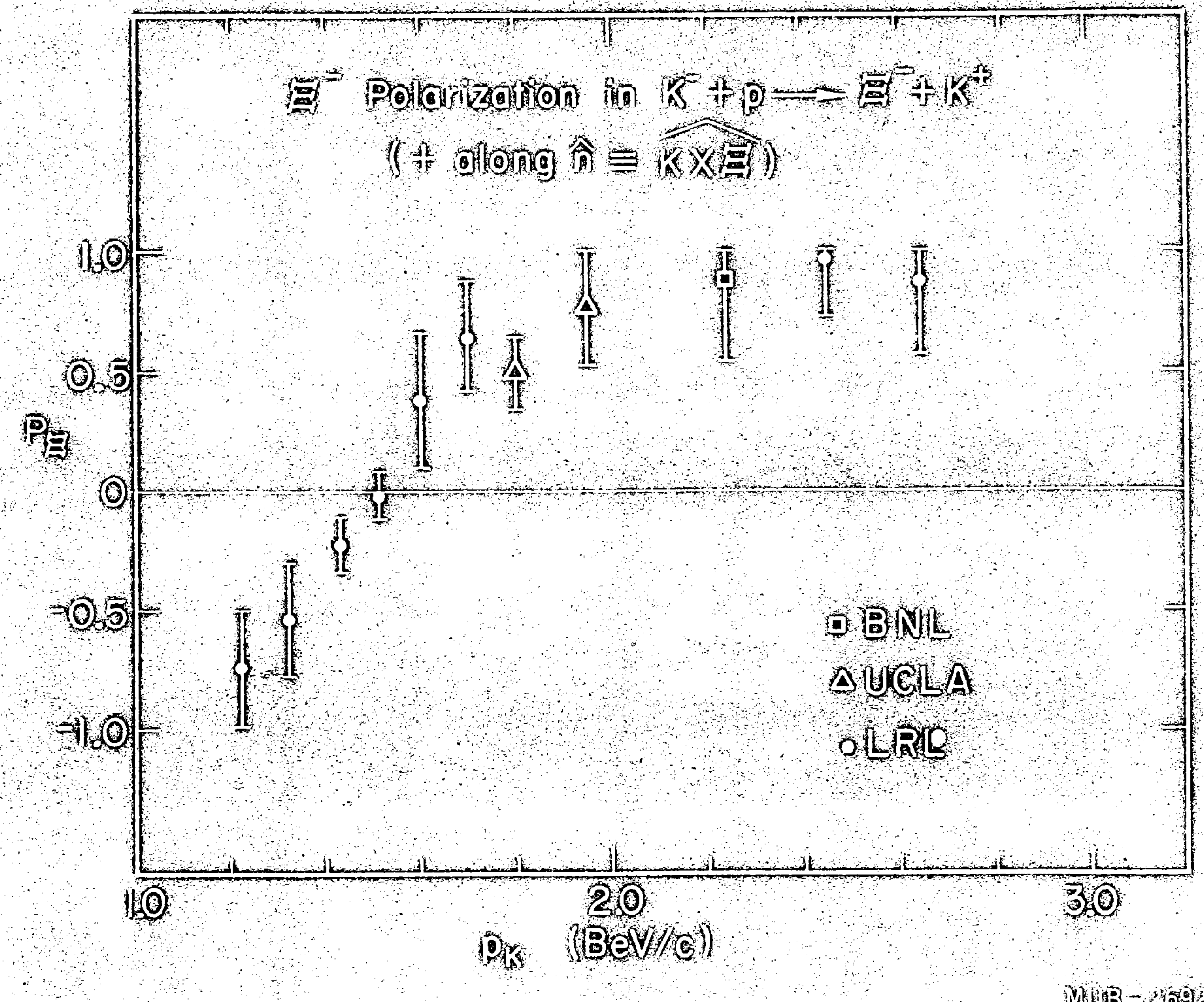

Ξ^- Polarization in $K^- + p \longrightarrow \Xi^- + K^+$
$(+ \text{ along } \hat{n} \equiv \widehat{K \times \Xi})$
1.0
0.5
P_Ξ
0
-0.5
-1.0
▫ BNL
△ UCLA
∘ LRL
1.0
2.0
3.0
p_K (BeV/c)
MUB-2692

FIG. (19)

BYERS-FENSTER MOMENT EXPRESSIONS

Weak Decay

even L — odd L

$$I(\theta,\phi) = \sum_{L,M} n_{L0}\, t_{LM}\, Y^*_{LM} + \Big(\sum_{L,M} n_{L0}\, t_{LM}\, Y^*_{LM}\Big)\,\alpha$$

Λ — α_Ξ

$$IP_{\parallel}(\;) = \alpha \sum n_{L0}\, t_{LM}\, Y^*_{LM} + \sum n_{L0}\, t_{LM}\, Y^*_{LM}$$

α_Ξ

$$IP_{\perp}(\theta,\phi) = -(\gamma + i\beta) \sum \frac{n_{L1}}{\text{[illegible]}} \sqrt{\frac{2L+1}{4\pi}}\, \mathcal{D}^L_{M1}(\phi,\theta,0)\, t_{LM}$$

$$\mathcal{L} = \prod_{k=1}^{N} \Big\{ I(k) + \alpha_\Lambda \Big[IP_{\parallel}(k)\, \hat{p}_k \cdot \hat{\Lambda}_k + IP_x\, \hat{p}\cdot\hat{x} + IP_y\, \hat{p}\cdot\hat{y} \Big] \Big\}$$

$$(2J+1)^2 = L(L+1)\, \frac{(\beta\, n_{L1}\, t_{LM})^2 + (\gamma\, n_{L1}\, t_{LM})^2}{(n_{L0}\, t_{LM})^2 (1-\alpha^2)}$$

FIG. 20

FIG. 21

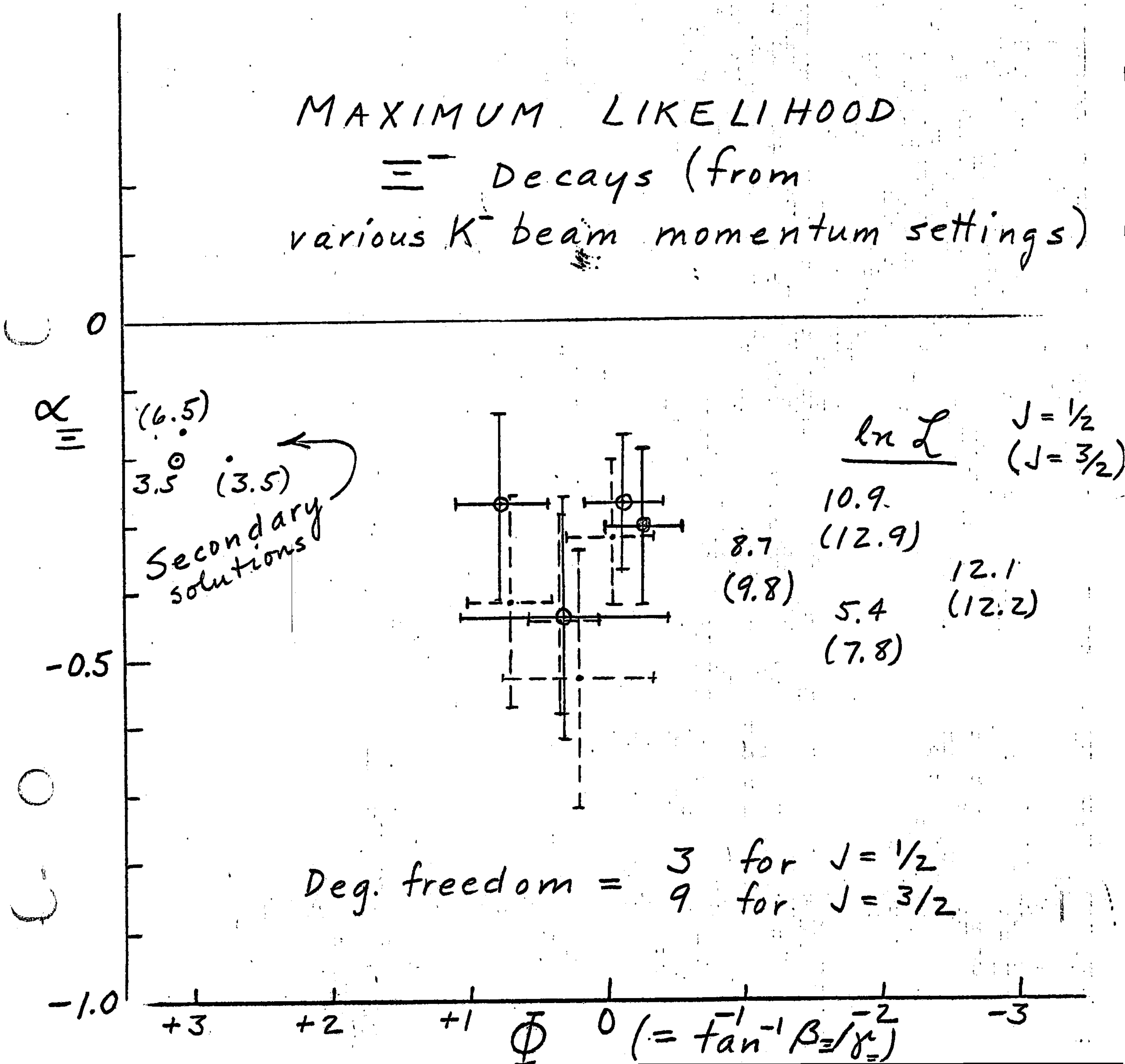
MAXIMUM LIKELIHOOD
Ξ⁻ Decays (from various K⁻ beam momentum settings)
α_Ξ
0
-0.5
-1.0
(6.5)
3.5
(3.5)
Secondary solutions
ln ℒ
J = ½
(J = 3/2)
10.9
(12.9)
8.7
(9.8)
12.1
(12.2)
5.4
(7.8)
Deg. freedom = 3 for J = ½
9 for J = 3/2
+3
+2
+1
0
-1
-2
-3
Φ (= tan⁻¹ β_Ξ/γ_Ξ)

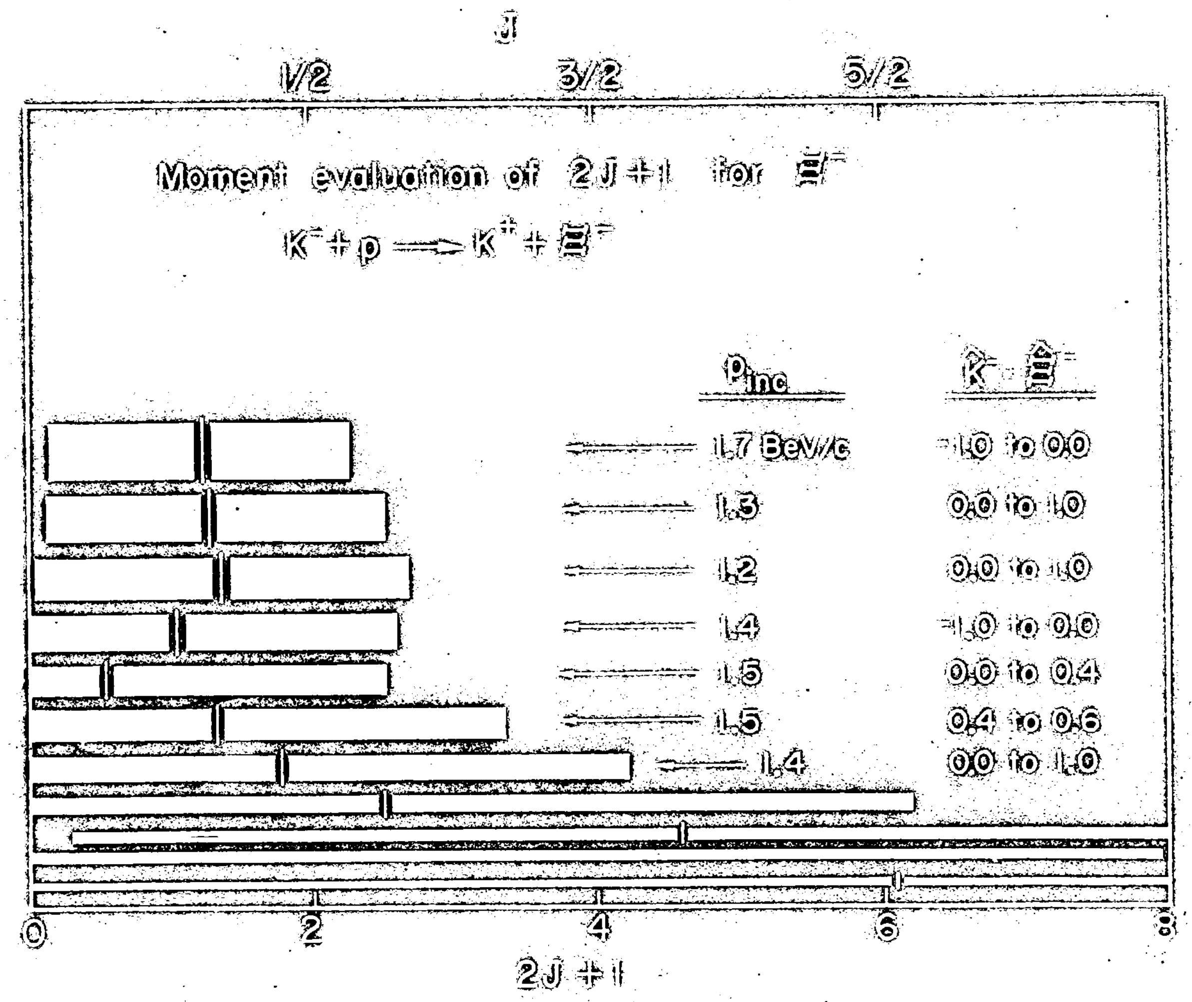

J
1/2
3/2
5/2
Moment evaluation of 2J + 1 for Ξ⁻
K⁻ + p ⟶ K⁺ + Ξ⁻
p_inc
1.7 Bev/c
1.3
1.2
1.4
1.5
1.5
1.4
-1.0 to 0.0
0.0 to 1.0
0.0 to 1.0
-1.0 to 0.0
0.0 to 0.4
0.4 to 0.6
0.0 to 1.0
0
2
4
6
8
2J + 1

FIG. 22

FIG. 23

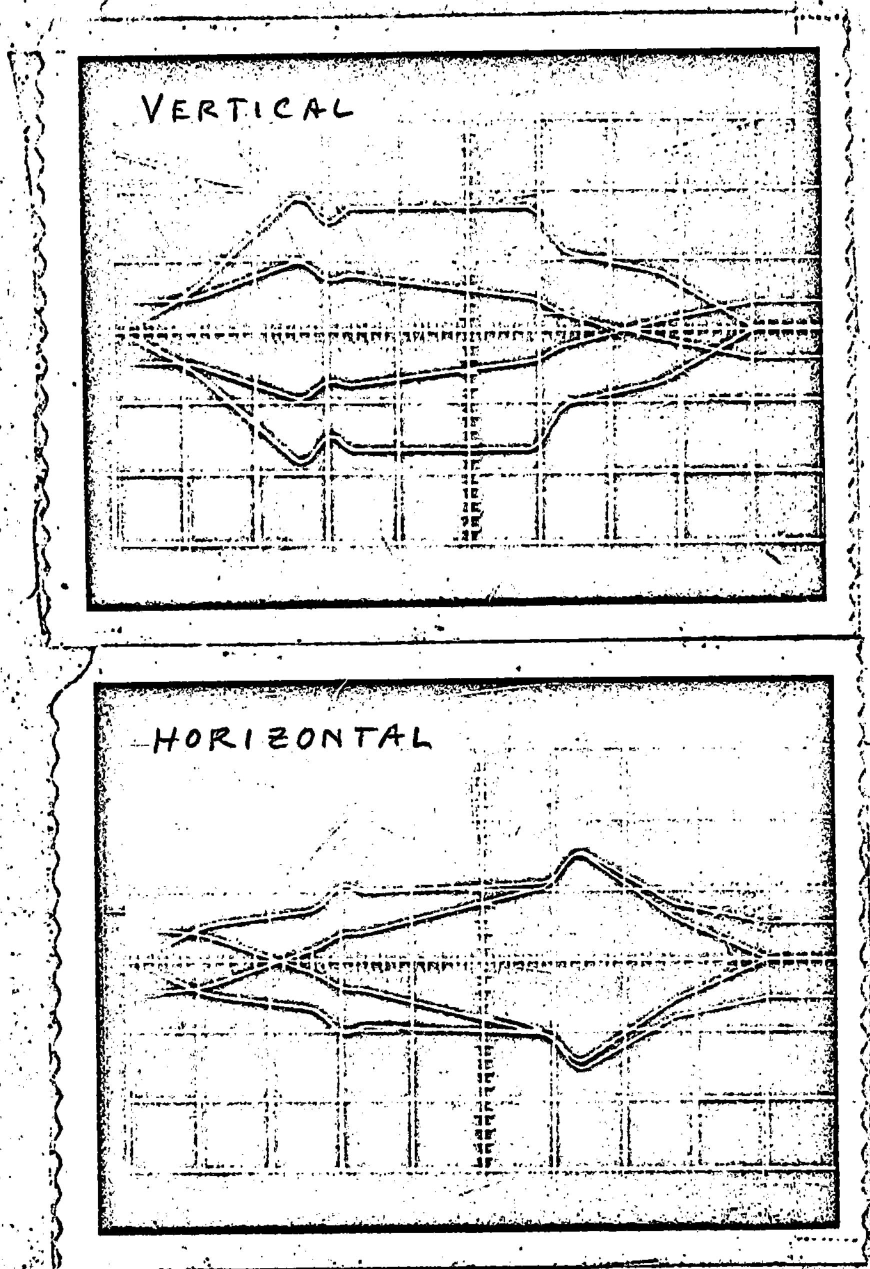

FIG. 24

$\Xi^- \pi^+$ vs. $K^\circ \pi^+$ at 2.45 BeV/c

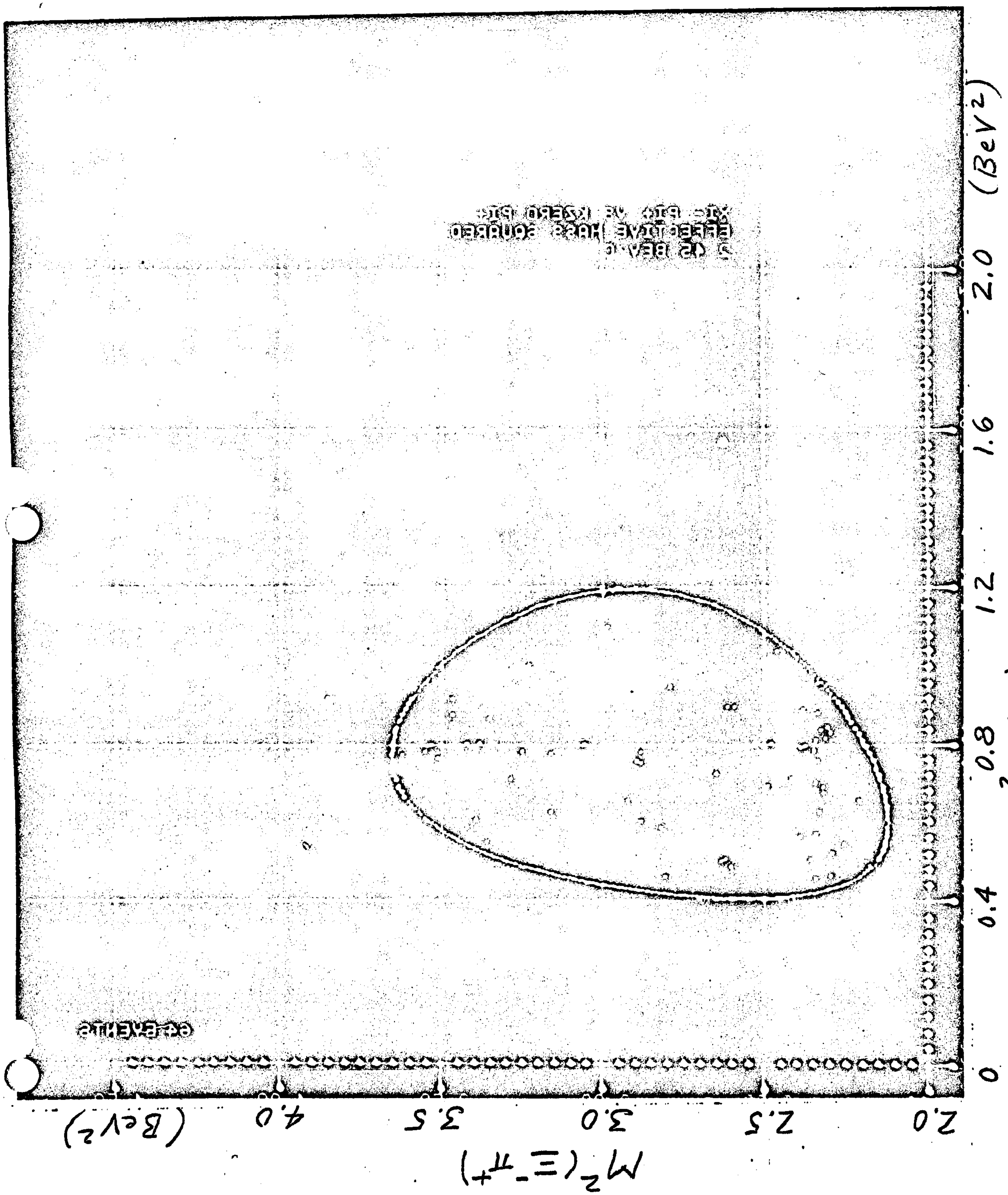

FIG. 25

$\Xi^- \pi^0$ vs. $K^+\pi^0$ at 2.45 BeV/c

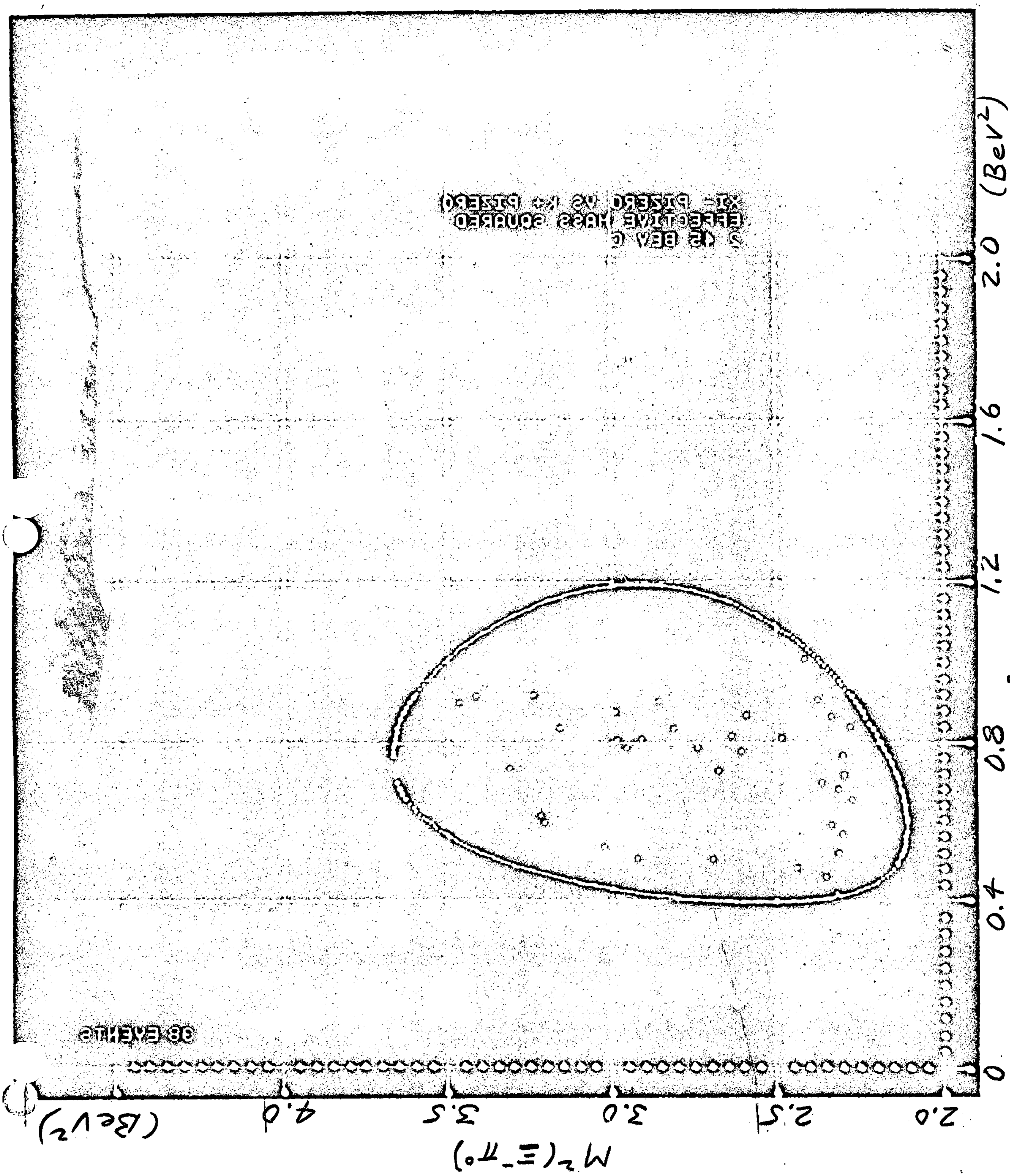

$\Xi^- \pi^+$ vs. $K^0 \pi^+$
at 2.45 – 2.70 BeV/c

FIG. 26

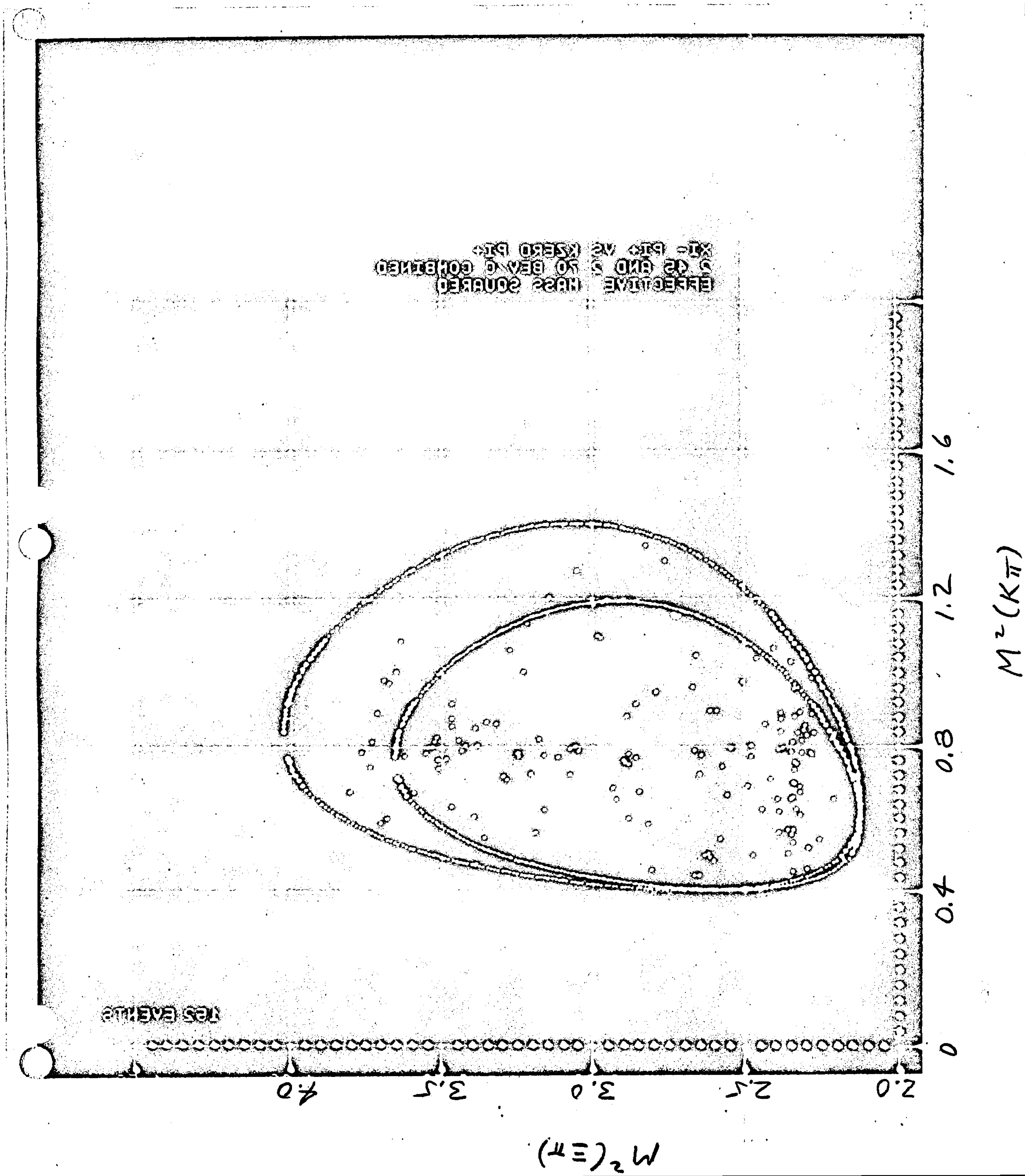

FIG. 27A

$\Xi^- \pi^0$ vs. $K^+ \pi^0$
at 2.45–2.70 BeV/c

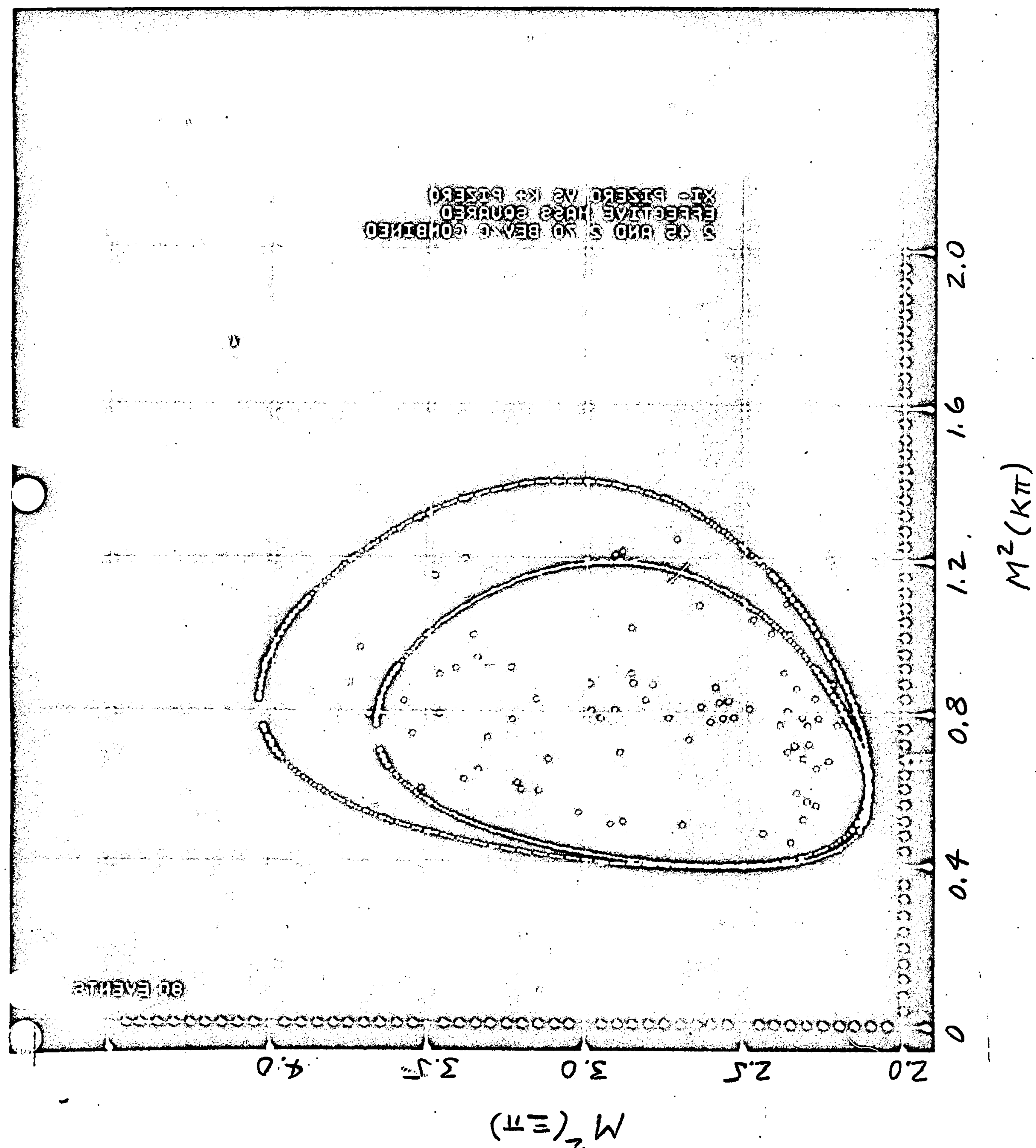

FIG. 27B

$\Xi\pi$ vs. $K\pi$ (both charges)
at 2.45 – 2.70 BeV/c

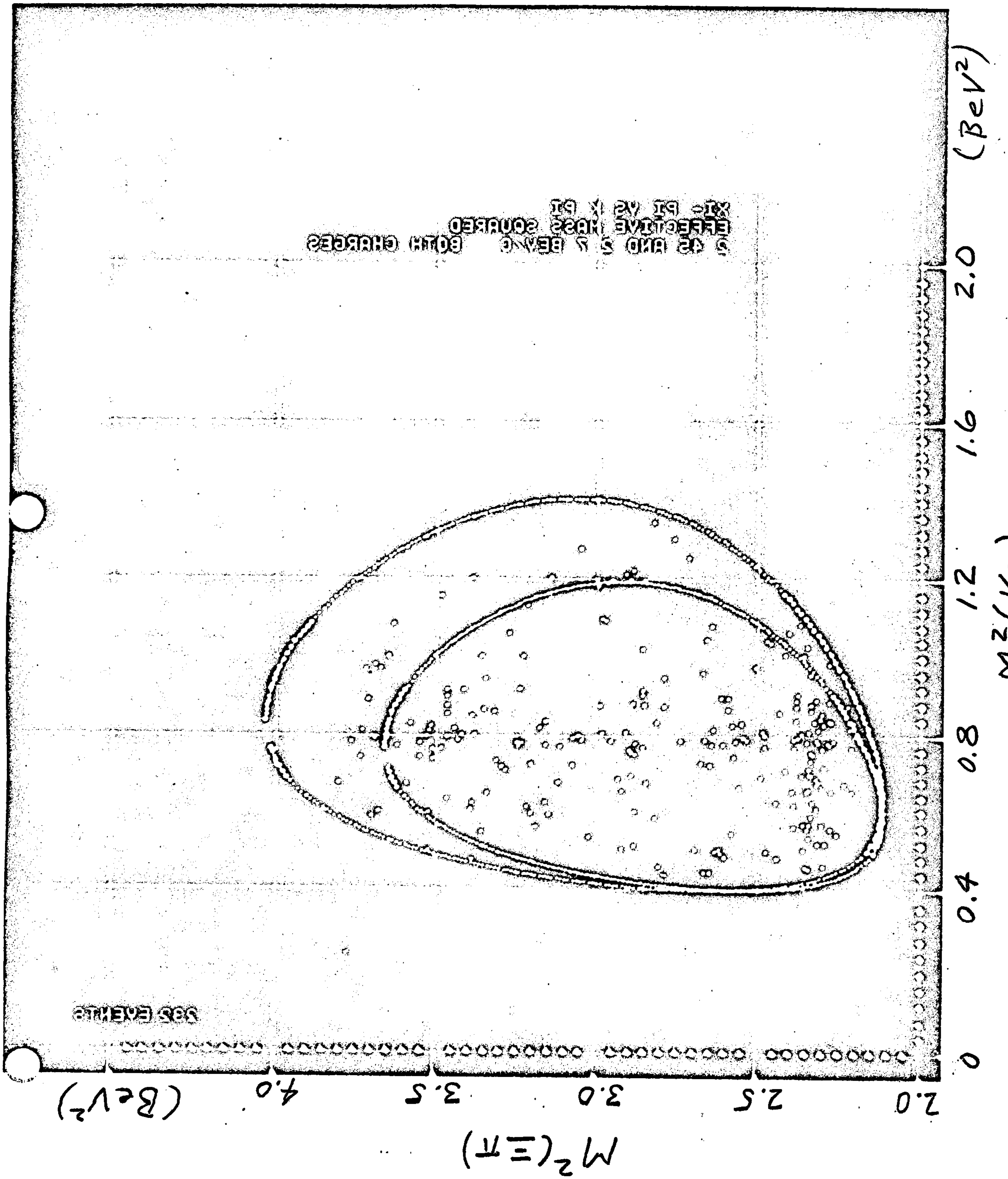

FIG. 28

(Sienna Conference)

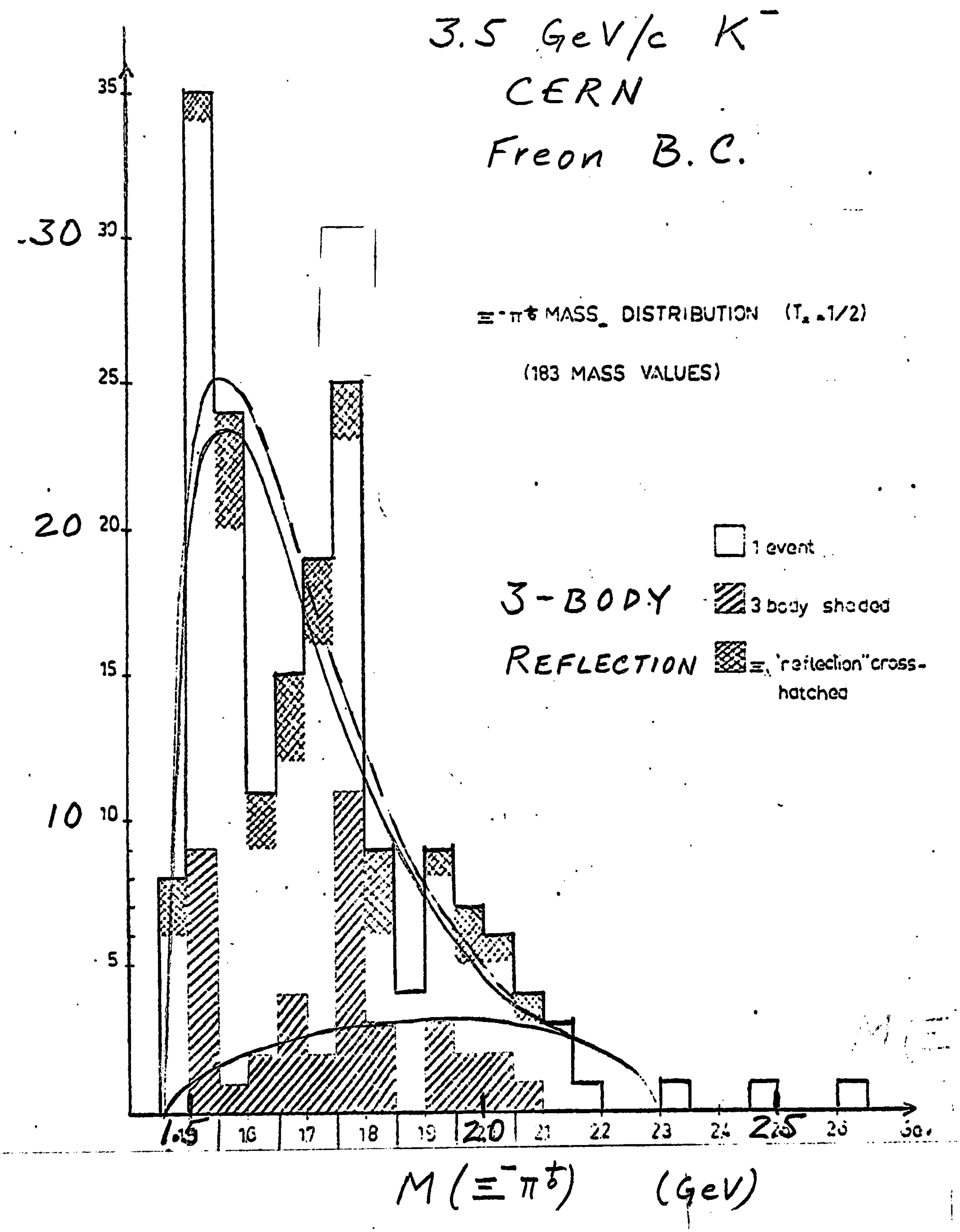

extra

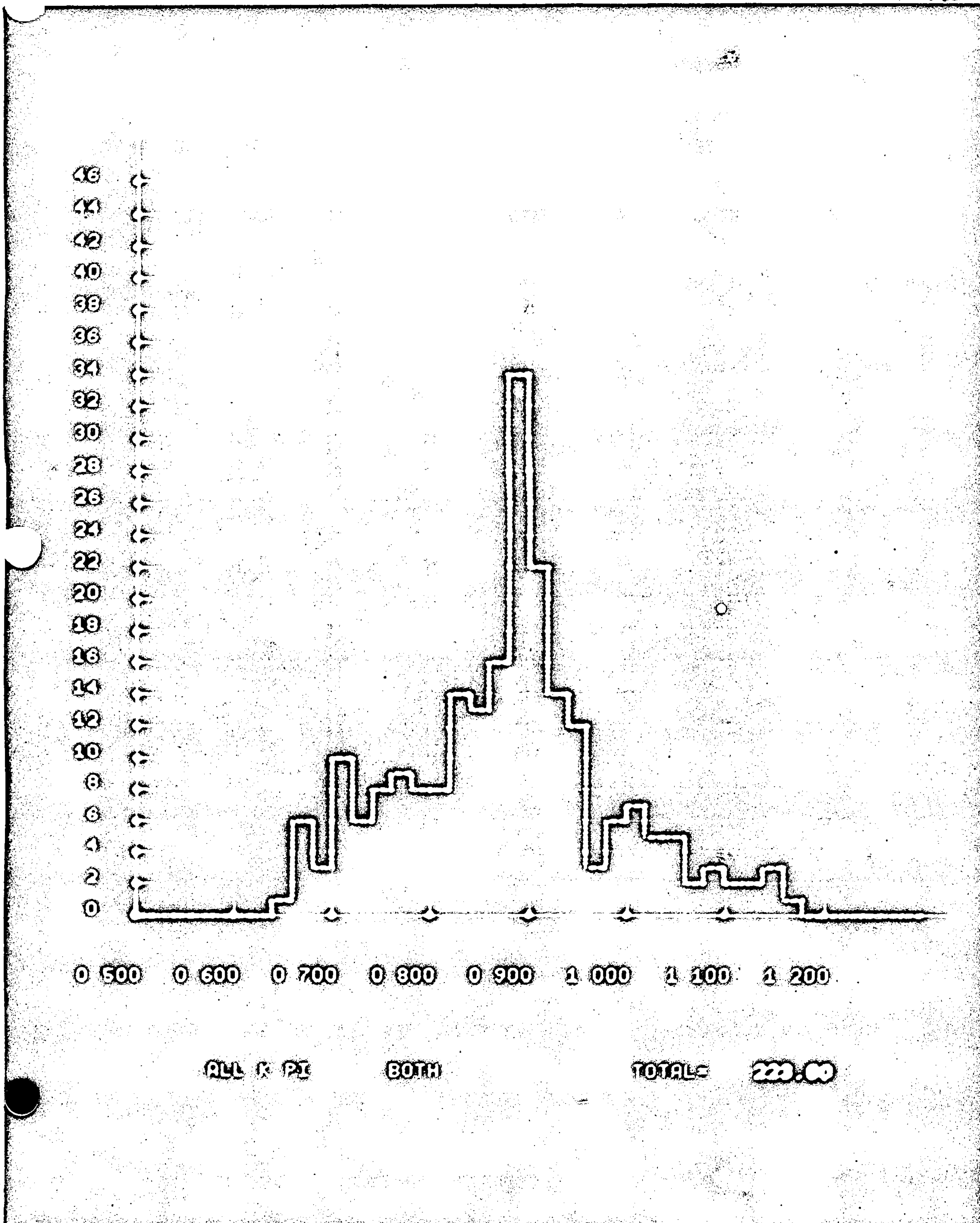

46
44
42
40
38
36
34
32
30
28
26
24
22
20
18
16
14
12
10
8
6
4
2
0
0 500
0 600
0 700
0 800
0 900
1 000
1 100
1 200
ALL K PI
BOTH
TOTAL=
220.00

FIG. (29)

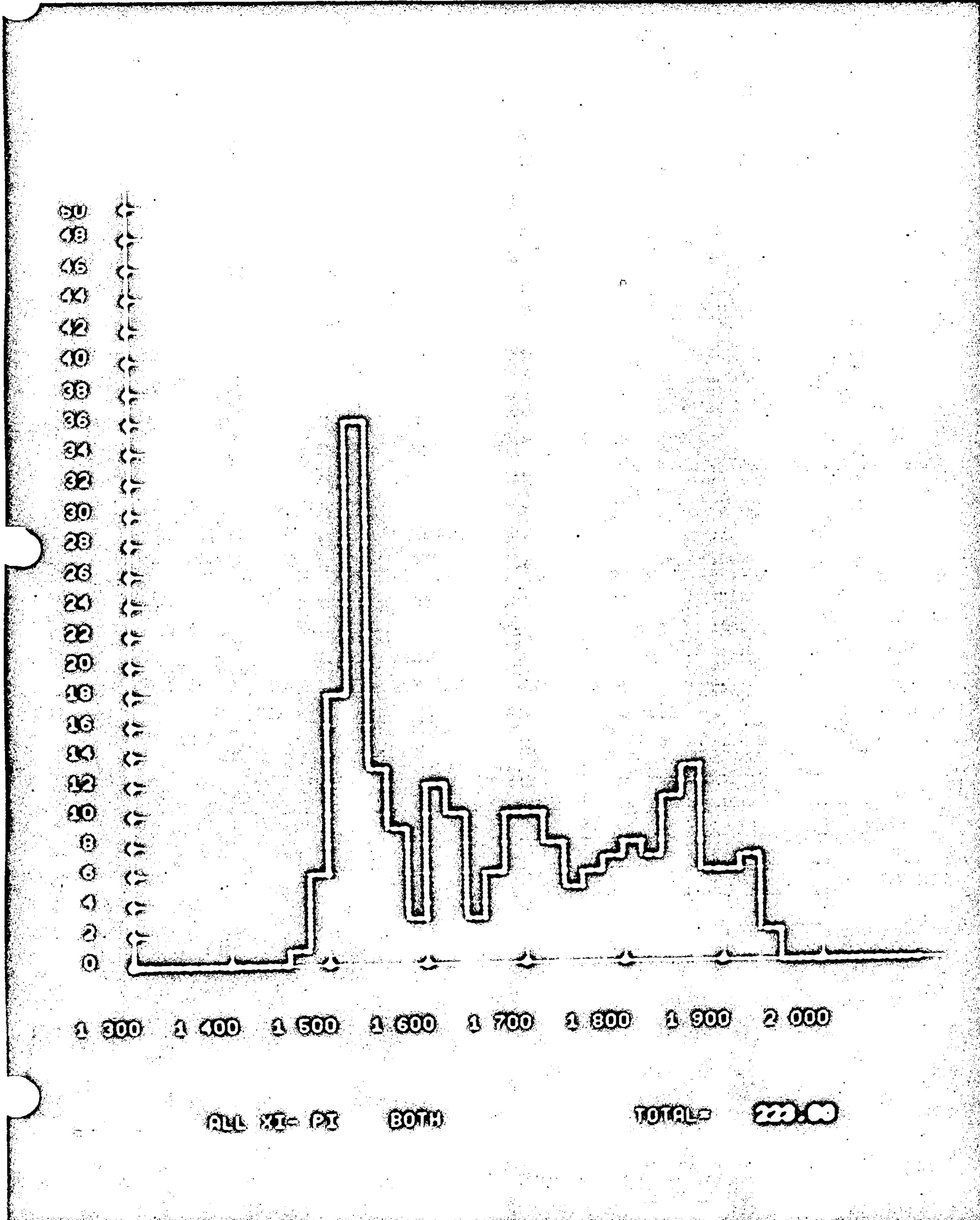

50
48
46
44
42
40
38
36
34
32
30
28
26
24
22
20
18
16
14
12
10
8
6
4
2
0
1 300
1 400
1 500
1 600
1 700
1 800
1 900
2 000
ALL XI- PI
BOTH
TOTAL=

FIG. (30)

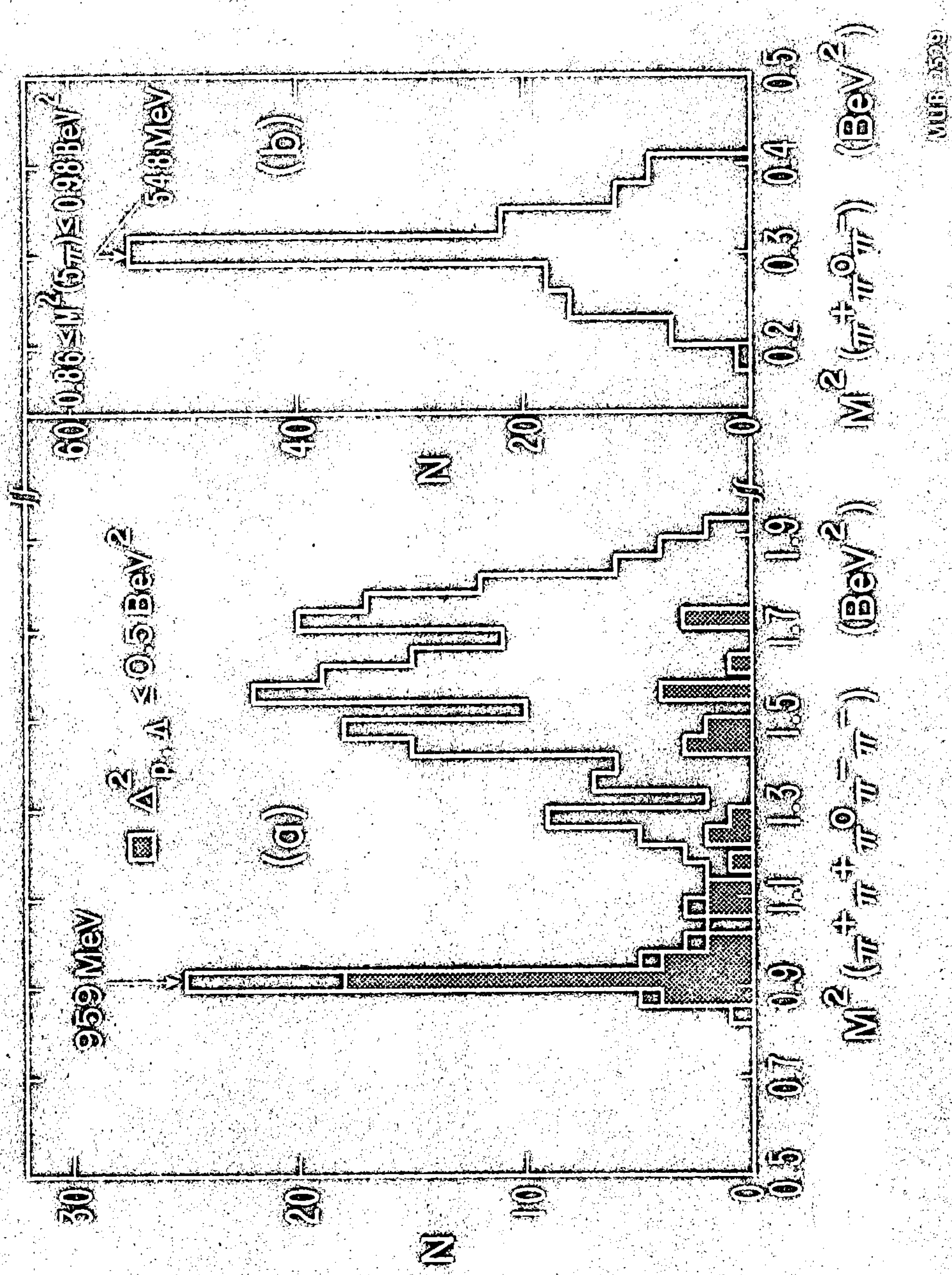

FIG. (31)

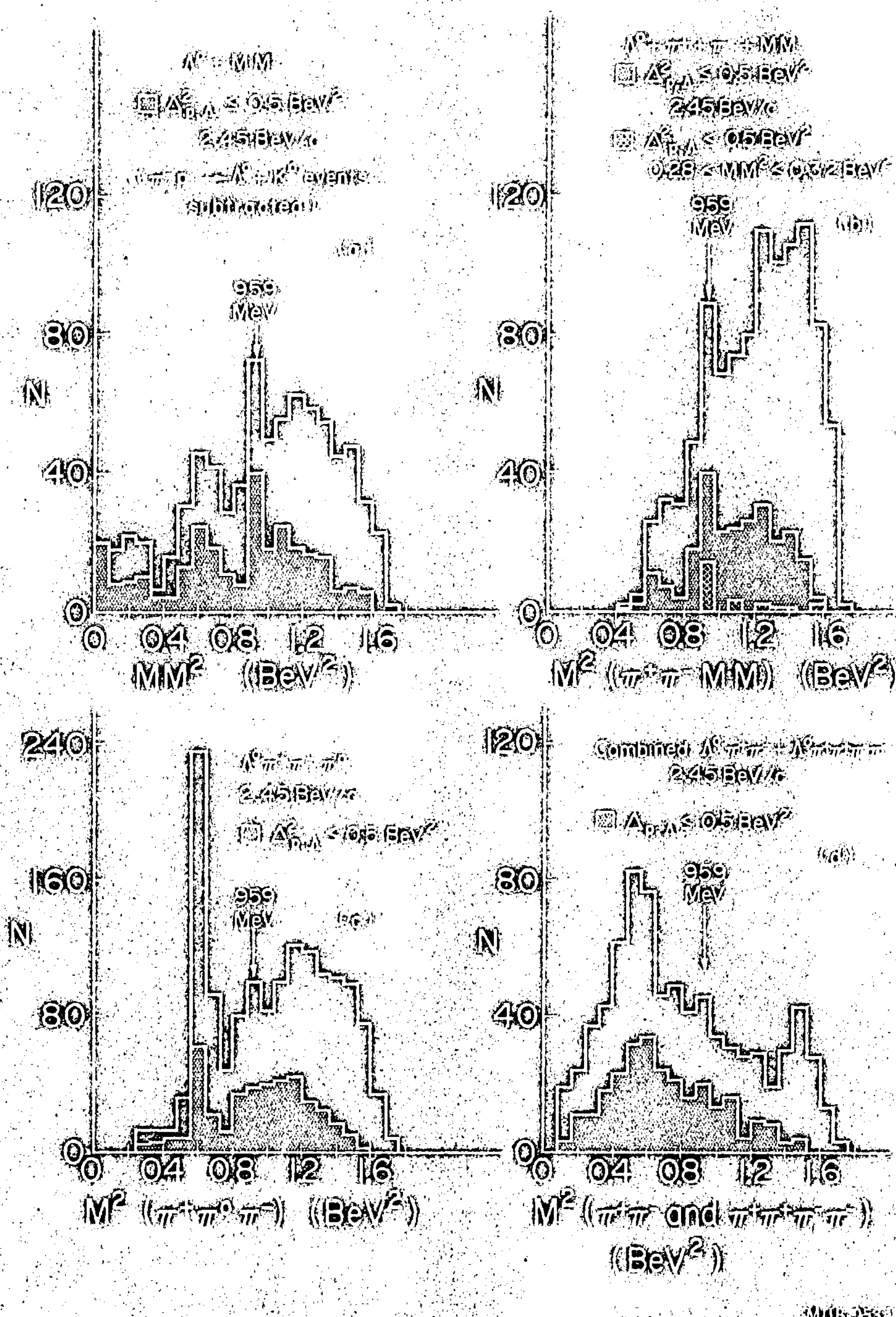

(a)
2.45 BeV/c
$\Delta^2_{p,\Lambda} \leq 0.5$ BeV^2
959 MeV
MM^2 (BeV^2)
(b)
2.45 BeV/c
$\Delta^2_{p,\Lambda} \leq 0.5$ BeV^2
$0.28 < MM^2 < 0.372$ BeV^2
959 MeV
M^2 ($\pi^+\pi^-$ MM) (BeV^2)
(c)
2.45 BeV/c
$\Delta^2_{p,\Lambda} \leq 0.5$ BeV^2
959 MeV
M^2 ($\pi^+\pi^0\pi^-$) (BeV^2)
(d)
2.45 BeV/c
959 MeV
M^2 ($\pi^+\pi^-$ and $\pi^+\pi^+\pi^-\pi^-$) (BeV^2)
N

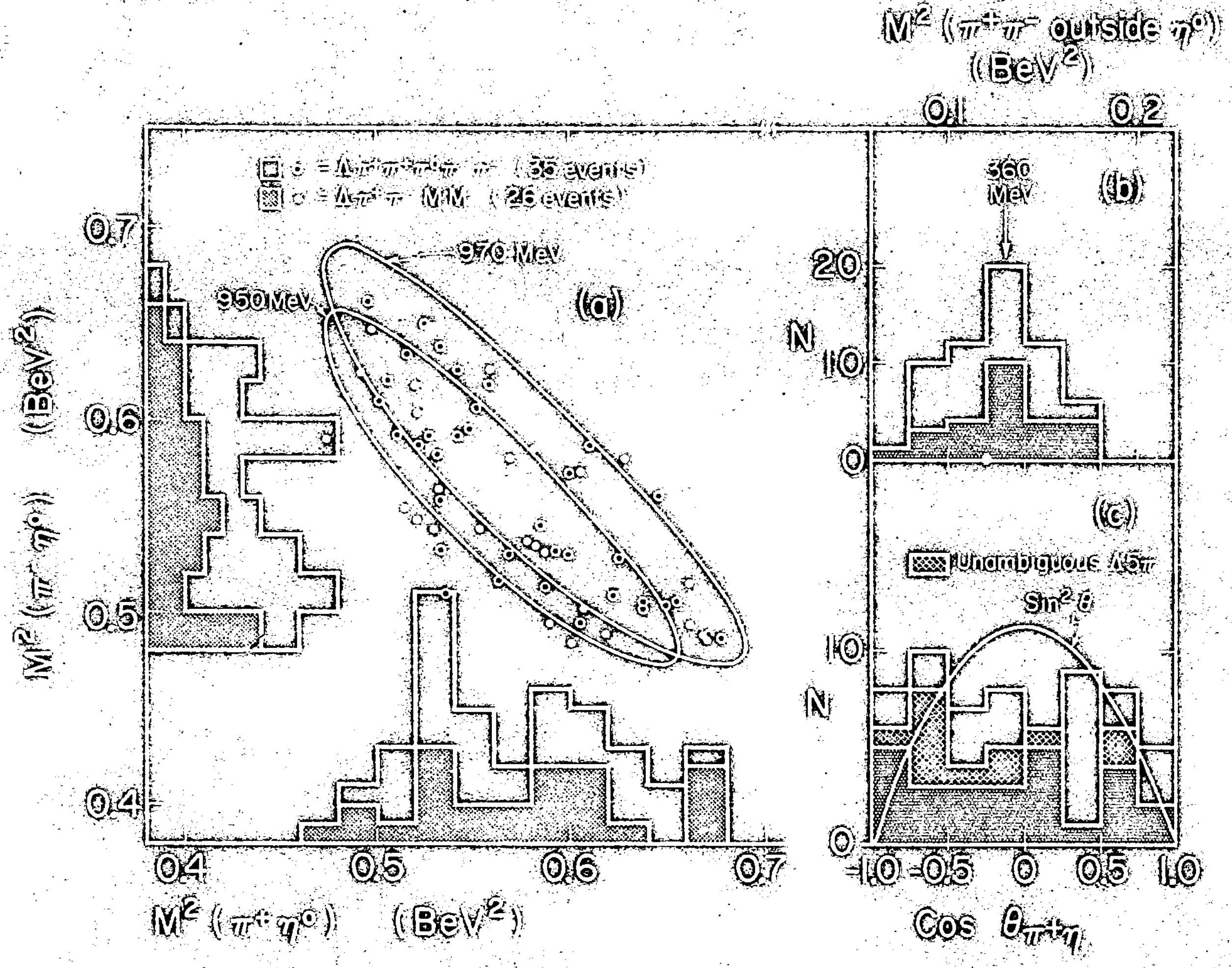

M² (π⁺π⁻ outside η°) (BeV²)
(35 events)
(26 events)
970 Mev
950 Mev
(a)
(b)
(c)
360 Mev
N
Unambiguous
Sin² θ
M² (π⁻ η°) (BeV²)
M² (π⁺ η°) (BeV²)
Cos θ

FIG. 32

SUBJECT NOTES ON THE OPERATION OF THE SPIRAL READER

NAME Lloyd/Solmitz

DATE May 20, 1964

The Spiral Reader (MPIIIb) is a vertex oriented device designed to measure bubble chamber events at a high rate and at a unit cost considerably less than other systems now employed in the field. Other machines are track oriented and are necessarily limited in speed because at some time in the operation of scanning or measuring "paths" must be established for each track by an individual. The Spiral Reader requires only that the operator make certain precision positionings of an x/y stage; it is not necessary to define paths which are the limiting factor of most measuring devices. For this reason the Spiral Reader has a distinct economic advantage over all other systems now in use in the field.

The present machine was originally conceived in 1958 and has undergone many changes in the intervening years. In this note we will outline the present situation and indicate our plans for the near future, with particular reference to the inclusion of a small digital computer in the Spiral Reader system. The Spiral Reader is expected to measure events of single vertex topology at rates in excess of 50 triads per hour within 4 months. The cost of the computer is $50K.

The Spiral Reader was operated during the Fall of 1963 and was used by Dr. Stanley Wojcicki in an experiment in K^- scattering. At the conclusion of this experiment of about 10,000 measurements, the machine was taken out of service for some necessary technical improvements. These improvements included the redesign and installation of an Automatic Video Gain Control and a detailed study of methods by which the machine could be operated with higher reliability. It was not economically feasible to continue to operate the machine under conditions which prevailed during most of Wojcicki's experiment. However, during this time the machine did measure for extended periods at 20 events per hour. To understand the potential measuring speed of this device, the conditions under which these measurements were made is outlined below.

During this period film was positioned by hand, the vertex positioned for measurement completely under the control of the operator and the indicative data for each event entered by the operator at the time of measurement. Operators referred to written lists for measurement information. Fiducials were measured manually with the x/y stage. In all present high performance machines at least some and usually all of these operations are performed automatically by the machine. It has been devices of this type that have improved the performance of Franckenstein and SMP. Precision coordinates were measured by positioning the x/y stage as done on Franckenstein. A positioning was made for each vertex, for an endpoint of each track and for each of the fiducials. This means that for a 2-prong measured in 3 views we required that the stage be positioned 3 views X (2 fiducials + 1 vertex + 3 tracks) = 18 times. It is quite impressive that even under these conditions the Spiral Reader has operated for long periods at such high measurement rates.

We will eliminate many of these time consuming positionings. The "crutch points" will be eliminated for the most part. At present the program FILTER finds tracks quite reliably without the aid of the crutch points but cannot choose the correct tracks from the fairly large number of variants which have been found. FILTER could be modified but because of the nature of the program we have determined that it should be rewritten in Fortran using a somewhat different approach. The new program is about 75% complete and will be ready in late June. Crutch points will still be used to identify short tracks. It is difficult to estimate the speed of the new program at this stage but we expect that it should process events at a rate somewhat faster than 4 seconds per triad on 7094.

A technique has been developed to identify and measure fiducials on 72 inch film automatically. All fiducials are digitized in one translation of the stage. The device is installed on the Spiral Reader and is undergoing final checkout and calibration.

Modifications have been completed to install a simplified version of the SP-V "Fly's Eye" film positioning system and frame number readout. This system will be ready for installation within 2 weeks.

The Spiral Reader at present is composed of the following major components:

1. Film transport
2. Stage drive and x/y scalers
3. Periscope drive and r/0 scalers
4. Video channel including scanning slit, periscope and Automatic Gain Control
5. Track detection logic
6. Electronics for logical sequencing of the measuring operation
7. Buffer memory and interlacing controls
8. Magnetic tape transport and control

We have found that in the past the reliability of many of these components to be less than adequate. An appendix by Tom Taussig will describe these difficulties in detail.

One of the more important difficulties with the Spiral Reader, aside from component reliability, has been the lack of an adequate automatic gain control. Variations in background light intensity of 10:1 are not unusual on 72 inch film; also, the angular velocity of the scan is constant and therefore the frequency response of the AGC must vary with radius to be effective. Such a device has been designed and installed over the past 2 months and recent measurements have shown very satisfactory results. The machine will now digitize tracks reliably in all areas of the chamber. The precision of precent measurements compares quite favorably to SMP or Franckenstein.

In the Spiral Reader we have a device which potentially can measure bubble chamber film at rates approaching an order of magnitude faster than Franckenstein and SMP and at a cost not significantly greater. It is clear therefore that if the demand exists to measure this volume of events we should immediately look to the most economic and reliable way to execute the project.

We propose the purchase of the Digital Equipment Corporation's PDP-4 computer as the basic control element, buffer memory, tape control unit and operator communication device in the Spiral Reader system. The PDP-4 is a fast, reliable, 18 bit, 4096 word digital computer with limited arithmetic capability but a very large and flexible array of input/output facilities well suited to our application. With this computer wewill eliminate many of the components which have proven so unreliable in the past. More important, we will gain the flexibility of software logic and immediate checks on data as it is produced. The devices to speed the operation now being installed will be simpler and less expensive because the decision making elements of each is the computer.

The Spiral Reader will operate in the future with prescanned film; information on event type and location of the event will be an input to the computer. The frame will be positioned and the stage moved to roughly center the vertex completely under computer control. Fiducials will be measured automatically and verified by the computer. The operator's duties will consist of centering the vertex precisely for the r/θ scan and to deciding if crutch points must be taken to eliminate ambiguities or to point out short tracks. The time limitations of the measurement will then be primarily film transport, the centering of the vertex by the operator and the r/θ scan itself which takes about 5 seconds per vertex.

The Jet Propulsion Laboratory has 4 PDP-4's in service. One of these is in an application quite similar to ours and in discussions with their engineers at Pasadena we have found that they are more than pleased with the flexibility and dependability of the PDP-4 in their installation.

NAME T. Taussig
DATE May 20, 1964

SUBJECT APPENDIX TO PHYSICS NOTE 509

SYSTEM RELIABILITY

A detailed study of the reliability of the Spiral Reader during the calendar year, 1963, shows that there were 208 separate occurrences of some failure in the system. The distribution of these failures into various component systems of the Spiral Reader shows that approximately 45% of these occurrences were not detectable by the operator or the maintenance man on duty. This means that most often the failures were not detected until the data that was produced by the machine had been processed by the 7094 system and returned to the experimenter for his evaluation. The time involved in this procedure often was measured in days and usually a minimum of 24 hours. Many of these failures are not major in that they can be repaired by maintenance people in a resonably short time. But without the aid of some on-line monitering device, these failures cannot be detected without a great deal of lost operating time. It can be seen that although these approximately 100 occurrences of undetected failures took only 5 hours on the average to repair one must add to this 5 hour average time at least 1 day per occurrence of lost time, thus, it is at approximately 63 days down time is turned into an actual 163 days of lost time due to failures. The main contribution to this down time is the memory buffer which accounts for 20% of all failures and, thus, approximately 1/2 of all the undectable failures. The buffer memory system was purchased commerically in approximately 1958 for use on a different project. As used in the Spiral Reader actually 2 memory buffers are used in parallel to make available a 36-bit word that is constructed from the 2 24-bit buffer memories. It is evident that these memories were designed very early in the state of the art of magnetic core buffers. There was very little, if any thought, given to adequate maintenance procedures. Access to the power supply components, for instance, requires approximately 2 hours of mechanical disassembly time. The electronic components that comprise the logic of the memory are of various mixtubes of type and carry very little continuity for the maintenance man. We have attempted to locate one of these memories that is not is use so that we could procure it and possibly use it for 100% spare parts as well as a test fixture in which to repair the boards that have failed in our active memories. A search for such a memory has thus far not been fruitful. 12% of the undetected failures were due to magnetic tape problems. The Ampex FR400 tape unit that was in use with the system for some time was, in October, 1963 replaced by an IBM 7330 tape transport at which time the tape troubles dropped to an undectable level. Other sections of the system such as Baldwin digitizer, amplifiers, and the servo amplifiers have been modernized and rebuilt in such a manner that they are easily serviceable and give very little maintenance trouble. The control logic of the Spiral Reader, on the other hand, does not give an excessive amount of trouble, but on occasion there arises a situation in which one would like to change somewhat the sequencing or operation of the machine. Although the design of this portion of the Spiral Reader was extremely well documented in a 2-inch thick binder, our experience agrees with the opinion of the original designer that it would be difficult, if not impossible, to make extensive changes to this protion of the machine.

In general, the problem of reliability is not one only of component reliability, but one of logical organization. The reliability of a computer stems not only from the fact that it uses fairly reliable logical elements, but also because it uses a minimum number of these elements and uses them repetitively to perform as many functions as possible commensurate with its required speed of operation. That is the information flow in a computer is mainly relegated to that between a reliable memory and 2 or 3 active registers. The various operations

SUBJECT
NAME
DATE

that the computer performs is done merely by manipulating the data contained in these registers. The logic that controls these manipulations is also stored in the memory and, thus, the same logical packages that transmit data information transmit the instructions for manipulating the data. Although initially conceived as a computer controlled measuring device, due to its evolution, it has grown to be a large system of sequential logic and sequentially gated data flow. The data that the Spiral Reader produces is passed through many gates in order to gather the information from the many registers in which it originates into the core buffer memory and from there through many gates so that it can be formatted properly for writing onto magnetic tape. This type of logical organization not only provides greater opportunities for electronic failures, but also increases the maintenance effort that is required to find and repair these faults.

Memo 510 is missing from the collection